Chapter 8
Using Nanoparticles as Gas Foam Stabilizing Agents for Enhanced Oil Recovery Applications

Yazan Mheibesh, Farad Sagala, and Nashaat N. Nassar

8.1 Introduction

8.1.1 Background

Oil recovery from a conventional reservoir involves three distinct but intimately connected recovery mechanisms: the primary recovery, which is the oil production using the inherent reservoir pressure; the secondary recovery, which is the recovery of oil by pressure maintenance operations including water flooding; and the enhanced oil recovery (EOR), which is the extraction of oil by either thermal, chemicals, or gas flooding techniques. The primary and secondary oil recovery mechanisms can recover up to one-third of the present oil in a reservoir while two-thirds of the oil will remain unrecovered [3, 76, 116, 144]. Tertiary or enhanced oil recovery (EOR) methods are targeted to economically produce 65% of the remaining hydrocarbon initially in place at the end of both the primary and secondary recovery mechanisms [65]. The performance of EOR is evaluated based on the macroscopic and microscopic efficiencies. The macroscopic displacement efficiency refers to the ability of the displacing fluid in contact with the reservoir in a volumetric sense both areally and vertically [65]. On the other hand, the microscopic displacement efficiency addresses the ability of the displacing fluid to mobilize the residual oil in the pore scale [35]. The microscopic displacement efficiency is closely related to the dimensionless capillary number which is the ratio between the viscous and interfacial forces. In a typical brine flooding (secondary recovery), the capillary number is within the range of (10^{-7}–10^{-6}) [84]. Increasing the capillary number to the range of

Y. Mheibesh · F. Sagala · N. N. Nassar (✉)
Department of Chemical and Petroleum Engineering, University of Calgary, Calgary, AB, Canada
e-mail: nassar@ucalgary.ca

N. N. Nassar et al. (eds.), *Nanoparticles: An Emerging Technology for Oil Production and Processing Applications*, Lecture Notes in Nanoscale Science and Technology, https://doi.org/10.1007/978-3-319-12051-5_8

(10^{-4}–10^{-3}) can reduce the residual oil saturation to 10% [79]. Moreover, the residual oil saturation reaches zero as the capillary number is increased to 10^{-2} [78]. To achieve this capillary number, the interfacial tension has to be within the range of (10^{-2}–10^{-3}) mN/m [153]. Although chemical EOR can effectively decrease the interfacial tension to ultralow values, it has not been applied widely in the past due to the high costs of chemicals and low oil prices [84].

The most common EOR method implemented in field applications is the gas EOR which contributes to about 39% of the entire world EOR project production [7, 10, 58]. Gas EOR methods include the injection of inert or hydrocarbon gases including methane, nitrogen, carbon dioxide, or air for reservoir pressure maintenance and residual oil recovery [142]. About 38% of US EOR project production is referred to as CO_2 injection [100]. The high focus on CO_2 implementation in EOR projects is attributed to minimizing the environmental aspects of the greenhouse emissions (GHE) as well as the desirable miscible properties of CO_2. However, the oil recovery from field applications of gas EOR is considered lower than anticipated as a result of early gas breakthrough and gravity override. Several applications of the oil industry involve utilizing foams including fire retardants and synthesis of porous materials [24, 25, 121], hydraulic fracturing [71, 130], and finally EOR [54]. Foam is considered one of the most promising technologies to overcome the gravity override and viscous fingering of gas EOR. Foams are capable of enhancing the macroscopic sweep efficiency of the gas flood by blocking the high permeable zones, increasing the apparent viscosity of gas, and diverting it towards unswept reservoir zones. Despite the high potential of foams in enhancing oil recovery, the stability of foams is still a major concern due to film thinning and bubble coalescence. One of the ultimate approaches to enhance the stability of surfactant-stabilized foams can be nanoparticles as suggested in the literature [108]. This is mainly attributed to nanoparticles and their ability to irreversibly adsorb and stabilize the foam liquid films [19, 74, 167]. The focus of this chapter is to summarize the main concepts of foam stability and the current status of foam stabilization by nanoparticles including the mechanisms and crucial parameters influencing foam stability. Moreover, remarkable studies also illustrate the role of nanoparticles in enhancing both the static and dynamic foam stabilities. Lastly, some field application overview and future commendations/research gaps for nanoparticle-stabilized foam are addressed in this chapter.

8.1.2 Need for Foam EOR

Theoretically, a miscible gas flood can recover most of the crude oil in a swept zone [152]. However, field applications showed that oil recovery by miscible CO_2 is much lower than anticipated which can go up to 20% of the OOIP [15]. The main obstacle of gas EOR is the low volumetric sweep efficiency due to the gravity override, the gas fingering, and reservoir heterogeneity, as depicted in Fig. 8.1 [26, 29,

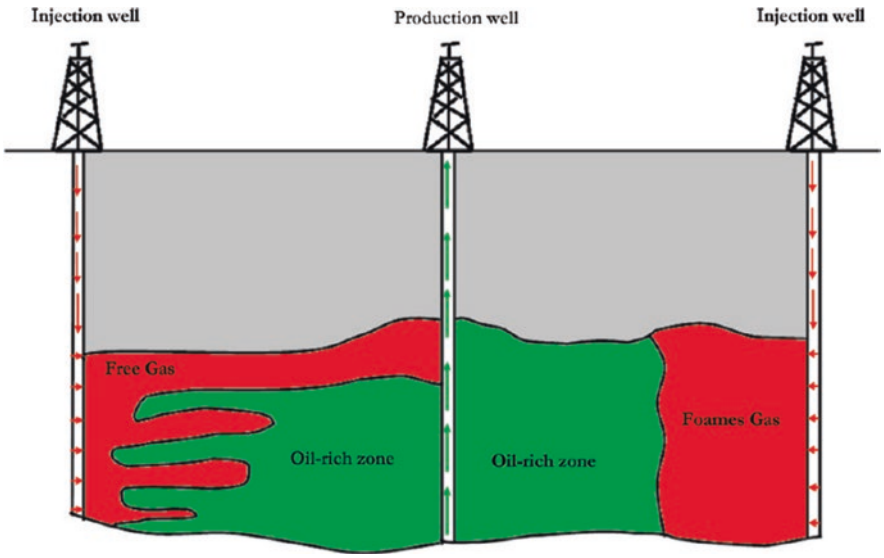

Fig. 8.1 Comparison between the volumetric sweep efficiency of gas and foam floods [60]. Permissions related to the material excerpted were obtained from ACS, and further permission should be directed to ACS; Farajzadeh, R., Andrianov, A., & Zitha, P. L. J. (2010). Investigation of Immiscible and Miscible Foam for Enhancing Oil Recovery. Industrial & Engineering Chemistry Research, 49(4), 1910–1919. doi: https://doi.org/10.1021/ie901109d

110]. The density difference between the gas and displaced fluid causes the gravity override of gas which results in an early gas breakthrough [5]. Moreover, the existence of fractured zones and heterogeneity in reservoir permeability can form high-mobility channels of the low-viscosity gas, thus lowering the macroscopic displacement efficiency of a gas flood [137, 141]. These drawbacks of gas flooding hinder the oil recovery by CO_2 gas flooding even though it has a high microscopic displacement efficiency [137]. Despite the high potential of surfactant flooding in recovering residual oil, it can only be implemented when oil prices are relatively high because of surfactant high costs and surfactants retention [94]. These addressed challenges of both gas and surfactant EOR methods led to conceptualizing of foam as a promising EOR approach [5, 179]. Literature suggests that generation of foam by a combination of both surfactant and gas flooding is cost-effective and enhances the sweep efficiency [5, 134]. Foam increases the sweep efficiency by reducing gas mobility via blockage of some flow channels, trapping gas so that its relative permeability will be reduced, and it can also increase the gas effective viscosity [5, 57, 97, 107, 134, 137].

In contrast with gas flooding, foam mainly recovers oil by the following mechanisms: it increases the viscosity of injected gas (the displacing fluid) for a more stable displacement process. Secondly, it diverts gas to more unswept oil-bearing zones by diverting gas from high permeable zones [5, 9, 60].

8.2 Foam Principles

One of the colloidal dispersion kinds is foam in which gas phase (internal/disperse phase) is dispersed in a continuous liquid phase (external phase). Gas bubbles are separated by a thin liquid film called lamellas which meet at a vertex called the plateau border. Figure 8.2a depicts a 2-D section of a foam surface. In two-dimensional slices of foam, the three lamellas meeting at the plateau border will have an angle of 120 (polyhedral angle). In three dimensions four lamellas will be meeting at the plateau border with an angle of 109.6 (tetrahedral angle). Finally, foams are thermodynamically unstable, and the arrangements of films in the foam are a result of both the surface tensions and contracting forces along with the liquid films [140].

The structure of gas bubbles in a foam can be either spherical or polyhedral cells. When the foam is wet or in a liquid phase, the shape of the gas bubbles will be spherical. However, due to the effect of gravity, foam can start drying resulting in a more polyhedral shape as shown in Fig. 8.2b [4, 18, 45, 46].

Surfactants are considered the most common foaming agent. The most common foam generation and evaluation methods of a solution containing foaming agents are the Bartsch method (shaking), the Bikerman method (sparging), and the Ross-Miles method. Based on the Bartsch method, foam is generated by mechanical shaking of a specific amount of solution placed in a closed container at a specific frequency [124]. In the Bikerman method, a specific volume of solution is placed in a cylinder while gas is being sparged at a specific flow rate through an orifice or porous disk placed at the bottom [124]. In the Ross-Miles method, a portion of the

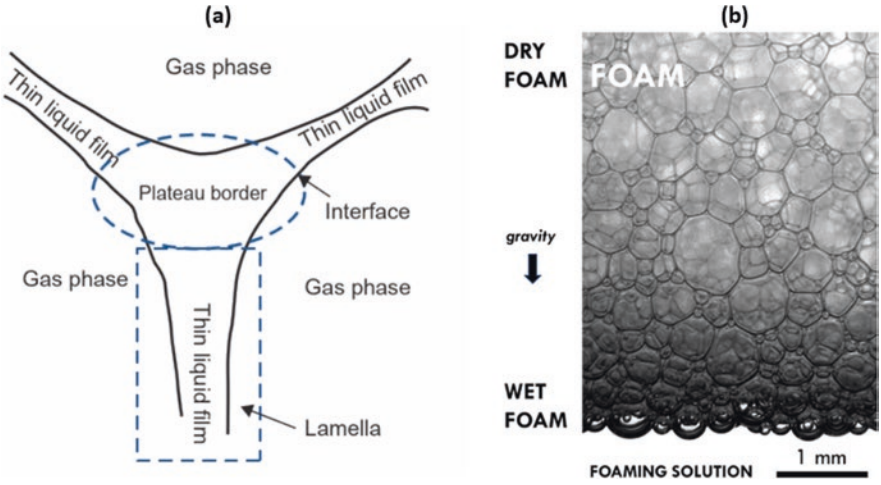

Fig. 8.2 (**a**) 2-D section of a foam [143]. Permissions related to the material excerpted were obtained from Elsevier and further permission should be directed to Elsevier; J. Sheng (2013). Enhanced Oil Recovery Field Case Studies. Oxford, UNITED STATES: Elsevier Science & Technology. (**b**) Wet and dry foam structures. Permissions related to the material excerpted were obtained from Elsevier and further permission should be directed to Elsevier [45]

solution is being placed in a cylinder while a portion of the liquid phase is being poured from the top to generate foam from a specific height [124].

The main concepts to be considered when dealing with the foaming behavior of a solution include foamability and foam stability. According to Carey and Stubenrauch [27], foamability characterizes the ability of a solution to produce foam which can be evaluated as the time needed to achieve a specific volume of foam. The rate at which surfactant molecules adsorb and the total amount of surfactant molecules adsorbed at the water/gas interface are the main factors controlling the foamability of a surfactant solution [27]. Thus, high foamability refers to a foam possessing a rapid surfactant adsorption rate, a high surface elasticity, and surface viscosity properties [27, 122]. The main principles of foam stability will be discussed in the following section.

8.3 Fundamentals of Foam Stability

A foaming agent that can be surfactant, macromolecule, or fine solids is required to generate foam by reducing interfacial energy thus increasing the interfacial area and reducing the mechanical energy input between the gas and liquid phases. To form a more stable foam, effects of foam destabilizing processes have to be minimized, including the film thinning (i.e., lamellas become thinner without changing the total surface area of the bubbles), coalescence (i.e., lamellas rupture, and gas bubbles merge to form bigger bubbles), and coarsening or Oswald ripening (i.e., gas flux from smaller to bigger bubbles). The main factors affecting foam stability include gravity drainage, capillary suction, surface elasticity, foam bulk, surface viscosity, repulsion, electric double layer, dispersion force attraction, and steric repulsion forces [140, 165].

According to the Young-Laplace equation, interfacial tension (σ) causes pressure difference (ΔP) to exist across a curved surface between the interface of gas (G) and liquid (L) phases. Equations (8.1 and 8.2) show the pressure difference (ΔP) across an interface of a wet foam bubble with a radius (R) where P_G, P_L are the pressure of the gas and liquid phases, respectively. Equation (8.3) shows the pressure difference of more complex foam bubbles with principal radii of curvature (R_1, R_2) [140].

$$\Delta P = P_G - P_L \tag{8.1}$$

$$\Delta P = \frac{2\sigma}{R} \tag{8.2}$$

$$\Delta P = \frac{\sigma}{\frac{1}{R_1} + \frac{1}{R_2}} \tag{8.3}$$

The Young-Laplace equation illustrates that the pressure inside a foam bubble (P_G) exceeds the outside pressure (P_L). Moreover, the pressure difference at the interface is also dependent on the foam bubble radius (R).

Due to variations in a foam bubble principal radii as shown in Fig. 8.3 between measured radius from a plateau border (R_B) and measured radius from a lamella (R_A), an additional pressure difference occurs between the liquid inside a film (P_A) and liquid in a plateau border (P_B). The pressure of a liquid in the foam film increases with an increase of measured radius. Thus, the liquid will flow from the film (relatively bigger radius R_A) to the plateau border (relatively smaller radius R_B) which causes film thinning resulting in lower foam stability [140].

Free energy of a gas bubble in foam increases with an increase in bubble size. As surfactant molecules adsorb a monolayer on the interface between a gas bubble and a liquid film, surface tension and free surface energy will be decreased. Thus, the thin liquid film will be stabilized due to surface tension reduction and increase in interfacial viscosity which provides mechanical resistance to film thinning and rupture. Equation (8.4) shows the general Gibbs adsorption for a binary isothermal system containing excess electrolyte. This equation thermodynamically describes the reduction of free surface energy due to surfactant adsorption when surfactant adsorption is considered as a monolayer while surface curvature is not great [140]

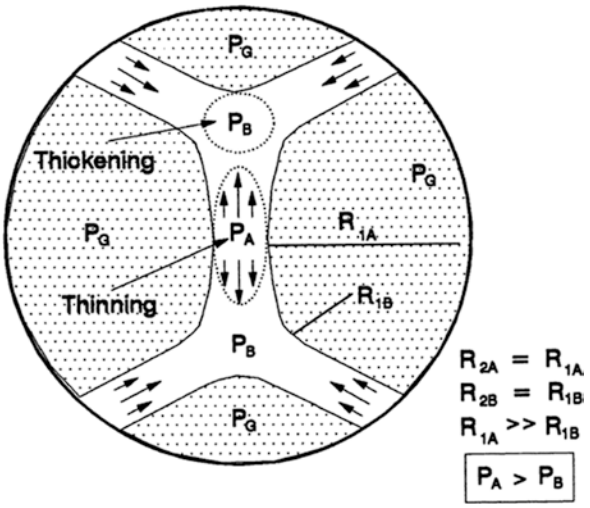

Fig. 8.3 Pressure difference across curved surfaces in a foam lamella due to variation in bubble principal radii. R_{1A} and R_{1B} are the radii from the right side of the liquid film, while R_{2A} and R_{2B} are from the left side of the liquid film [140]. Permissions related to the material excerpted were obtained from ACS, and further permission should be directed to ACS; Schramm, L. L., & Wassmuth, F. (1994). Foams: Basic Principles. In Foams: Fundamentals and Applications in the Petroleum Industry (Vol. 242, pp. 3–45): American Chemical Society

$$\Gamma_s = -\left(\frac{1}{RT}\right)\left(\frac{d\sigma}{d\ln C_s}\right) \tag{8.4}$$

where (Γ_s) is the surface excess of surfactant (mol/cm^2), (R) is the gas constant, (T) is the absolute temperature, (σ) is the surface or interfacial tension, and (C_s) is the solution concentration of surfactant in (M). Due to gravity forces, the liquid starts draining from liquid films until it is being balanced by capillary forces as described previously by the Young-Laplace equation. As a result, the thinning process leads to further foam collapse [140]. Surface elasticity of foam films increases foam ability to withstand deformations without rupturing. When a foam film is stabilized by surfactant adsorption undergoes a sudden expansion, the expanded portion of the film will have a lower degree of surfactant adsorption compared to the unexpanded film portion due to the increase in surface area. Thus, surface tension increases locally providing resistance for more film expansion by producing an immediate surface contraction by viscous forces. Hence, liquid flows from the low-surface tension region to the high-surface tension region as shown in Fig. 8.4. The diffusion of surfactant from bulk liquid to the expanded foam portion can be more quick in thick films compared to thin foam films. In thin foam films, not enough surfactant molecules will be transferred and adsorbed on the interface and achieve equilibrium quickly after film expansion. This phenomenon is called the Gibbs-Marangoni effect which is significant in stabilizing foam against thin film rupture and rapid deformation. This effect explains why a foam having low film surface tension cannot stabilize foam, because it does not having sufficient surface elasticity to reach equilibrium after surface expansion or contraction [140].

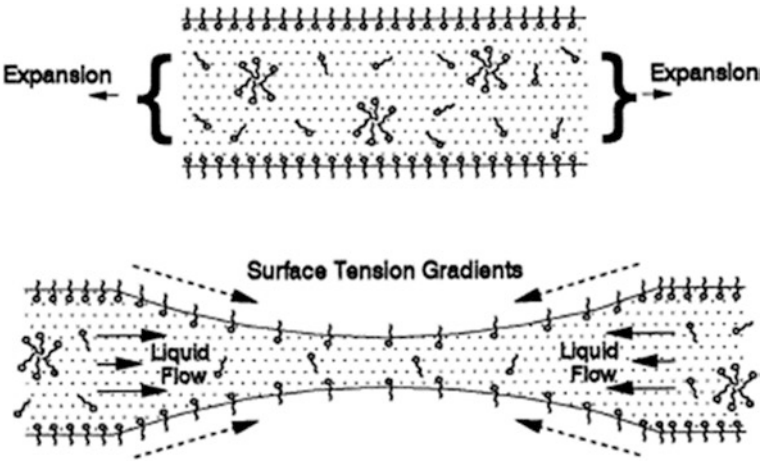

Fig. 8.4 Surface tension gradients in a film due to expansion [140]. Permissions related to the material excerpted were obtained from ACS, and further permission should be directed to ACS; Schramm, L. L., & Wassmuth, F. (1994). Foams: Basic Principles. In Foams: Fundamentals and Applications in the Petroleum Industry (Vol. 242, pp. 3–45): American Chemical Society

To form a stable foam, both lower surface tension and surface elasticity properties are required. Surface elasticity in foams is a dynamic property measuring the resistance against the creation of surface tension gradients and the rate of disappearance of these gradients in the system. In foam stability studies, there are two types of surface elasticity, the Gibbs and the Marangoni surface elasticities. The Gibbs surface elasticity (E_G) is an equilibrium surface measurement occurring when the number of surfactant molecules in the thin foam is very low so that the surfactant cannot restore surface concentration equilibrium after deformation. The Marangoni surface elasticity (E_M) is a nonequilibrium or time-dependent surface measurement occurring when there is enough amount of surfactant molecules in the foam for restoring the surface concentration equilibrium. Figure 8.5 compares between Gibbs and Marangoni surface elasticities after surface expansion. Equation (8.5) shows the Gibbs surface elasticity for a foam film (E_G) where (σ) is the surface tension and (A) is the geometric area of the surface. The surface elasticity for foam accounts for the effect of two gas/liquid interfaces so factor 2 is introduced in Eq. (8.5) [140].

$$E_G = \left(\frac{2\, d\sigma}{d \ln A} \right) \tag{8.5}$$

Viscous forces in foam, including both the surface and bulk viscosities, can affect the rate of bubble coalescence and film drainage. These forces can indirectly

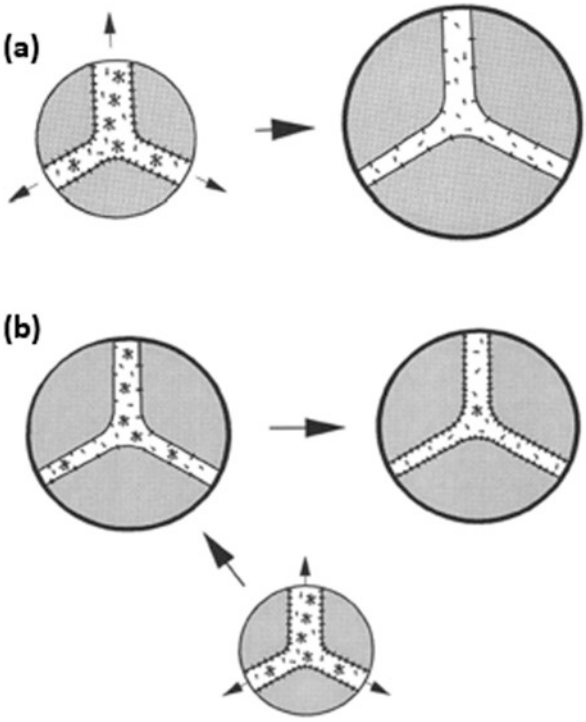

Fig. 8.5 Illustration of (**a**) Gibbs surface elasticity measurement occurring when the number of surfactant molecules is very low, (**b**) Marangoni surface elasticity measurement occurring when enough number of surfactant molecules exists in the foam for restoring the surface concentration equilibrium after film expansion [140]. Permissions related to the material excerpted were obtained from ACS, and further permission should be directed to ACS; Schramm, L. L., & Wassmuth, F. (1994). Foams: Basic Principles. In Foams: Fundamentals and Applications in the Petroleum Industry (Vol. 242, pp. 3–45): American Chemical Society

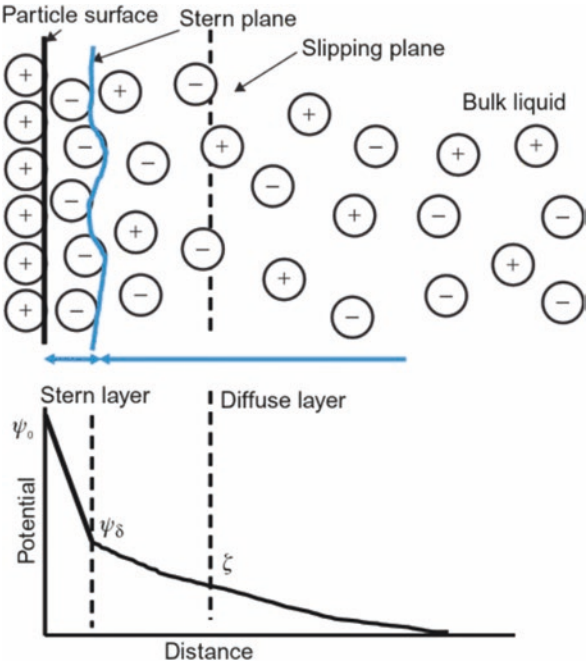

Fig. 8.6 Illustration of ELD of a charged foam lamella [143]. Permissions related to the material excerpted were obtained from Elsevier, and further permission should be directed to Elsevier; J. Sheng (2013). Enhanced Oil Recovery Field Case Studies. Oxford, United States: Elsevier Science & Technology

stabilize foam by resisting foam film thinning and rupturing processes. Thinning of thick foam lamellas is mainly resisted by bulk viscosity, while surface viscosity hinders the thinning of thin films [140].

A foam film stabilized by ionic surfactants adsorbed on the interface influences the distribution of nearby ions. Thus, ions with the same charge are repelled, while counter-charged ions are attracted to the film interface. This results in an electric double layer (ELD) consisting of both inner adsorbed ions and a diffuse layer. The diffuse layer consists of attracted ions by electric forces, and thermal motion will be formed. Depending on foam film thickness and charge density, the ELD opposes foam film thinning process when the charged interfaces of both film interfaces approach each other due to repulsive forces. Figure 8.6 depicts an electric double layer on one side of a foam film and the electric potential for a charged foam lamella [140].

Moreover, disjointing pressure, hydrostatic pressure difference between gas bubbles and bulk liquid, plays a significant role in keeping lamellas interfaces apart from each other. It accounts for electrical, dispersion, and steric (Van der Waals) forces operating across the foam lamellas [140].

8.4 Effect of Nanoparticles on Foam Stabilization

Despite the advantages of foam in increasing the oil recovery over conventional gas enhanced oil recovery processes, solely stabilized foams by surfactants have undesirable properties hindering foam flooding applications in enhanced oil recovery

projects. Low foam stability in harsh reservoir conditions such as high temperature and salinity makes conventional foams fail to meet the production requirements [98]. Moreover, adsorption of surfactants to the rock surface and surfactant decomposition in harsh reservoir environments results in weak foam formation resulting in poor sweep efficiency [7, 97].

Generally, dispersed solids help in the formation of more stable foams. They can increase the foam bulk viscosity and provide more foam film mechanical stability by solid adsorption on the gas/liquid interface [140]. Several studies showed that nanoparticles can play a significant rule in foam stability at high temperatures and salinity conditions by synergistic effect or physicochemical interactions between nanoparticles and surfactants [7]. Adsorption of nanoparticles on the liquid-gas interface enhances the foam dilatational elasticity and hinders the water flow at the bubble surface, thus preventing bubble coarsening, and slows down film thinning [47, 83, 113].

8.4.1 Mechanisms of Foam Stabilized by Surfactant and Nanoparticles

Interactions between nanoparticles-interface, surfactants-interface, and nanoparticles-surfactants count for foam film stabilization. There are several mechanisms of foam stabilization by nanoparticles proposed in the literature including particle detachment energy, particle arrangement during film drainage, maximum capillary pressure of coalescence, and the growing of aggregates [7, 146].

8.4.1.1 Particle Detachment Energy

Adsorption of nanoparticles at the film interface between gas and liquid is irreversible. The affinity of nanoparticles at the liquid interface is affected by the hydrophilic or lipophilic characters of the nanoparticles [129]. The required energy to remove a particle from the gas/liquid interface (ΔE) is expressed in Eq. (8.6) when the gravity and buoyancy forces are neglected due to the small size of the nanoparticles [20].

$$\Delta E = \pi R^2 \sigma_{aw} \left(1 \pm \cos\theta\right)^2 \tag{8.6}$$

where (ΔE) is the energy required to remove a particle from the interface, (R) is the nanoparticle radius, (σ_{aw}) is the gas/water interfacial tension, and (θ) is the contact angle between nanoparticles and the liquid. The sign in the bracket is negative for transfer from water and positive for transfer from oil or gas phase. This equation explains that the reduction in interfacial tension at the interface by surfactants can

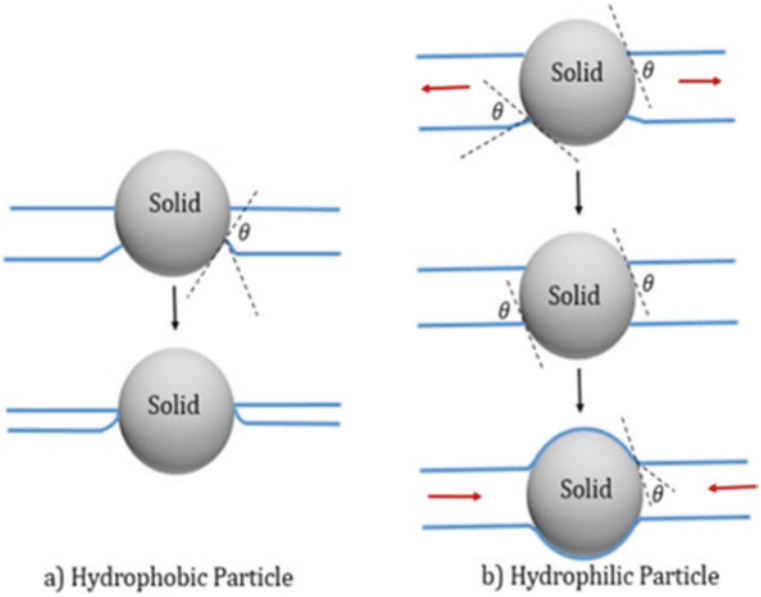

Fig. 8.7 Contact angle between solid particle and surfactant solution: (**a**) Hydrophobic particle ($\theta > 90°$), (**b**) hydrophilic particle ($\theta < 90°$) [7]. Permissions related to the material excerpted were obtained from ACS, and further permission should be directed to ACS; AlYousef, Z., Almobarky, M., & Schechter, D. (2017). Enhancing the Stability of Foam by the Use of Nanoparticles. Energy & fuels, 31(10), 10620–10627

lower the detachment energy resulting in lower foam stability. In the case of the high hydrophilic ($\theta < 30°$) or hydrophobic ($\theta > 150°$) particle wettability, the detachment energy will be reduced resulting in lower foam stability [146]. Figure 8.7 depicts the lipophile and hydrophile characterization of nanoparticles depending on contact angles between solids and liquid.

8.4.1.2 Particle Arrangement During Film Drainage

Depending on the wettability of the solid, adsorbed nanoparticles inside a thin film can form either a monolayer of bridging particles, a bilayer of closed-packed particles, or a network of particles aggregates as shown in Fig. 8.8 [77]. The network of particle aggregates occurs when there is an excess of solids inside the foam films. It is considered the most effective mechanism in foam stabilization because it keeps the gas bubbles separated by resisting dragging, hence slowing foam coalescence and liquid drainage [7].

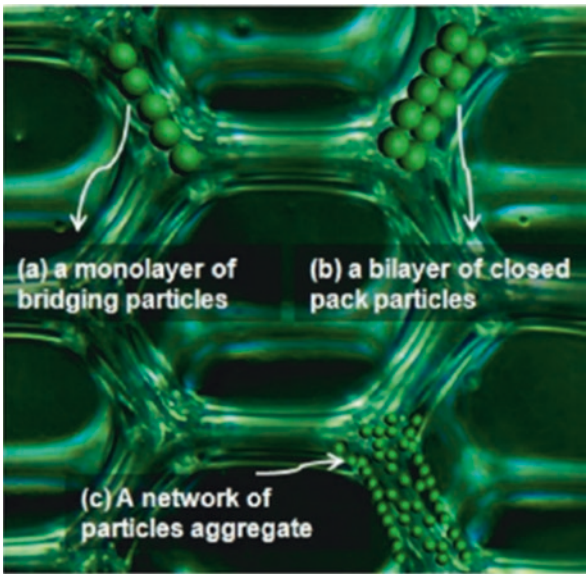

Fig. 8.8 Particle arrangement during film drainage [146]. Permissions related to the material excerpted were obtained from ACS, and further permission should be directed to ACS; Singh, R., & Mohanty, K. K. (2015). Synergy between Nanoparticles and Surfactants in Stabilizing Foams for Oil Recovery. Energy & Fuels, 29(2), 467–479. doi: https://doi.org/10.1021/ef5015007

8.4.1.3 Maximum Capillary Pressure of Coalescence

With the presence of nanoparticles adsorbed to the foam films, the maximum capillary pressure a liquid film can withstand before rupture increases [42]. This threshold pressure is referred to as the maximum capillary pressure of coalescence ($P_c^{\max}$) which results in more foam stability as $P_c^{\max}$ increases [146]. In the absence of nanoparticles, foam films are flat, while they do not have to be flat in the presence of nanoparticles, which provides a barrier against film thinning [7]. Equation (8.7) expresses that the maximum capillary pressure of coalescence ($P_c^{\max}$) is dependent on the packing parameter (p), air/liquid interfacial tension, particles radius (R), and contact angle (θ).

$$P_c^{\max} = p\frac{2\sigma_{aw}}{R}\cos\theta \tag{8.7}$$

In the case of hydrophobic solids ($\theta > 90°$), the film ruptures due to liquid drainage. On the other hand, if the solid particles are hydrophilic ($\theta < 90°$), liquid film starts thinning until it becomes flat as capillary pressure moves the liquid towards the solid particles [7, 146]. As a result, the film thinning process will be stopped which helps in maintaining foam stability, as shown previously in Fig. 8.7.

8.4.1.4 Growing Aggregates

The stability of foam films can be increased by nanoparticles as a result of particle aggregation and cork formation. Using silica nanoparticles at high concentrations (concentration > 2 wt.%,) helps in improving foam stability by increasing film viscosity [7, 28].

8.4.2 Experimental Techniques of Foam Stability Evaluation

The main experimental methods of foam stability by surfactant-nanoparticles for enhanced oil recovery include bulk stability tests, interfacial and dilatational elasticity experiments, and foam displacement tests [175]. In static foam tests, the decay of foam height, bubble size, and gas quality are evaluated over time both in the presence and absence of crude oil. These experiments indicate the effect of nanoparticles on slowing foam decay and coalescence rate. Interfacial tension and dilatational elasticity experiments evaluate the stability of foam films under expansion and contraction effects. Finally, foam displacement tests evaluate the ability of foam in increasing apparent viscosity of the displacing fluid, enhancing the flood mobility ratio, and its effect on oil recovery.

8.4.2.1 Bulk Foam Stability Tests

In bulk foam stability tests, foam generated by gas and the surfactant-nanoparticle dispersion is received in a transparent cylindrical testing tube to assess the foam physical properties over time. Foamability can be indicated by the change in foam height, bubble size distribution, and liquid holdup as a function of time. Effects of temperature, pressure, salinity, surfactant concentration, nanoparticle concentration, and crude oil could be evaluated in this type of foamability test. In this method, foam stability can be evaluated based on foam height and half-life time, bubble size distribution, vertical foam film, and confocal laser scanning microscopy tests.

Foam Height and Half-Life Time

As the generated foam is received in a cylindrical column, it starts decaying with time. The measured height of the foam column at a given time indicates foam stability. The time of foam height decay is slower in more stable foams. Half-life time is the time required for a foam column to decay to its half original height. Normalized foam height can be expressed as shown in Eq. (8.8). This test can be used to evaluate the effect of surfactants and/or nanoparticle concentrations on foam stability when the foam is in contact with crude oil. Figure 8.9 shows a typical diagram of a foam stability device used for bulk foam stability evaluation.

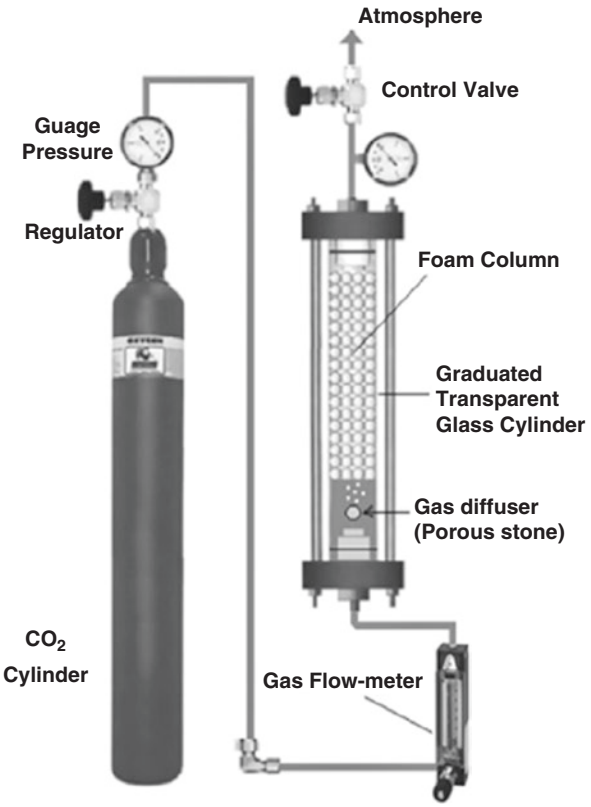

Fig. 8.9 Typical foam evaluation device for bulk foam stability evaluation [16]. Permissions related to the material excerpted were obtained from Elsevier, and further permission should be directed to Elsevier; Bayat, A. E., Rajaei, K., & Junin, R. (2016). Assessing the effects of nanoparticle type and concentration on the stability of CO_2 foams and the performance in enhanced oil recovery. Colloids and Surfaces A: Physicochemical and Engineering Aspects, 511, 222–231. doi: https://doi.org/10.1016/j.colsurfa.2016.09.083

$$\text{Normalized foam height} = \frac{\text{foam height @ time}(t)}{\text{foam height @ foam formation}} \tag{8.8}$$

Bubble Size Evaluation

Investigation of bubble size distribution helps in understanding the foam coalescence and film rupture mechanisms, especially by the use of microscopic pictures. Generally, the radius of foam bubbles is small when the foam is formed, but the size of the gas bubbles starts growing as a result of lamella rupturing. The effect of absorbed nanoparticles at the liquid films on delaying foam rupture can be studied by this method [97]. Figure 8.10 compares the gas bubble sizes of several surfactant solutions and surfactant-nanoparticle solutions. Foam coarsening was delayed in the case of the surfactant-nanoparticles solution, while foam bubble sizes of surfactant solution increased relatively faster indicating lower foam stability. Analyzing the foam bubble size and size distribution helps in understanding the effect of nanoparticles in enhancing foam stability as introduced by Xue et al. [171]. The

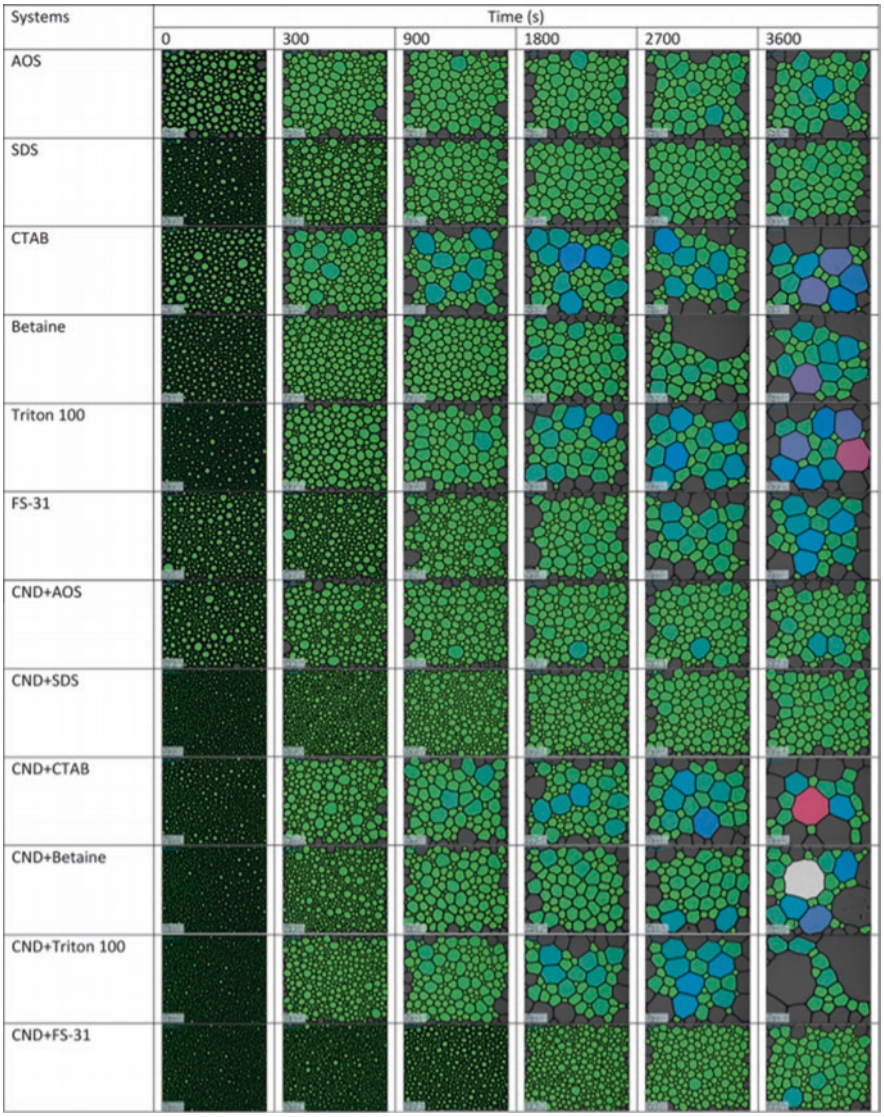

Fig. 8.10 Comparison between bubble sizes with time of foam stabilized by surfactants only and foam stabilized by surfactant-carbon nanodot (CND) [136]. Permissions related to the material excerpted were obtained from ACS, and further permission should be directed to ACS; Sakthivel, S., Adebayo, A., & Kanj, M. Y. (2019). Experimental Evaluation of Carbon Dots Stabilized Foam for Enhanced Oil Recovery. Energy & Fuels, 33(10), 9629–9643. doi: https://doi.org/10.1021/acs.energyfuels.9b02235

captured picture of foam morphology generated in a glass bead pack over time was used to calculate the Sauter mean diameter (D_{sm}) and the dimensionless polydispersity (U_{poly}) as expressed in Eqs. (8.9) and (8.10). A smaller change in foam Sauter

mean diameter over time indicates higher foam stability and delayed foam coarsening and coalescence. The insignificant change in the polydispersity indicates more uniformity in bubble shape over time [171, 175].

$$D_{sm} = \frac{\Sigma D_i^3}{\Sigma D_i^2} \tag{8.9}$$

$$U_{\text{poly}} = \frac{1}{D_{med}} \frac{\Sigma D_i^3 \left| D_{med} - D_i \right|}{\Sigma D_i^3} \tag{8.10}$$

where D_{sm} and U_{poly} are the Sauter mean diameter and the Polydispersity averaged over at least 100 bubbles. D_i and D_{med} are the diameter of a foam bubble and the median of the volume-averaged bubble diameter in the foam, respectively.

Vertical Foam Film Tests

In these tests, microscopes are used to observe the foam morphology to understand the effects of surfactants and/or nanoparticles on film thinning, film thickness, foam stability, and the location of adsorbed surfactants and/or nanoparticles. These tests show that nanoparticles can form three-dimensional networks enhancing the foam bubbles [146]. Figure 8.11 compares between a vertical foam film stabilized by surfactant only and a foam film stabilized by the surfactant-nanoparticle mixture. It shows that the surfactant-nanoparticle mixture delayed both the foam film thinning and rupturing. In Fig. 8.12b, when nanoparticles with fluorescence properties were used, nanoparticles were shown to be adsorbed at the interface and the Gibbs-Plateau border.

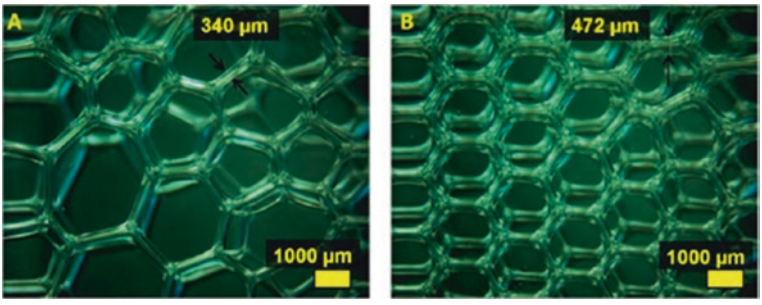

Fig. 8.11 Comparison between foam film morphologies and thicknesses of (**a**) foam stabilized by surfactant, (**b**) foam stabilized by surfactant and nanoparticles [146]. Permissions related to the material excerpted were obtained from ACS, and further permission should be directed to ACS; Singh, R., & Mohanty, K. K. (2015). Synergy between Nanoparticles and Surfactants in Stabilizing Foams for Oil Recovery. Energy & Fuels, 29(2), 467–479. doi: https://doi.org/10.1021/ef5015007

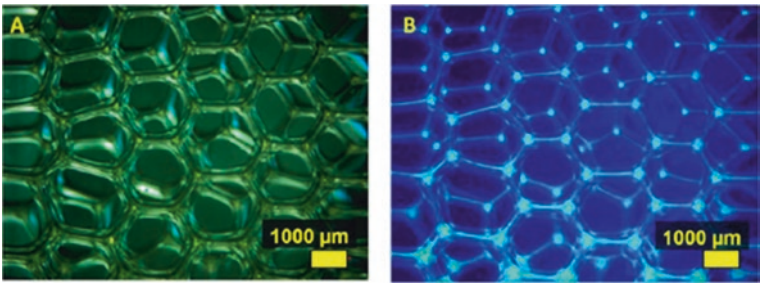

Fig. 8.12 Vertical foam film stabilized by surfactant-nanoparticle mixture captured at (**a**) visible light, (**b**) UV light [146]. Permissions related to the material excerpted were obtained from ACS, and further permission should be directed to ACS; Singh, R., & Mohanty, K. K. (2015). Synergy between Nanoparticles and Surfactants in Stabilizing Foams for Oil Recovery. Energy & Fuels, 29(2), 467–479. doi: https://doi.org/10.1021/ef5015007

8.4.2.2 Interfacial Tension and Dilatational Viscoelasticity Measurements

Interfacial tension and viscoelastic modulus are important parameters for the evaluation of foam generation and stability. In the absence of crude oil, surface tension controls the foam generation [7]. An increase in the viscoelastic modulus of foam films enhances foam stability against contraction and expansion [97]. Experiments of emulsions stabilized by surfactants and numerical simulations indicated that higher surface dilatational elasticity may decrease the Oswald ripening rates thus increasing foam stability [63, 113, 159]. In the presence of crude oil, interfacial tension properties between gas, water, and oil (σ_{wg}, σ_{wo}, σ_{og}) can be used to evaluate the effect of oil on foam stability, as will be discussed in the coming sections. The viscoelastic modulus (ε) in (mN/m) is expressed in Eq. (8.11) [97], where (γ) is the interfacial tension in (mN/m) and (A) is the surface area in (m^2).

$$\varepsilon = \frac{d\gamma}{d \ln A} \tag{8.11}$$

8.4.2.3 Application of Foam in the Porous Media Experiments

The effect of stabilized foam by surfactant-nanoparticle solution on enhancing oil recovery can be tested using porous media experiments. Micromodels, sand packs, and core flooding can be used for testing the foam apparent viscosity and its effect on oil recovery and mobility ratio enhancements. Micromodels can be used to study the pore scale effect of foam in EOR processes and its physical structure within the porous media at lower pressure experiments [118]. Core flooding experiments can mimic EOR processes under real reservoirs conditions. From differential pressure drop data in porous media experiments, apparent viscosity and mobility reduction factor can be calculated. An increase in pressure drop in foam flooding experiments

is related to the increase in gas apparent viscosity [111]. Apparent foam viscosity (μ_{app}) in a core flooding experiment is mathematically expressed in Eq. (8.12) [111].

$$\mu_{app} = \frac{k\Delta P}{u_t L} \tag{8.12}$$

where k is the core permeability, ΔP is the pressure difference, u_t is the total superficial velocity, and L is the core length.

Steady-state foam flow behavior can be classified into low-quality and high-quality foam regimes concerning the gas volumetric fraction in the total injected fluids or the foam quality (f_g) [30, 135]. Low-quality foam regime is characterized by a high superficial velocity of water (U_w) and low superficial velocity of gas (U_g) [22]. When the superficial velocity of gas (U_g) is high whereas the superficial velocity of water is low (U_w), foam flow regime is considered a high-quality foam regime [22]. These flow regimes can be clearly distinguished in the pressure gradient (ΔP) contours concerning superficial velocities of gas and water as illustrated in Fig. 8.13. The nearly vertical (ΔP) contours express the high-quality regime, while the nearly horizontal (ΔP) contours express the low-quality foam regime [22].

Higher apparent foam viscosity significantly attributes in higher foam strength [5]. Pressure gradient and apparent foam viscosity increase with the increase in the foam quality in the low-quality foam regime [37, 107]. Then, both the pressure gradient and the apparent foam viscosity decrease with the increase in the foam quality in the high-quality foam regime [37, 107]. Effect of increase in foam quality on the pressure and the apparent foam viscosity in foam displacement experiments in porous media is illustrated in Fig. 8.14.

The behavior of foam bubbles varies in the porous media in the different foam regimes. In the low-quality foam regime, foam bubbles are spaced and separated by thick liquid films [75, 107]. Hence, as the foam quality increases, apparent foam viscosity will also increase [37, 56, 135]. On the other hand, foam bubbles are packed and separated by individual liquid films in the high-quality foam regime [75, 107]. Moreover, as the foam quality increase in the high-quality foam regime, apparent foam viscosity will decrease as a result of an increase in the gas saturation and capillary pressure [61]. Hence, the foam will be unstable due to foam bubble coarsening [61]. Overall, in the high-quality foam regime, foam is stable when capillary pressure is lower than a limiting capillary pressure (P_c^*) [37]. Figure 8.15 expresses the concept of the limiting capillary pressure at which foam becomes unstable when foam quality is increased.

Injected foam in porous media can be either continuous or discontinuous gas foam as illustrated in Fig. 8.16. Gas bubbles in the discontinuous gas foam are separated by liquid lamellas, while gas channels are connected in the case of continuous gas foam [56, 107]. Accounting for this behavior is essential for understanding the foam mobility in porous media [5]. Discontinuous gas foam is capable of increasing apparent viscosity, while continuous gas foam can only reduce the gas relative

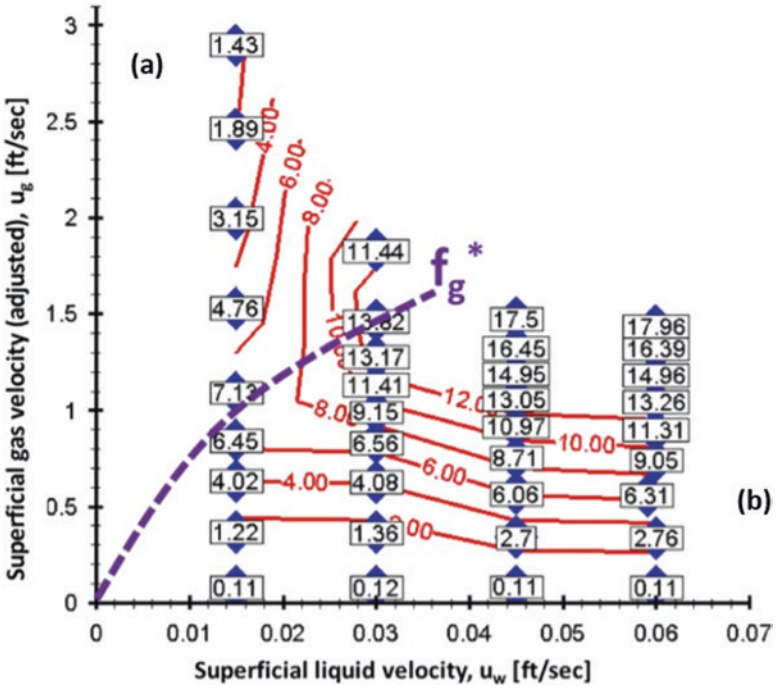

Fig. 8.13 Pressure gradient (psi/ft) contours as a function of gas and water superficial velocities of nitrogen gas foam in a horizontal pipe (0.5 wt% FA-406, 0.38/0.5 in ID/OD nylon pipe): (**a**) high-quality foam regime, (**b**) low-quality foam regime [62]. Permissions related to the material excerpted were obtained from Elsevier, and further permission should be directed to Elsevier; Gajbhiye, R. N., & Kam, S. I. (2011). Characterization of foam flow in horizontal pipes by using two-flow-regime concept. Chemical Engineering Science, 66(8), 1536–1549. doi: https://doi.org/10.1016/j.ces.2010.12.012

permeability [75, 107]. Hence, for the best mobility control foam, gas has to be discontinuous [5].

The ratio of total mobility of gas/brine to foam mobility is called the mobility reduction ratio (*MRF*). A higher reduction factor indicates higher foam stability [81]. It can be calculated from the ratio of pressure drop across the core during foam flooding (ΔP_f) to the pressure drop of the gas-only (ΔP_g). Equation (8.13) expresses the mobility reduction factor [81].

$$MRF = \frac{\left[\frac{kA\Delta P}{QL}\right]_f}{\left[\frac{kAvP}{QL}\right]_g} = \frac{\Delta P_f}{\Delta P_g} \tag{8.13}$$

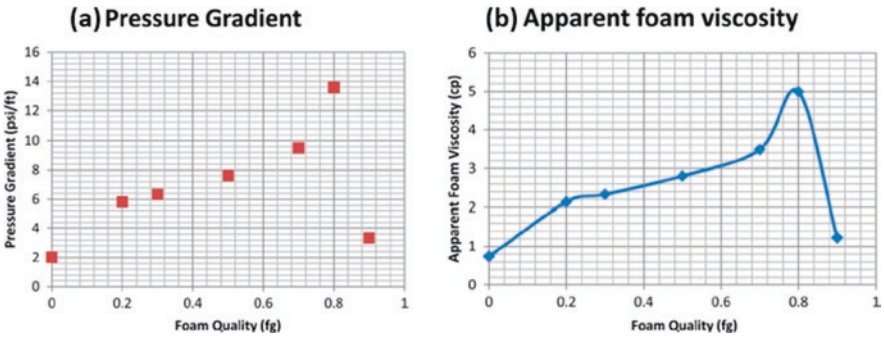

Fig. 8.14 Effect of increasing foam quality on (**a**) pressure gradient, (**b**) apparent foam viscosity. Carbonate core was used to construct these figures, while total injection rate was (0.05 ft^3/d) [5]. Permissions related to the material excerpted were obtained from ACS, and further permission should be directed to ACS; Al Sumaiti, A., Shaik, A. R., Mathew, E. S., & Al Ameri, W. (2017). Tuning Foam Parameters for Mobility Control using CO2 Foam: Field Application to Maximize Oil Recovery from a High Temperature High Salinity Layered Carbonate Reservoir. Energy & Fuels, 31(5), 4637–4654. doi: https://doi.org/10.1021/acs.energyfuels.6b02595

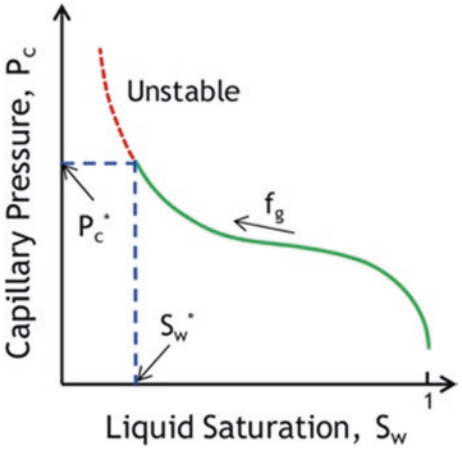

Fig. 8.15 Limiting capillary pressure concept for foam stability [61]. Permissions related to the material excerpted were obtained from ACS, and further permission should be directed to ACS; Farajzadeh, R., Lotfollahi, M., Eftekhari, A. A., Rossen, W. R., & Hirasaki, G. J. H. (2015). Effect of Permeability on Implicit-Texture Foam Model Parameters and the Limiting Capillary Pressure. Energy & Fuels, 29(5), 3011–3018

where k is the core permeability, A is the cross-sectional area of the core, ΔP is the pressure drop Q is the injection rate, and L is the core length. The subscripts f and g are for the foam and gas, respectively.

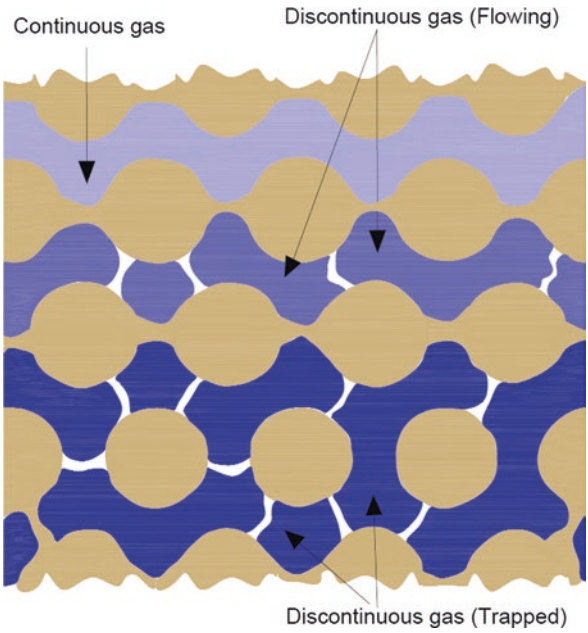

Fig. 8.16 Illustration of continuous and discontinuous gas (flowing and trapped) foams flow in porous media

8.5 Critical Parameters Influencing Foam Stability

In this section, the main crucial parameters influencing foam stability are discussed extensively.

8.5.1 Temperature

Generally, literature results suggest that increasing the temperature of a foam dispersion has a detrimental effect on foam stability. Static foam stability measurements indicate a decline in foam half-life time of liquid drainage as the temperature is increased [97, 163]. Moreover, the interfacial tension between gas and water increases, while dilatational viscoelasticity modulus decreases as a result of temperature elevation as depicted in Fig. 8.17 [97]. Consequently, both the foam stability and foam generation rate are declined with the increase in foam dispersion temperature [13, 97, 115, 156, 175, 177]. As a result, apparent foam viscosity can also decrease with the increase in temperature [8, 170].

The reduction of foam stability with the increase in temperature is attributed to several reasons. Increasing temperature cause ineffective adsorption of surfactant molecules and nanoparticles at foam lamellae as a result of thermal agitation and energetic movement of nanoparticles and surfactant molecules [97, 175, 177]. Increasing the temperature also contributes to decreasing the foam viscosity due to

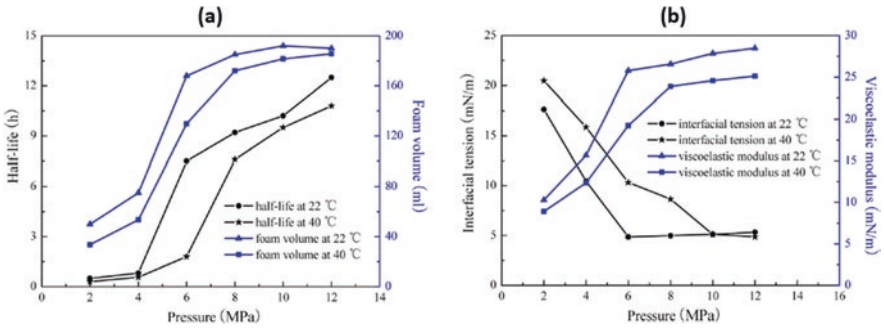

Fig. 8.17 Effect of increasing temperature from 22 to 40 °C and pressure from 2 to 12 MPa on CO_2 foam properties of SDS/SiO_2 dispersion: (**a**) foam volume and half-life time, (**b**) interfacial tension and viscoelastic modulus [97]. Permissions related to the material excerpted were obtained from ACS, and further permission should be directed to ACS; Li, S., Li, Z., & Wang, P. (2016). Experimental Study of the Stabilization of CO_2 Foam by Sodium Dodecyl Sulfate and Hydrophobic Nanoparticles. Industrial & Engineering Chemistry Research, 55(5), 1243–1253. doi: https://doi.org/10.1021/acs.iecr.5b04443

the escalation of both the gas diffusion and liquid drainage from the foam films [148, 172, 175]. Hence, the foam stability is crucially impacted as a result of foam film thinning and Ostwald ripening. Furthermore, an increase in water evaporation rate also contributes to foam film thinning [97, 175, 177].

8.5.2 Pressure

Increasing pressure can increase foam stability as suggested by Li et al. [97] In their study, CO_2 foam stability of SDS/SiO_2 dispersion was enhanced as indicated from half-life time, foam volume, surface tension, and viscoelastic measurements when pressure was increased from 2 to 12 MPa. Figure 8.17 indicates the increase in foam half-life time, volume, viscoelastic modulus, and the decrease in surface tension due to the increase in pressure. Moreover, generated CO_2 foam volume and density was increased gradually as pressure was raised as shown in Fig. 8.18. Li et al. [97] attributed the increase in foam volume and the enhancement of foam stability as pressure was increased due to the phase change of CO_2. The density of CO_2 increases dramatically from the gas phase to the supercritical phase. Hence, the fluid discharged from the CO_2 foam will be decreased as explained by Li et al. [97] which enhanced the foam stability in addition to resulting in desirable interfacial property behavior.

However, Emrani and Nasr-El-Din [53] reported the opposite effect of increasing pressure on CO_2 foam stability of AOS/SiO_2 at 75°F. It was claimed that the increase in CO_2 solubility with the increase in pressure decreased the foam half-life time leading to a faster liquid drainage rate as shown in Fig. 8.19. Finally, further research needs to be conducted to explain the causes of such completely different behavior of foam half-life time and volume when pressure is increased.

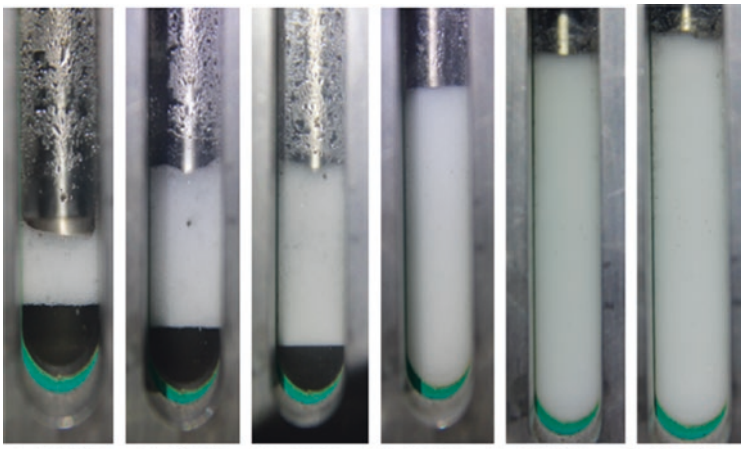

Fig. 8.18 Morphology of CO_2 foam of SDS/SiO_2 foam at pressure 2–12 MPa [97]. Permissions related to the material excerpted were obtained from ACS, and further permission should be directed to ACS; Li, S., Li, Z., & Wang, P. (2016). Experimental Study of the Stabilization of CO_2 Foam by Sodium Dodecyl Sulfate and Hydrophobic Nanoparticles. Industrial & Engineering Chemistry Research, 55(5), 1243–1253. doi: https://doi.org/10.1021/acs.iecr.5b04443

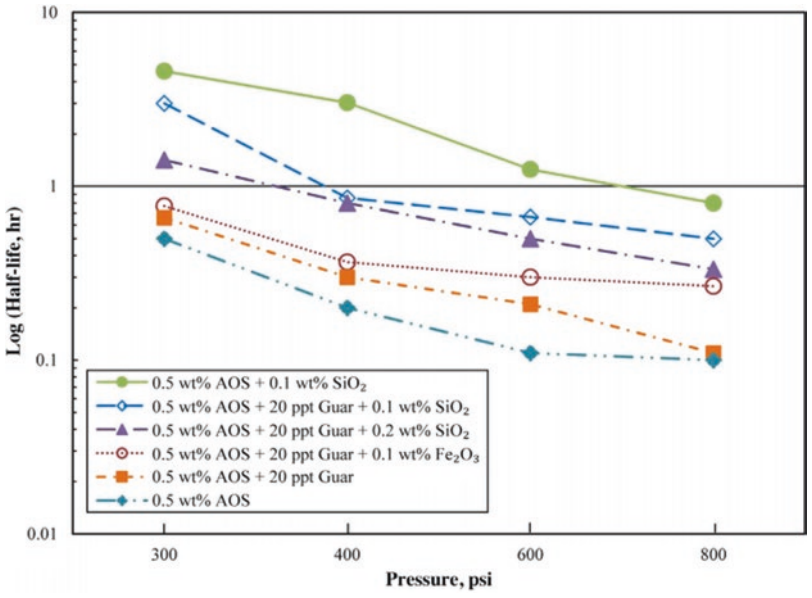

Fig. 8.19 Effect of pressure on CO_2 foam half-life time of AOS/SiO_2 at 25 °C while SiO_2 concentration was fixed at 0.1 wt.% [52]. Permissions related to the material excerpted were obtained from Elsevier, and further permission should be directed to Elsevier; Emrani, A. S., & Nasr-El-Din, H. A. (2017a). An experimental study of nanoparticle-polymer-stabilized CO_2 foam. Colloids and Surfaces A: Physicochemical and Engineering Aspects, 524, 17–27. doi: https://doi.org/10.1016/j.colsurfa.2017.04.023

8.5.3 *Salinity*

The presence of electrolytes is a crucial parameter influencing both the stability of surfactant molecules and nanoparticles in a foam dispersion. The stability of a surfactant-stabilized foam depends on both the concentration and the type of cation salts whether it is a monovalent, divalent, or multivalent. Kumar and Mandal [93] studied the effect of NaCl concentration on foam height for several surfactants including SDS, CTAB, and Tween 80. Their results indicated a relative increase in foam height after 50 min as salt concentration was less than 1 wt.% NaCl. However, as salinity was increased above 1 wt.% NaCl, foam height after 50 min declined. Figure 8.20 summarizes the effect of NaCl salinity on foam height after 50 min, while concentrations of SDS, CTAB, and Tween 80 were at the critical micelle concentration. Impact of salinity on a surfactant-stabilized foam increases due to the presence of divalent or multivalent ions. This is mainly due to the high tendency of surfactants to influentially react with existing cations such as Ca^{2+} and Mg^{2+} in formation brines which results in surfactant precipitation [162, 175].

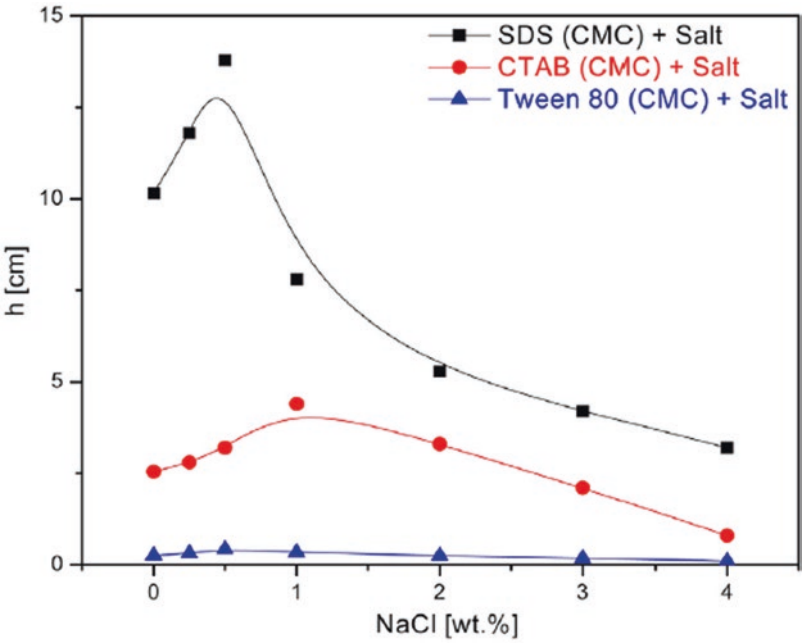

Fig. 8.20 Effect of salt concentration on foam height after 50 min in the presence of different surfactants [93]. Permissions related to the material excerpted were obtained from Elsevier, and further permission should be directed to Elsevier; Kumar, S., & Mandal, A. (2017). Investigation on stabilization of CO_2 foam by ionic and nonionic surfactants in presence of different additives for application in enhanced oil recovery. Applied Surface Science, 420, 9–20. doi: https://doi.org/10.1016/j.apsusc.2017.05.126

Derjaguin-Landau-Verwey-Overbeek (DLVO) theory suggests that the stability of a nanoparticle-stabilized foam is controlled by the sum of the repulsive electrostatic forces and the Van der Waals forces [173, 175]. The Van der Waals attraction forces become greater than the electrostatic repulsion forces as a result of the increase in solution salinity [21, 172]. This can be indicated from the low zeta potential measurements [44, 91]. Hence, the presence of a high concentration of monovalent and divalent ions can cause nanoparticle aggregation resulting in either stabilizing or destabilizing foam depending on the location of agglomeration (liquid phase, continuous liquid phase, or at the gas/liquid interface) [175].

According to Yekeen et al. [175], moderate aggregation of nanoparticles due to the presence of electrolytes at the gas/liquid interface can enhance foam stability. On the other hand, excessive particle accumulation at the interface or in the liquid phase can prevent the migration of nanoparticles to the gas/liquid interface which will eventually destabilize the foam.

8.5.4 Zeta Potential and pH

Zeta potential measures the magnitude of electrostatic repulsion/attraction between suspended particles and is considered a major property in evaluating the stability of colloidal dispersions and emulsions [117]. More stable emulsions possess higher magnitudes of electrostatic forces and consequently higher zeta potential measurements [117]. The major property affecting the zeta potential of a colloidal dispersion is the pH. Adding an acid to an emulsion reduces the magnitude of zeta potential, while adding an alkali increases the magnitude of the zeta potential [17].

In acidic environments, protonation of surfactants occurs, resulting in a reduction in the molecules' surface-active properties. As a result, surfactant aggregation can occur. Hence, it is more favored to keep an emulsion in the alkali environment for more stability [34].

Singh, Panthi, Weerasooriya, and Mohanty [150] evaluated the effect of pH alternation on the foam stability of tristyrylphenol propoxy carboxylate (TSP-PO45-COOH). This is an anionic surfactant which contains a carboxyl group which is a pH-sensitive unit as shown in Fig. 8.21. This surfactant dispersion was able to produce a fine bubble texture (bubble size <200 μm) in the alkali pH range. However, decreasing the pH by either adding acid or CO_2 injection resulted in foam destabilization behavior. Singh et al. [150] explained that the protonation of the carboxyl unit is responsible for foam destabilization. Moreover, the acidic pH causes a cloudy/unclear surfactant solution due to aggregation as reported from DLS and TEM test as shown in Fig. 8.22. Figure 8.23 shows the foam behavior due to pH alternation.

Recently, several surfactants were reported to generate stable foams in acidic environments including switchable amine surfactants. Switchable amine surfactants such as Ethomeen C/12, Duomeen TTM, and Duomeen CTM perform as nonionic surfactants in neutral pH and convert to cationic surfactants at low pH due to

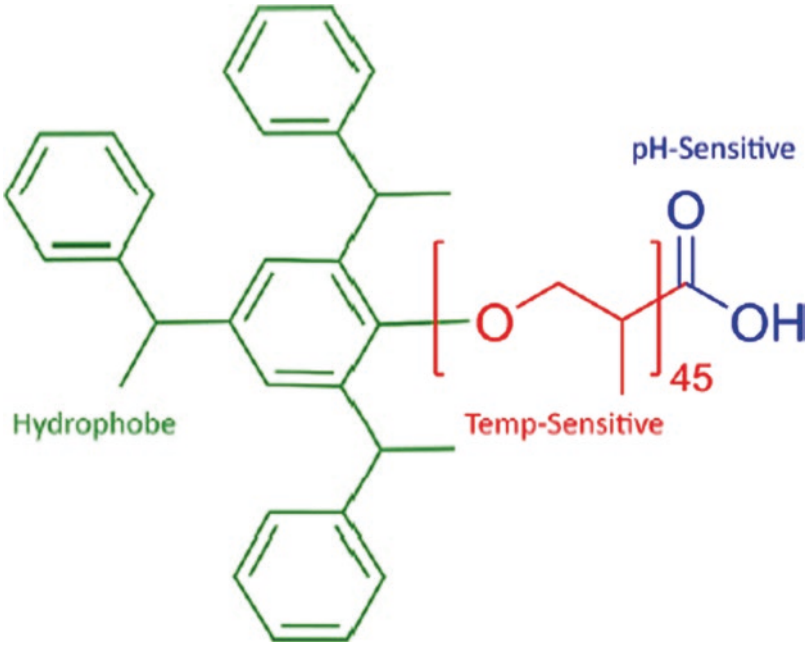

Fig. 8.21 Structure of TSP-PO45-COOH [150]. Permissions related to the material excerpted were obtained from ACS, and further permission should be directed to ACS; Singh, R., Panthi, K., Weerasooriya, U., & Mohanty, K. K. (2018). Multistimuli-Responsive Foams Using an Anionic Surfactant. Langmuir, 34(37), 11010–11020. doi: https://doi.org/10.1021/acs.langmuir.8b01796

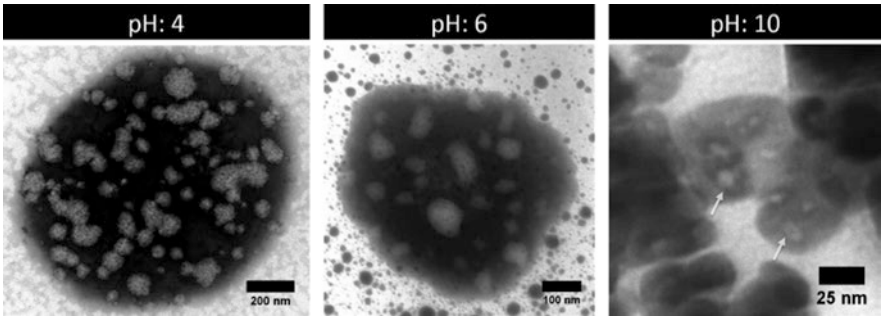

Fig. 8.22 TEM pictures showing the effect of pH alternation on growing aggregates of TSP-PO45-COOH surfactant [150]. Permissions related to the material excerpted were obtained from ACS, and further permission should be directed to ACS; Singh, R., Panthi, K., Weerasooriya, U., & Mohanty, K. K. (2018). Multistimuli-Responsive Foams Using an Anionic Surfactant. Langmuir, 34(37), 11010–11020. doi: https://doi.org/10.1021/acs.langmuir.8b01796

Fig. 8.23 Effect of pH alternation on foam stability of TSP-PO45-COOH surfactant [150]. Permissions related to the material excerpted were obtained from ACS, and further permission should be directed to ACS; Singh, R., Panthi, K., Weerasooriya, U., & Mohanty, K. K. (2018). Multistimuli-Responsive Foams Using an Anionic Surfactant. Langmuir, 34(37), 11010–11020. doi: https://doi.org/10.1021/acs.langmuir.8b01796

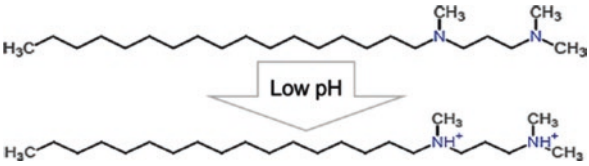

Fig. 8.24 Schematic of protonation of a switchable surfactant from the nonionic to the cationic form due to protonation at low pH conditions [38]. Permissions related to the material excerpted were obtained from ACS, and further permission should be directed to ACS; Rattanaudom, P., Shiau, B.-J., Suriyapraphadilok, U., & Charoensaeng, A. (2021). Effect of pH on silica nanoparticle-stabilized foam for enhanced oil recovery using carboxylate-based extended surfactants. Journal of Petroleum Science and Engineering, 196, 107729. doi: https://doi.org/10.1016/j.petrol.2020.107729

protonation as shown in Fig. 8.24 [32, 33, 50]. These surfactants are capable of producing stable CO_2 at pH between 4 and 6 [31].

Generally, stable nanoparticle dispersion at a specific pH range can enhance surfactant foam stability. Rattanaudom, Shiau, Suriyapraphadilok, and Charoensaeng [128] compared the effect of pH alternation on the N_2 foam stability of an anionic carboxylate extended surfactant with the effect of the addition of partially hydrophobic silica nanoparticles to the surfactant solution. Their results indicated that the presence of nanoparticles increased the foam half-life time when pH was increased from 3 to11 as displayed in Fig. 8.25. Figure 8.26 shows the zeta potential of the surfactant dispersion at 0.5 wt.% concentration and the 0.5 wt% surfactant dispersion with 100 ppm hydrophobic silica nanoparticles.

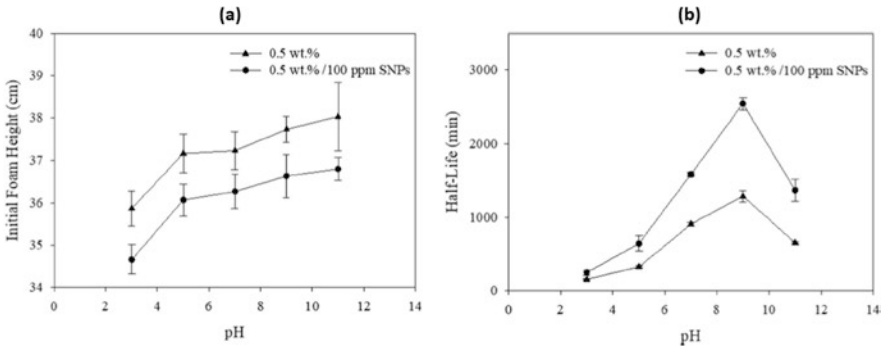

Fig. 8.25 Comparison between the effect of pH alternation on foam stability of carboxylate surfactant at 0.5 wt.% with the addition of hydrophobic silica nanoparticles at 100 ppm concentration: (**a**) foam initial height, (**b**) foam half-life time [128]. Permissions related to the material excerpted were obtained from Elsevier, and further permission should be directed to Elsevier; Rattanaudom, P., Shiau, B.-J., Suriyapraphadilok, U., & Charoensaeng, A. (2021). Effect of pH on silica nanoparticle-stabilized foam for enhanced oil recovery using carboxylate-based extended surfactants. Journal of Petroleum Science and Engineering, 196, 107729. doi: https://doi.org/10.1016/j.petrol.2020.107729

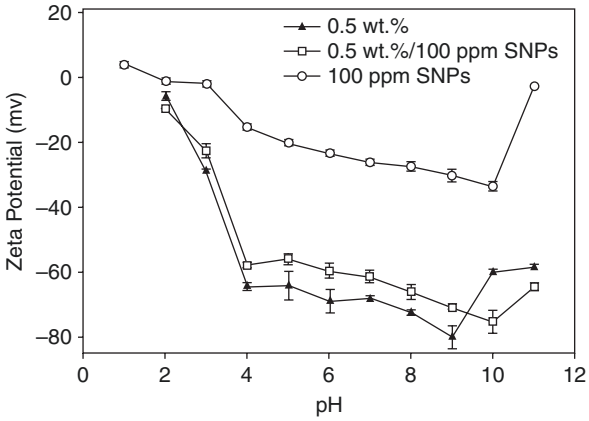

Fig. 8.26 Zeta potential of 0.5 wt.% surfactant solution, 0.5 wt.% surfactant, and 100 ppm silica solution and nanoparticle dispersion at 100 ppm concentration [128]. Permissions related to the material excerpted were obtained from Elsevier, and further permission should be directed to Elsevier; Rattanaudom, P., Shiau, B.-J., Suriyapraphadilok, U., & Charoensaeng, A. (2021). Effect of pH on silica nanoparticle-stabilized foam for enhanced oil recovery using carboxylate-based extended surfactants. Journal of Petroleum Science and Engineering, 196, 107729. doi: https://doi.org/10.1016/j.petrol.2020.107729

8.5.5 Gas Type

Foam performance and properties crucially depend on the gas types used for foam generation. The main gases utilized in gas EOR include methane, carbon dioxide, nitrogen, and air. In foam stability studies, carbon dioxide, nitrogen, and air received the most attention since they are nontoxic, nonflammable, and cost-effective [175].

Compared to CO_2, N_2 and air can form a stable foam in both ambient and reservoir conditions. Aarra, Skauge, Solbakken, and Ormehaug [2] evaluated the properties of N_2 and CO_2/AOS surfactant foams due to pressure variation (30–280 bar) while temperature and gas quality were fixed at 50 °C and 80%, respectively. Core flooding experiments in a Berea sandstone core indicated that N_2 was able to form a stable foam at both low and high pressures. However, the pressure drop in the CO_2 foam core flooding was significantly decreased as pressure was increased from 30 to 280 bar. Figure 8.27 compares the differential pressure of N_2 and CO_2 foams core flooding experiments at both low and high pressures.

The change in CO_2 foam properties between ambient and reservoir conditions is attributed to the phase change of CO_2 from the subcritical to the supercritical state. Moreover, the high solubility of CO_2 in water increases gas diffusion between foam bubbles resulting in both lamella rapturing and film thinning [68, 175]. Due to the high solubility of CO_2, less gas volume generates foam compared to less soluble gases such as N_2 [1, 174]. Furthermore, dissolved CO_2 gas in water produces carboxylic acid which also influences foam stability and film thickness via screening of the Van der Waals and electrostatic forces [11, 59].

Despite the physical change of CO_2 at high pressure and temperature conditions, several surfactants and nanoparticles were reported to be capable of generating stable supercritical CO_2 foams. Mainly, switchable amine surfactants [5, 38], the

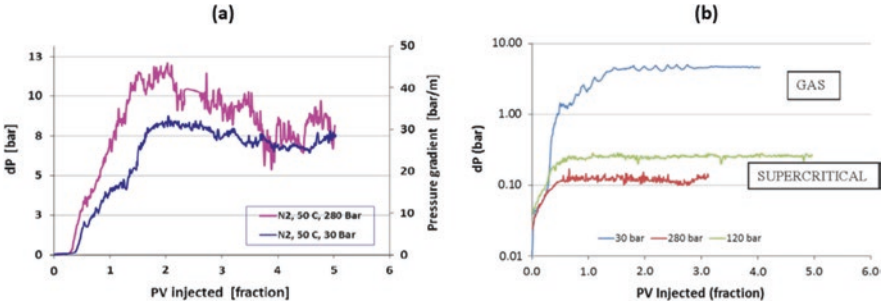

Fig. 8.27 Pressure gradient of foam core flooding experiments at both low and high pressure conditions of (**a**) N_2, (**b**) CO_2 while temperature and gas quality were 50 °C and 80%, respectively [2]. Permissions related to the material excerpted were obtained from Elsevier, and further permission should be directed to Elsevier; Aarra, M. G., Skauge, A., Solbakken, J., & Ormehaug, P. A. (2014). Properties of N2- and CO_2-foams as a function of pressure. Journal of Petroleum Science and Engineering, 116, 72–80. doi: https://doi.org/10.1016/j.petrol.2014.02.017

zwitterionic surfactant LDMAA [170], and the anionic surfactant AMPHOAM [170] can produce supercritical CO_2 foams at elevated pressure and temperature conditions. Organic ligand-graphed silica nanoparticles also showed the ability to stabilize supercritical CO_2 foams [8]. These surfactants and nanoparticles will be explained in further detail in the following sections.

8.5.6 Crude Oil

Crude oil is composed of complex mixtures of hydrocarbon and nonhydrocarbon components. Main hydrocarbon components include paraffin, aromatics, and naphthenes, while nonhydrocarbons contain sulfur, nitrogen, and oxygen compounds [112]. The variety of oil composition can significantly influence both the physical and chemical properties of any petroleum fluid [119, 160]. Hence, crude oil properties are significant in evaluating foam stability whether it will not destabilize the foam or only spread on liquid films or even enter the foam lamellas [111]. The main concepts discussed in the literature for evaluating the effect of crude oil on foam stability include the spreading and entering coefficients, lamella number, bridging coefficient, and the pseudo-emulsion film theory [160].

8.5.6.1 The Spreading and Entering Coefficients

To explain foam stability qualitatively in the presence of crude oil, the following coefficients can be used: spreading (S) and entering (E) coefficients as expressed in Eqs. (8.14) and (8.15). Negative values of the entering (E) and spreading coefficients (S) indicate that the oil does not affect foam stability. On the other hand, a positive value of S indicates that oil will spread on the foam films causing film rupture as depicted in Fig. 8.28 [160].

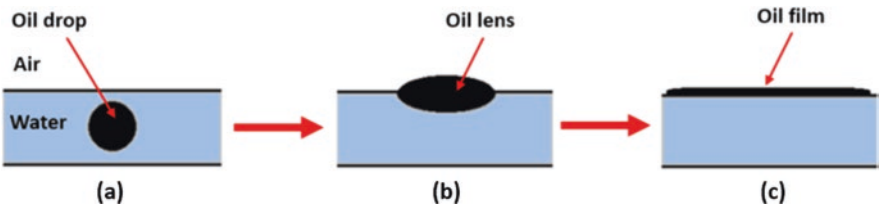

Fig. 8.28 Illustration of: (**a**) oil drop within the solution, (**b**) non-spreading oil system ($S < 0$), and (**c**) spreading system ($S > 0$) [103]. Permissions related to the material excerpted were obtained from ACS, and further permission should be directed to ACS; Lobo, L., & Wasan, D. T. (1993). Mechanisms of aqueous foam stability in the presence of emulsified nonaqueous-phase liquids: structure and stability of the pseudoemulsion film. Langmuir, 9(7), 1668–1677. doi: https://doi.org/10.1021/la00031a012

$$S = \sigma_{wg} - \sigma_{wo} - \sigma_{og} \tag{8.14}$$

$$E = \sigma_{wg} + \sigma_{wo} - \sigma_{og} \tag{8.15}$$

where σ_{wg}, σ_{wo}, and σ_{og} are the gas and water interfacial tensions with oil.

8.5.6.2 The Bridging Coefficient

When the value of the bridging coefficient (B) as expressed in Eq. (8.16) is positive, the presence of crude oil will destabilize the foam films regardless of the sign of the spreading coefficient (S). Figure 8.29 illustrates the bridging effect of oil in a foam liquid film ($B > 0$) [7, 41, 70, 111, 131, 160].

$$B = \sigma_{wg}^2 + \sigma_{wo}^2 - \sigma_{og}^2 \tag{8.16}$$

where σ_{wg}, σ_{wo}, and σ_{og} are the gas and water interfacial tensions with oil.

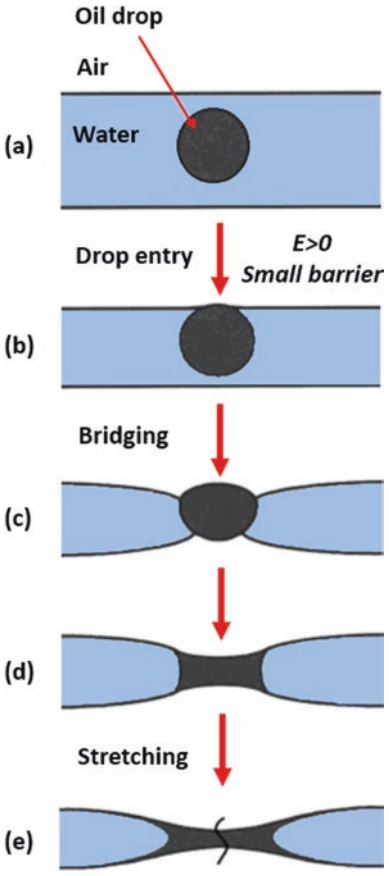

Fig. 8.29 Illustration of oil bridging-stretching mechanism of foam film destruction: (**a**–**c**) formation of an oil bridge, (**c**–**e**) stretching of an oil bridge due to uncompensated capillary pressures at the oil-water and oil-air interfaces, and (**e**) oil bridge rupture at the its thinnest central region [43]. Permissions related to the material excerpted were obtained from ACS, and further permission should be directed to ACS; Denkov, N. D., Cooper, P., & Martin, J.-Y. (1999). Mechanisms of Action of Mixed Solid–Liquid Antifoams. 1. Dynamics of Foam Film Rupture. Langmuir, 15(24), 8514–8529. doi: https://doi.org/10.1021/la9902136

8.5.6.3 Lamella Number

Lamella number (L) as expressed in Eq. (8.17) represents the tendency of oil to become emulsified and imbibed into foam films. When lamella number is less than 1, spreading and entering coefficients are negative which results in a more stable foam. When lamella number is between 1 and 7, the oil will moderately destabilize the foam which results in a negative spreading and positive entering coefficients. Finally, when the lamella number is greater than 7, the oil will destabilize the foam, and both S and E will be positive. Figure 8.30 illustrates the effect of oil on the stability of three types of foam (A, B, C) and the variations of the foam lamella number [138, 139, 160]

$$L = \frac{0.15\sigma_{wg}}{\sigma_{wo}} \tag{8.17}$$

where σ_{wg} and σ_{wo} are the water/gas and the water/oil interfacial tensions, respectively.

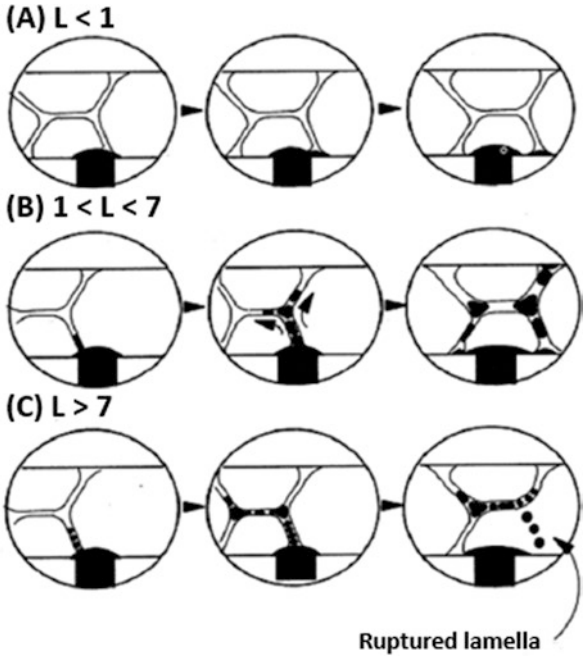

Fig. 8.30 Comparison between foam stability in contact with oil of: (**a**) foam type A ($L < 1$), (**b**) foam type B ($1 < L < 7$), and (**c**) foam type C ($L > 7$) [138]. [2]. Permissions related to the material excerpted were obtained from Elsevier, and further permission should be directed to Elsevier; Schramm, L. L., & Novosad, J. J. (1990). Micro-visualization of foam interactions with a crude oil. Colloids and Surfaces, 46(1), 21–43. doi: https://doi.org/10.1016/0166-6622(90)80046-7

8.5.6.4 Pseudo-Emulsion Film

Foam stability in presence of oil is significantly related to the stability of pseudo-emulsion films [90, 109, 127, 164]. A pseudo-emulsion film is defined as the thin liquid film existing between an oil droplet and the gas phase [160]. The oil will remain in the liquid lamella if the pseudo-emulsion film is stable, whereas oil may form a lens at the gas/water interface if the pseudo-emulsion film is ruptured. Hence, foam can break down [160]. Figure 8.31 expresses the possible configurations of the oil depending on the pseudo-emulsion film stability.

8.5.7 Surfactants

Foaming agents or surfactants are required for foam generation. Surfactant molecules stabilize liquid films via adsorption at the water/gas interface. Hence, the water molecules at the interface are replaced by a layer of surfactant molecules with a lower energy level [120, 166]. The selection of the appropriate surfactants for any EOR project is a challenging task. Surfactant concentration, hydrophilic-lipophilic balance (HLB), gas type, temperature, pH, and salinity are crucial factors impacting the effectiveness of foam stabilization by surfactants. The main surfactants reported in the literature for possessing foamability and foam stabilization properties for EOR applications are summarized in Table 8.1.

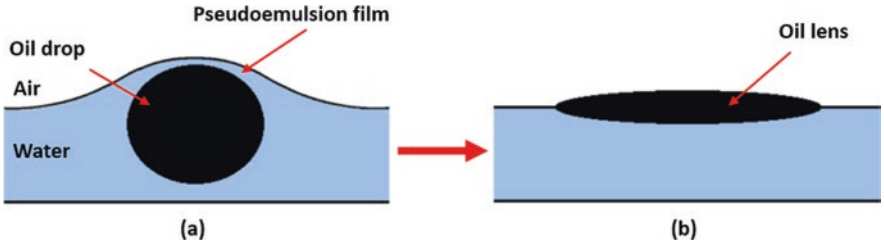

Fig. 8.31 (**a**) Stable pseudo-emulsion film, and (**b**) unstable pseudo-emulsion film [103]. Permissions related to the material excerpted were obtained from ACS, and further permission should be directed to ACS; Lobo, L., & Wasan, D. T. (1993). Mechanisms of aqueous foam stability in the presence of emulsified nonaqueous-phase liquids: structure and stability of the pseudo-emulsion film. Langmuir, 9(7), 1668–1677. doi: https://doi.org/10.1021/la00031a012

Table 8.1 Main surfactants tested for foam stabilization

Surfactant type	Short name	Chemical name	Reference
Anionic	APS	Alcohol propoxy sulfate	[117]
	AOS	Alpha olefin sulfonate	[117]
	SDS	Sodium dodecyl sulfate	[9]
	AMPHOAM	–	[170]
	AES	Sodium fatty alcohol polyoxyethylene ether sulfate	[123]
	FRC-1	–	[104]
	ENORDET A031	–	[6]
Cationic	CTAB	Dodecyl trimethyl ammonium bromide	[27]
	Ethomeen C/12	Bis(2-hydroxyethyl cocoalkylamine)	[38]
	Duomeen TTM	*N*,*N*,*N*′ -trimethyl-*N*′ -tallow-1,3-diaminopropane	[38]
	Duomeen CTM	*N*,*N*,*N*′ -trimethyl-*N*′ -coco-1,3-diaminopropane	[38]
Zwitterionic	FS	Perfluoroalkyl betaine surfactant	[9]
	LDMAA	Lauryldimethylammonio acetate	[170]
	LAPB	Lauramidopropyl betaine	[66]
	OA-12	$C_{14}H_{31}NO$	[163]
Nonionic	C_{12}DMPO	Dodecyl dimethyl phosphine oxide	[27]
	FC	Fluorochemical	[9]
	β-$C_{12}G_2$	*n*-dodecyl-β-D-maltoside	[23]
	Triton CG-110	Alkyl polyglucoside	[147]
	Tween 80	Polysorbate 80	[93]
	TX-100	$C_{34}H_{62}O_{11}$	[163]
	$C_{12}E_{23}$	Lauryl alcohol polyoxyethylene ether	[99]

8.5.8 Nanoparticles

Extensive foam stability studies suggest that nanoparticles may be a promising technique for enhancing both the static and dynamic foam stability. Insofar, it was proved that nanoparticles are capable of increasing foam half-life time, delay the foam bubble coalescence and coarsening rates, and maintain small bubble sizes with time. Moreover, they significantly increase the viscoelastic modulus of liquid while decreasing the gas/water surface tension. Foam displacement experiments indicated that nanoparticles could play a significant role in maintaining higher foam apparent viscosities. Hence, they contribute to better foam stability. Nanoparticle type, surface wettability, size, and concentration are the main crucial factors influencing the effectiveness of nanoparticles in enhancing foam stability.

8.5.8.1 Nanoparticle Type

Several nanoparticle types have been investigated for foam stabilization including silica nanoparticles, metal oxides, graphene oxides, and ash materials. Silica nanoparticles are the most common type of nanoparticles applied in foam stability studies [175]. Bayat et al. [16] studied the effect of nanoparticle type on the stability of CO_2 foam. Evaluated nanoparticles were silica (SiO_2), hydrophilic metal oxide including aluminum oxide (Al_2O_3), titanium dioxide (TiO_2), and copper oxide (CuO) at an optimum concentration of 0.008 wt.%. Static and dynamic foam stability experiments indicated that SiO_2 and Al_2O_3 were the best nanoparticles types for stabilizing CO_2 foam. The foam half-life times of SiO_2, Al_2O_3, TiO_2, and CuO were 28.1, 24.6, 20.1, and 17.9 min, respectively. Finally, total oil recoveries by foam displacement in sand packs achieved by SiO_2, Al_2O_3, TiO_2, and CuO were 71.7%, 65.7%, 58.2%, and 57.3%, respectively.

Several researchers evaluated the potential of fly ash, particulate matter (PM), and graphene oxides as a CO_2 foam stabilizer [48, 67, 95, 106, 149]. Fly ash or PM is a waste material produced from coal power generation plants [106, 149]. Although fly ash materials are cheap and can be used as CO_2 foam stabilizers, the grain sizes are too large for injection in the reservoirs [149]. To minimize the sizes of fly ash materials, high-frequency ultrasonic grinding (ball milling process) was used [48, 149, 175]. However, producing nanoparticles from fly ash material requires several steps of dilution which makes the quantification of the concentration of the produced nanoparticles very challenging [48, 67]. Similarly, particle growth of graphene oxides causes it to be unsuitable for implementation in reservoirs [14]. Literature results suggest that nanoparticles can improve the stability of foam without the respect of the nanoparticle types [175], especially if it poses the optimum surface wettability, size, and concentration, as explained in the next section.

8.5.8.2 Nanoparticle Surface Wettability

Surface wettability of nanoparticles plays a significant role in foam generation by nanoparticles and provides an essential indication of the particle surface activity [175]. Literature results demonstrated that the hydrophilic-lipophilic balance (HLB) and the hydrophilic-CO_2-philic balance (HCB) contributes to the surface wettability of nanoparticles [175]. Hence, the correct choice of HCB is crucial for the generation of nanoparticle-stabilized CO_2 foams [168].

The wettability of nanoparticles can usually be indicated via the measurement of the contact angle at the gas/liquid interface [36]. The ideal contact angle reported in the literature for foam stabilization by nanoparticles is within the range of 40–70° [77, 85, 97, 125, 146, 156], According to other researchers, the contact angle is preferred to be in the range of 60–90° [98]. As the nanoparticles possess the optimum contact angle, it will be adsorbed efficiently and irreversible at the gas/water interface due to the highly associated particles' detachment energy [19, 74, 167].

Table 8.2 Selected nanoparticles surface modification from the literature

Nanoparticle type	Surface modification/surfactant/polymer	Hydrophilicity/contact angle	Reference
Silica (SiO_2)	Polyethene glycol (PEG)	Hydrophilic	[55]
	Methylsilylmodifed (Siu)	Partially hydrophobic	[168]
	Methyl coated with dichloro dimethyl silane	30°	[118]
	PEG, physical mixing with AOS	Hydrophilic	[146]
	Surface modified, physical mixing with SDS	Partially hydrophobic/122.22°	[97]
	Alumina-coated, surface modifier, physical mixing with AOS	Hydrophilic	[147]
	Surface modified, physical mixing with CTAB	Hydrophilic/38.63°	[98]
	Physical mixing with viscoelastic surfactant (VES) and AOS		[81]
	Physical mixing with TX-100, SDBS, CTAB, or OA-12 surfactants	Hydrophilic	[163]
	Saline modified, physical mixing with linear alcohol ethoxylate (C12-C16) surfactant	Less hydrophilic	[133]
	Physical mixing with polymer (PAM)	Hydrophilic	[126]
	Coated with dimethylsiloxane, physical mixing with FRC1 anionic surfactant	Hydrophobic	[104]
	Physical mixing with lauryl alcohol polyoxyethylene ether ($C_{12}E_{23}$) nonionic surfactant	Hydrophilic	[99]
	Surface modified by silane KH560, physical mixing with ethoxylated amine surfactant	Hydrophilic	[181]
Fly ash	Physical mixing with AOS	Hydrophilic	[48]
Iron oxide (Fe_3O_4)	Physical mixing with AOS	Hydrophilic	[51]
	Surface modification by 4-methyl-2-pentanone, physical mixing with SDS and HPAM	Contact angles (12.7°, 20.6°, 57.5°, and 97.3°)	[102]

On the other hand, at contact angles, less than 30° or higher than 150°, particles' detachment energy will be reduced [175].

According to Yekeen et al. [175], several techniques can be used to modify the surface wettability of nanoparticles for foam stabilization. Firstly, the extent of salinization can be altered by dichloro dimethyl silane. Secondly, surface-active agents (surfactants or polymers) can be coated on the surface of the nanoparticles. Thirdly, surface modification of the nanoparticles can be achieved by in situ hydrophilization of the nanoparticles or mixing it with surfactants. Table 8.2 summarizes the main approaches of nanoparticle surface modification illustrated in the literature.

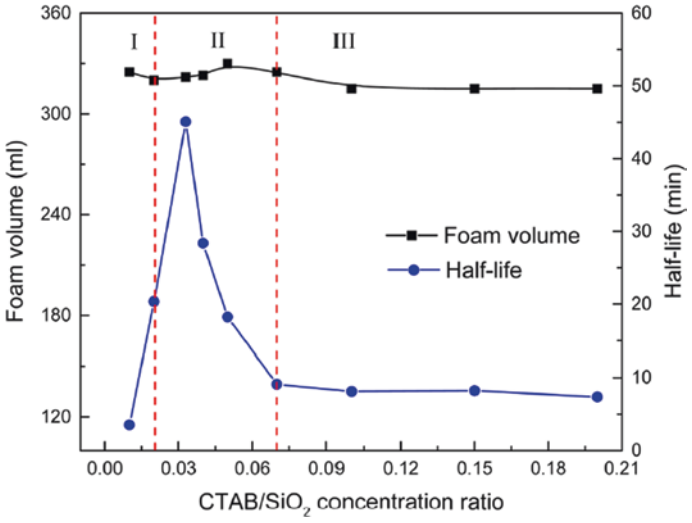

Fig. 8.32 Effect of CTAB/hydrophilic silica nanoparticle concentration ratio on CO_2 foam stability [98]. Permissions related to the material excerpted were obtained from ACS, and further permission should be directed to ACS; Li, S., Qiao, C., Li, Z., & Wanambwa, S. (2017). Properties of Carbon Dioxide Foam Stabilized by Hydrophilic Nanoparticles and Hexadecyltrimethylammonium Bromide. Energy & Fuels, 31(2), 1478–1488. doi: https://doi.org/10.1021/acs.energyfuels.6b03130

8.5.8.3 Effect of Nanoparticles Size

The performance of nanoparticles in foam stabilization is crucially impacted by the size of nanoparticles [85]. Generally, foam stability decreases as the size of the nanoparticles increases, and smaller nanoparticles generate more stable foams [175]. Tang, Xiao, Tang, and Jiang [158] studied the effect of silica nanoparticle size variation (sizes in the range of 20–700 nm) on the stability of SDS air foams. Their results indicated that smaller size nanoparticles are better for foam stabilization. Moreover, foam apparent viscosity also increases with decreasing the size of nanoparticles [89]. Figure 8.32 compares the apparent viscosity of CO_2 foam stabilized by varied sizes of silica nanoparticles (12–80 nm).

Smaller sizes of nanoparticles attribute to better foam stability for several factors. Mainly, smaller nanoparticles can migrate faster than bigger nanoparticles to the gas/water interface [40]. Hence, the adsorption and concentration of nanoparticles at the gas/water interface will increase providing more liquid film stability [89, 175]. Moreover, the attachment energy of nanoparticles at the gas/water interface is increasing with the increase in particle size [154, 172].

8.5.8.4 Effect of Nanoparticle Concentration

Literature results indicated that nanoparticle concentration is crucial for the evaluation of foam stability. At low nanoparticle concentration, the number of nanoparticles adsorbed at the water/gas interface could be not sufficient for enhancing the stability of the liquid film [175]. Kim, Taghavy, DiCarlo, and Huh [88] demonstrated that beyond a threshold of nanoparticle concentration, adsorbed nanoparticles at the gas/water interface become sufficient for enhancing the stability of the liquid. As the nanoparticle concentration in the solution increases, more nanoparticles will be adsorbed at the gas/water interface contributing to enhancing the liquid film elastic properties and slowing down both the liquid drainage and film thinning processes [175]. However, beyond the optimum nanoparticle concentration, aggregation of nanoparticles can impact the foam stability negatively [86]. According to Z. Li et al. [96], nanoparticle aggregation results in particles exerting gravity force exceeding the foam bubble anti-deformation capacity. Consequently, film thinning rate increases as a result of liquid discharge under the gravity effect of the aggregated nanoparticles [175]. The synergistic effect between nanoparticles and surfactants enhances the foam stabilization process. However, optimum nanoparticle concentration will be significantly impacted by the type of surfactant utilized, its chain length, and concentration [175]. Investigated synergy effect between silica nanoparticles and surfactants for CO_2 foam stabilization demonstrated that foam half-life time increases as the surfactant-nanoparticle concentration is increased until it reaches an optimum concentration ratio [97, 98]. However, beyond this optimum concentration ratio, the foam will be destabilized, as shown in Fig. 8.32.

S. Li et al. [98] explained that increasing the concentration ratio between CTAB and the hydrophilic silica nanoparticles (original contact angle with water is 38.63°) between 0.02 and 0.07 achieved the most stable foam (7 times the stability of CTAB alone) as shown in region (II) in Fig. 8.32. However, there was no obvious synergistic effect due to further increase in the CTAB/SiO_2 concentration ratio (region III), which results in lower foam stability compared to the region (II).

8.6 Various Studies Conducted on Foam Stability Using Nanoparticles

Foam studies can be conducted by using nitrogen, methane, and carbon dioxide. Literature results are expressed based on different gas types used for foam generation.

8.6.1 Nitrogen

Singh and Mohanty [145] evaluated the effect of alumina-coated silica nanoparticles on the stability of immiscible N_2 foam. These hydrophilic nanoparticles were unable to stabilize foam without the addition of a PG surface modifier. PG surface

modifier was able to change the wettability of nanoparticles to partially hydrophobic thus helping in the formation of more stable and fine foam bubbles at nanoparticle concentration of 1 wt.% and surface modifier of (0.05 wt.%). [7] showed that anionic alpha olefin sulfonate (0.5 wt.%) and surface-modified silica nanoparticle (0.5 wt.%) solution was able to stabilize foam in the prescience of crude oil. Foam half-life time was increased as the concentration of nanoparticles was increased. Moreover, the increase in surfactant-solid dispersion salinity to 1 wt.% of NaCl showed a desirable effect on enhancing foam stability and delaying foam height decay. On the other hand, in the absence of crude oil, the addition of solids had a minor effect on foam stability.

Nitrogen foam stabilized by surfactants-nanoparticles can have the ability to increase oil recovery after water flooding. According to Singh and Mohanty, oil recovery by N_2 foam stabilized by 0.5 wt.% Titon nonionic surfactant increased the oil recovery by 13.4% OOIP after water flooding. On the other hand, oil recovery by N_2 foam stabilized by 0.05 wt.% PG surface modifier and 1 wt.% alumina-coated silica nanoparticles increased the oil recovery by 22.6% OOIP after water flooding. This indicates that stabilizing N_2 foam by nanoparticles does not only increase the oil recovery, but it also helps in lowering the amount of surfactant concentration required [7, 145].

Evaluation of foam stability by calculation of spreading, entering, and bridging coefficients helps in understanding the effects of change of experimental conditions such as salinity on foam stability. [7] showed that blends of nanoparticles were not able to stabilize foam since crude oil had an antifoaming effect which can be expressed by positive values of the bridging coefficient (B) for both 0 and 1 wt.% of nanoparticles as shown in Table 8.3. On the other hand, when solution salinity was increased to 1 wt.% of NaCl, the bridging coefficient (B) became negative, or crude oil was no longer acting as an antifoaming agent. It is worth mentioning that the value of entering coefficient (E) stayed positive when salinity was increased. This indicates that the crude oil had affected the foam stability to some extent, whereas the foam was still relatively stable since oil drops were not spreading on the surface of foam films. This can be indicated by the negative values of the spreading coefficient (S). Table 8.4 shows a selected nitrogen foam studies from the literature and the oil displacement recovery for each experiment.

Table 8.3 Spreading (S), entering (E), and bridging (B) coefficients calculated from IFT measurements at 25 °C [7]

	0 wt.% NaCl		1 wt.% NaCl	
Coefficient	0 wt.% NPs	1 wt.% NPs	0 wt.% NPs	1 wt.% NPs
S	−5.5	−5.1	−4.5	−3.9
E	5.7	4.7	1.8	1.3
B	39	8.7	−74.9	−72.4

Permissions related to the material excerpted were obtained from ACS, and further permission should be directed to ACS; AlYousef, Z., Almobarky, M., & Schechter, D. (2017). Enhancing the Stability of Foam by the Use of Nanoparticles. Energy & fuels, 31(10), 10620–10627

Table 8.4 Evaluation of the effect of surfactant-nanoparticle dispersion on oil recovery

Nanoparticle type	Surfactant/ surface modifier	Nanoparticle surface modification	Experimental conditions									Gas	Oil recovery	Reference
			Temperature (C °)	Pressure (psi)	Salinity	Nanoparticle concentration	Surfactant concentration	Core lithology	ϕ	k (md)	Gas quality (%)			
Alumina-coated silica	Non anionic (triton)	From hydrophilic to partially hydrophobic	Room temperature	750	–	0	0.5 wt.%	Sandstone	20%	442	80	Immiscible N_2	13.4% additional after water flooding	[145]
Alumina-coated silica	PG	From hydrophilic to partially hydrophobic	Room temperature	750	–	1 wt.%	0.05 wt.% surface modifier	Sandstone	22%	585	90	Immiscible N_2	22.6% additional after water flooding	[145]
Surface-modified silica	Anionic AOS	Surface-modified	25	1200	1 NaCl wt.%	0	0.5 wt.%	Sandstone	21.84%	1.55	90	N_2	41.45% total recovery after water and foam flooding	[7]
Surface-modified silica	Anionic AOS	Surface-modified	50	1200	1 NaCl wt.%	0.5 wt.%	0.5 wt.%	Sandstone	20.55%	1.69	90	N_2	49.05% total recovery after water and foam flooding	[7]

8.6.2 Carbon Dioxide

CO_2 has many advantages over other gases such as N_2 and CH_4 which makes it the most favorable gas in enhanced oil recovery. Mainly, it can achieve a supercritical state at most reservoir conditions, and it can be miscible in crude oil which helps in improving the microscopic displacement efficiency of residual oil [64]. Injected CO_2 foam can be either in the supercritical state or normal CO_2. Several researchers confirmed the ability of nanoparticles in stabilizing CO_2 foams. Surface-modified nanoparticles have the following advantages in foam stabilization. They can stabilize CO_2 foam under high temperature and high salinity concentrations [77, 80, 92, 161, 180]. Nanoparticles can migrate in the porous media and are less prone to adsorb on the surface of rock formations compared to surfactants [69, 178]. Since the molecules of CO_2 lacks a permanent dipole, the hydrocarbon chain of a surfactant will be more inclined towards the water phase instead of being at the gas/liquid interface due to the weak Van der Waals forces [169]. In contrast, the surface-modified nanoparticles can have an affinity for both CO_2 and water which increases the binding forces between CO_2 and water resulting in more foam stability [155]. Due to the high solubility of CO_2 in water, gas diffusion between bubble films results in bubble coarsening thus decreasing the foam lifetime as a result of the Ostwald ripping effect [171]. Adsorption of nanoparticles on the gas/liquid interface can reduce the gas diffusion by contact area reduction between gas bubbles and liquid films [97]. Literature suggests that CO_2 foam can be stabilized either by brine-nanoparticle solution or by the surfactant-nanoparticle solution. In the following sections, the main results of CO_2 foam studies are discussed.

8.6.2.1 CO_2 Foam Stabilization by Brine-Nanoparticle Solution

These studies mainly focus on the in situ generation of stabilized CO_2 foam in porous media without the need for surfactants. To mitigate problems of surfactant retention during enhanced oil recovery, surface-modified nanoparticles can be used for CO_2 foam formation and stabilization. Nanoparticles such as silica, fly ash, or nano-clay can be commercially fumed by using polyethene glycol or PEG process and cost USD 4/lb [82]. Espinoza et al. [55] investigated the effect of surface-modified silica nanoparticles on increasing supercritical CO_2 foam viscosity by using two types of surface-modified silica nanoparticles: hydrophilic coated nanoparticles with polyethene glycol and salt-tolerant nanoparticles. These nanoparticles were able to form stable foam and increase the flow resistance by 2–18 times compared to the CO_2 brine solution without nanoparticles by using only (0.5 wt.%) of nanoparticle concentration. The study was performed at 95 °C and 1350–1400 psi in a column of 180-micrometer glass beads. This study indicated that the threshold shear rate is independent of the ratio between the injected CO_2/brine ratio. Yu, An, Mo, Liu, and Lee [176] used other surface-modified silica nanoparticles that were able to increase the apparent foam viscosity and mobility by 1.5–2.5 times and 9 times higher than CO_2/brine solution when nanoparticle concentration was between 2500 and 10,000 ppm. Moreover, a sandstone core flooding experiment that was

conducted by the same research team showed that the pressure drop increased from 50 to 870 psi when brine and CO_2 foam stabilized by nanofluid was used at 5000 ppm concentration. However, despite their promising results of controlling CO_2 mobility, this nanofluid cannot form foam when salinity is higher than 2 wt.% NaCl due to nanoparticle agglomeration.

Yu et al. [178] evaluated the effect of supercritical CO_2 foam stabilized by (5000 ppm) silica nanoparticles on oil recovery via core flooding experiments. Two sandstone cores were used (permeability was 31 and 270 mD), salinity was (2 wt.% NaCl), and temperature and pressure were 20 °C and 1200 psig, respectively. Additional oil recovery in the two sandstone cores by CO_2-nanofluid after brine flooding was 48.7% and 35.8% OOIP. At the end of the core flooding experiment, one of the cores (31 mD) was tested against nanoparticle retention in the porous media. Nanoparticles losses were found to be 3.3% of the total injected in the core flooding experiment. It is expected that minor nanoparticles losses in reservoir flooded by nanoparticle-stabilized foams were due to strong attractions between the nanoparticles and the gas/liquid interface [12]. According to A. Worthen et al. [168] methyl-coated silica nanoparticles can form more stable foams than polyethene glycol (PEG)-coated silica nanoparticles. Nguyen et al. [118] demonstrated that 50% of methyl-coated silica nanoparticles were able to stabilize CO_2 foam for 10 days at a concentration of 1 wt.%. On the other hand, bare silica nanoparticles and 75% methyl-coated silica nanoparticles were not able to generate foam when mixed with CO_2, while sodium dodecyl sulfate (SDS) formed less stable foam. Moreover, due to the coalescence of SDS surfactant foam, foam density decreased from 31 to 9 bubbles/mm^2, while bubble diameter increased from 83 to 198 μm during the experiment period (20 h). During the same experiment period, methyl-coated silica nanoparticles were able to maintain a foam density of 29 bubbles/mm^2 with a diameter of 72 micrometers, and changes were negligible for the next 10 days as shown in Fig. 8.33.

To evaluate the stability of CO_2 foam stabilized by methyl-coated silica nanoparticles in presence of crude oil, Nguyen et al. [118] performed gas flooding experiments by using CO_2 and CO_2 foam stabilized by nanoparticles in a micromodel saturated with medium to heavy oil (API gravity of 24) at 22 °C and 600 psi. Water flooding resulted in a recovery of 41% OOIP. When water flooding was followed by CO_2 injection, additional recovery was 5% OOIP. On the other hand, CO_2 foam stabilized by nanoparticles resulted in 15% OOIP additional oil recovery. Figure 8.34 compares the oil recovery and the macroscopic displacement efficiency for brine, CO_2, and CO_2 foam floods in a micro model.

Nguyen et al. [118] reported a reduction in the oil-in-water emulsion sizes in the case of nanoparticle-stabilized CO_2 foam. This effect is attributed to the active nanoparticles at the oil-water interface. This mechanism contributes to enhancing the oil recovery by CO_2 foam. Similarly, in EOR methods, smaller oil-in-water emulsion sizes improve the recovery rates [39]. By using fluorescence imaging at the microscale, Nguyen et al. [118] were able to quantify the sizes of oil-in-water and water-in-oil emulsion sizes as shown in Fig. 8.35. Oil-in-water emulsion sizes in the CO_2 flooding were reported to have an average size of 7.8 μm, while it was

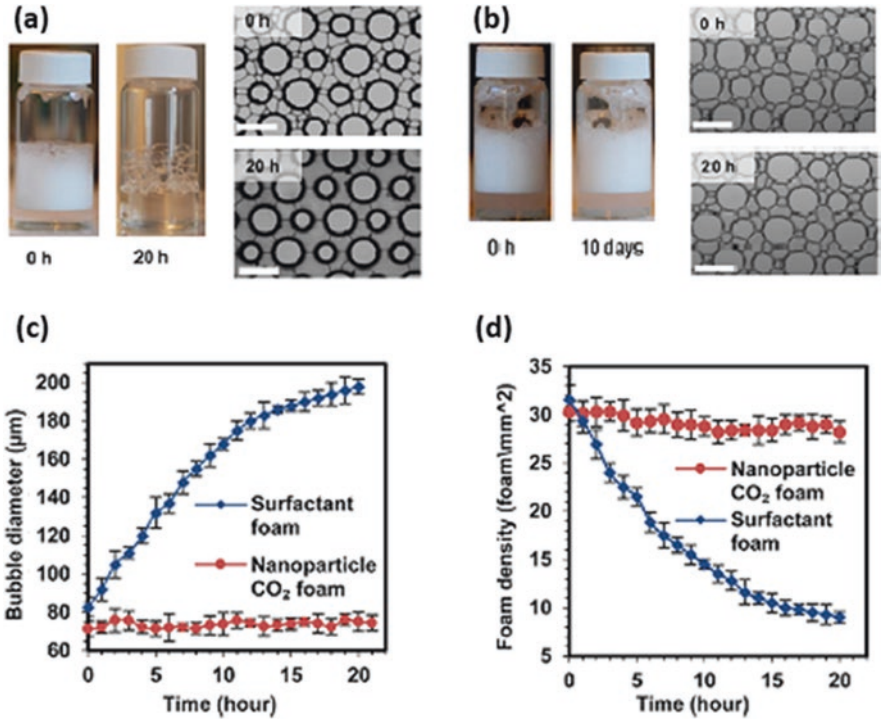

Fig. 8.33 (**a**) Foam sample stabilized only by SDS surfactant, (**b**) foam stabilized by nanoparticles, (**c**) change in bubble diameter of nanoparticle-stabilized foams with time, (**d**) change in foam density of surfactant- and nanoparticle-stabilized foams with time [118]. Permissions related to the material excerpted were obtained from ACS, and further permission should be directed to ACS; Nguyen, P., Fadaei, H., & Sinton, D. (2014). Pore-Scale Assessment of Nanoparticle-Stabilized CO2 Foam for Enhanced Oil Recovery. Energy & Fuels, 28(10), 6221–6227. doi: https://doi.org/10.1021/ef5011995

1.7 μm in the case of CO_2 nanoparticle foam. Thus, surface-active nanoparticles were able to reduce the oil-in-water emulsion sizes by 80%.

Alzobaidi et al. [8] demonstrated the effect of surface-modified silica nanoparticles on the increasing CO_2 foam apparent viscosity at harsh reservoir conditions. Silica nanoparticles utilized in their study were low coverage (LC), medium coverage (MC), and high coverage (HC) organic ligand nanoparticles. Nanoparticle dispersions of concentration of 1 wt.% were stabilized when salinity was 15 wt.% TDS at 3000 psi. Glass bead pack and sandstone core flooding experiments demonstrated the significant role of coated silica nanoparticles in maintaining high CO_2 foam viscosity up to 35 cP and bubble sizes in the order of 40 μm. Figure 8.36 compares the apparent foam viscosity against foam quality for the three types of nanoparticles at pressure, temperature, and salinity of 3000 psig, 25 °C, and 15 wt.% TDS, respectively. The apparent foam viscosity increased as the coverage of the silica nanoparticles increases from low coverage to high coverage. Moreover, apparent viscosity

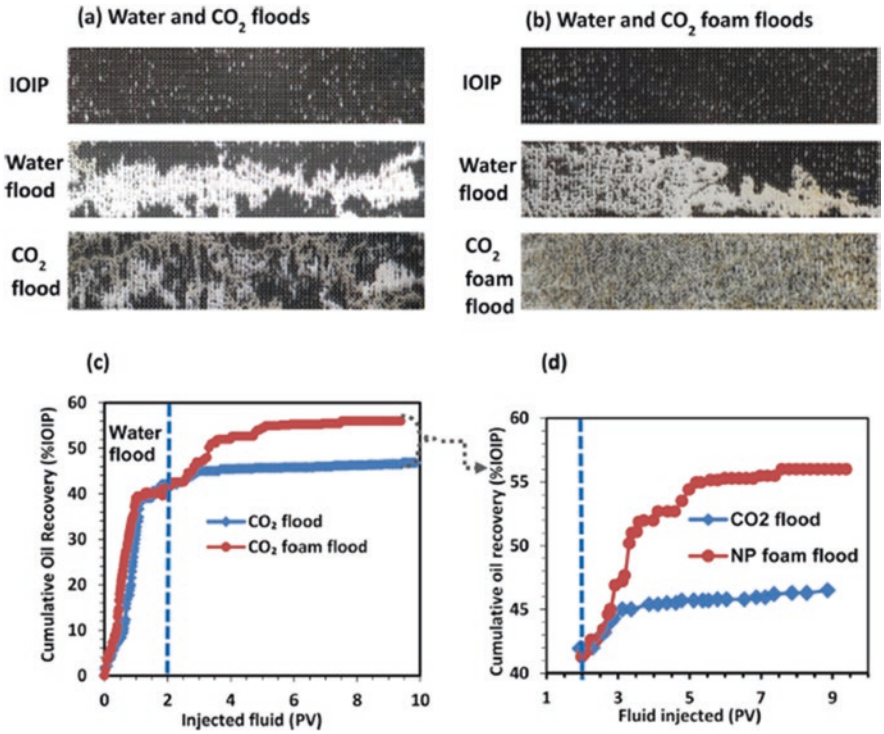

Fig. 8.34 Comparison between (**a**) water and CO_2 floods, (**b**) water and CO_2 foam stabilized by 50% methyl-coated silica nanoparticles [118]. Permissions related to the material excerpted were obtained from ACS, and further permission should be directed to ACS; Nguyen, P., Fadaei, H., & Sinton, D. (2014). Pore-Scale Assessment of Nanoparticle-Stabilized CO_2 Foam for Enhanced Oil Recovery. Energy & Fuels, 28(10), 6221–6227. doi: https://doi.org/10.1021/ef5011995

increased with an increase in foam quality; then it started decreasing after the transition foam quality (85%). Figure 8.37 compares the bubble sizes and apparent foam viscosity against foam quality for the MC and HC nanoparticles at pressure, temperature, and salinity of 3000 psig, 80 °C and 15 wt.% TDS, respectively. Finally, in core flooding experiments by using Boise and Berea sandstone cores, apparent foam viscosity was 26 cP at pressure, temperature, salinity, and foam quality of 3000 psig, 70 °C, 15 wt.% TDS, and 75%, respectively.

Rognmo et al. [132] performed another study on the effect of surface-modified silica nanoparticles on supercritical CO_2 at high salinity and pressure. Silica nanoparticles were surface modified to enhance hydrophobicity and salt tolerance. Nanoparticle dispersion at a concentration of 1500–5000 ppm was stable at a temperature of 40 °C for 75 days at salinity up to 20 wt.% NaCl and 5 wt.% $CaCO_3$. Moreover, nanoparticle dispersion dynamic stability was also tested at a concentration of 3000 ppm at temperatures 20, 60, and 120 °C and salinity between 15 and 25 wt.%. Constant pressure drop when the injection rate was fixed revealed that nanoparticle dispersion was stable. Rognmo et al. [133] evaluated the effect of

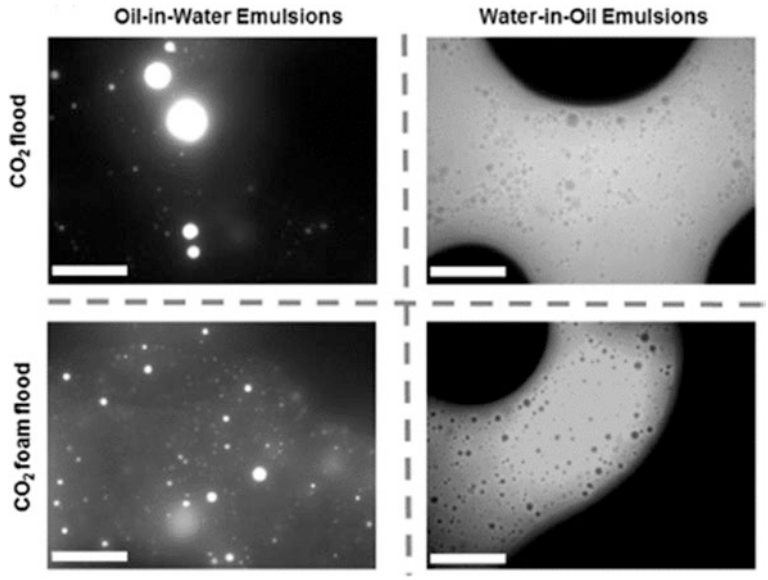

Fig. 8.35 Comparison between the oil-water and water-in-oil emulsion sizes in the cases of CO_2 and CO_2 foam floods [118]. Permissions related to the material excerpted were obtained from ACS, and further permission should be directed to ACS; Nguyen, P., Fadaei, H., & Sinton, D. (2014). Pore-Scale Assessment of Nanoparticle-Stabilized CO2 Foam for Enhanced Oil Recovery. Energy & Fuels, 28(10), 6221–6227. doi: https://doi.org/10.1021/ef5011995

co-injection of brine-silica nanoparticle dispersion and supercritical CO_2 at a foam quality of 70% and salinity of 1 wt.% NaCl on oil recovery and pressure drop. Surfactant used was a linear alcohol ethoxylate (C12–C16) at a concentration of 10,000 ppm. Core flooding experiments of 12 Bentheimer sandstone core plugs at 90 bar and 60 °C indicated that supercritical CO_2-nanoparticle dispersions enhanced the oil recovery compared to the injection of supercritical CO_2 and brine. The average increase in the oil recovery and the pressure drop gradient (calculated from the end of water flooding) of co-injection of supercritical CO_2 and brine (70% foam quality) was 8.2% OOIP and 39%, respectively. On the other hand, co-injection of 1500 ppm nanoparticles, 10,000 ppm surfactant dispersion, and supercritical CO_2 (70% foam quality) increased the oil recovery by 10.1–14.4% OOIP, while the increase in the pressure drop gradient was between 68 and 118%. Finally, injection of 5000 ppm nanoparticle dispersion and supercritical CO_2 at 70% foam quality increased the oil recovery by 15.4% OOIP, and the increase in the pressure drop gradient was 191%. On the other hand, co-injection of 1 wt.% of linear alcohol ethoxylate and supercritical CO_2 at foam quality of 70% increased oil recovery by 15.9% OOIP, while the pressure drop decreased by 13%. This indicates that the generated foam was not stable without the addition of silica nanoparticles. Figure 8.38 demonstrates the additional oil recovery and increase in pressure drop when nanoparticles were used compared to CO_2 flood and brine flood without

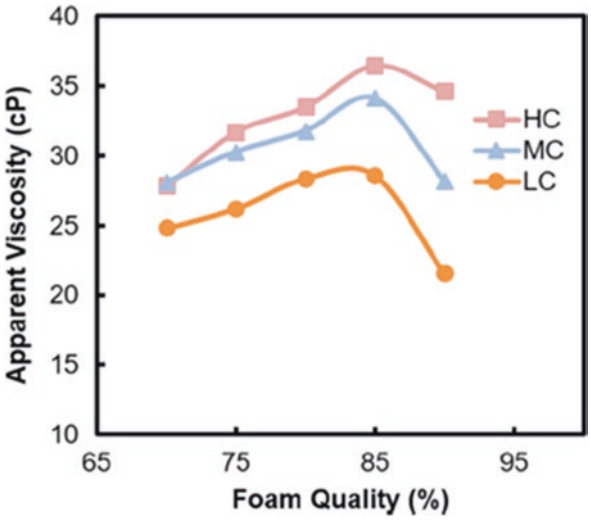

Fig. 8.36 Comparison between apparent viscosity behavior of the three types of nanoparticles with the increase in foam quality at pressure = 3000 psig, temperature = 25 °C, and salinity = 15 wt.% TDS [8]. Permissions related to the material excerpted were obtained from ACS, and further permission should be directed to ACS; Alzobaidi, S., Lotfollahi, M., Kim, I., Johnston, K. P., & DiCarlo, D. A. (2017). Carbon Dioxide-in-Brine Foams at High Temperatures and Extreme Salinities Stabilized with Silica Nanoparticles. Energy & Fuels, 31(10), 10680–10690

co-injection of surfactant (baseline). Figure 8.39 summarizes the average increase in oil recovery and pressure drop of each case as explained above.

Bayat et al. [16] assessed the effect of hydrophilic metal oxides (Al_2O_3, TiO_2, CuO) on enhancing the stability of CO_2 foam and increasing oil recovery. Best foam stability was obtained at nanoparticle concentration of 0.008 wt.% for all nanoparticle types. Evaluation of foam morphology and bubble size indicated that the bubble sizes of CO_2 foam stabilized by Al_2O_3, TiO_2, and CuO nanoparticles were 400, 500, and 600 μm, respectively. Hence, Al_2O_3 nanoparticles are better in CO_2 foam stabilization than TiO_2 and CuO nanoparticles since bubble coalescence rate was slower. Figure 8.40 compares the morphology and bubble sizes of CO_2 foam stabilized by SiO_2, Al_2O_3, TiO_2, and CuO nanoparticles. Increment in oil recovery by using CO_2 foam stabilized by Al_2O_3, TiO_2, and CuO nanoparticles was 12.3, 6.5, and 5.1% OOIP, respectively, while oil recovery increased by 17.4% OOIP in the case of CO_2 foam stabilized by SiO_2.

Graphene oxides (GO) are surface-active particles capable of the creation of very stable emulsions with organic solvents [87]. Amphiphilicity of GO is dependent on the particle sizes [105]. Smaller GO particles tend to have higher hydrophilicity due to the high density of –COOH on its edges and epoxy groups on the particle surface [105]. Thus, amphiphilicity of GO oxides can be altered by changing particle size or by partially reducing the particle oxygen content [101].

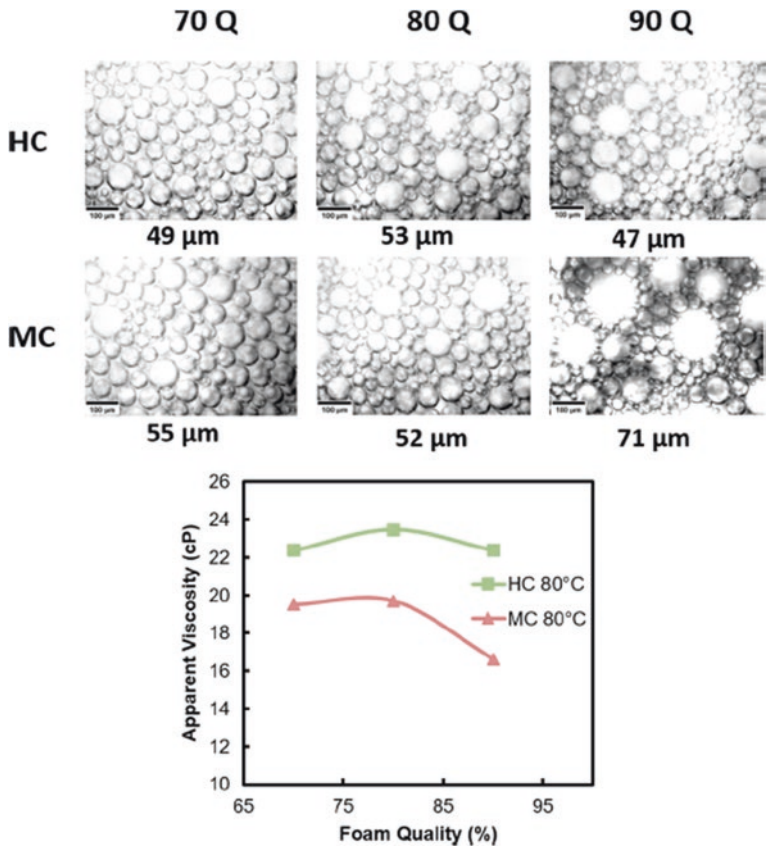

Fig. 8.37 Comparison between CO_2 foam bubble sizes and apparent viscosity of HC and MC nanoparticles at pressure = 3000 psig, temperature = 80 °C, and salinity = 15 TDS% [8]. Permissions related to the material excerpted were obtained from ACS, and further permission should be directed to ACS; Alzobaidi, S., Lotfollahi, M., Kim, I., Johnston, K. P., & DiCarlo, D. A. (2017). Carbon Dioxide-in-Brine Foams at High Temperatures and Extreme Salinities Stabilized with Silica Nanoparticles. Energy & Fuels, 31(10), 10680–10690

Partially reduced GO were efficient in stabilizing CO_2 in water which can improve foam stability due to large surface area of these particles [101]. Barrabino et al. [14] reduced the size of graphene oxides from 4–30 µm to 260–295 nm and tested their ability to produce stable CO_2 foams with synthetic seawater. Their study revealed that GO was able to generate foam, but the partially reduced graphene oxides and graphene in the nano range had a determinant effect on CO_2 foamability. Barrabino et al. [14] reported that nanographene can be partially reduced to achieve less hydrophilicity while considering the reduction angle. Table 8.5 summarizes selected studies of CO_2 foam stabilization by nanoparticles for enhancing oil recovery and maintaining high apparent foam viscosity.

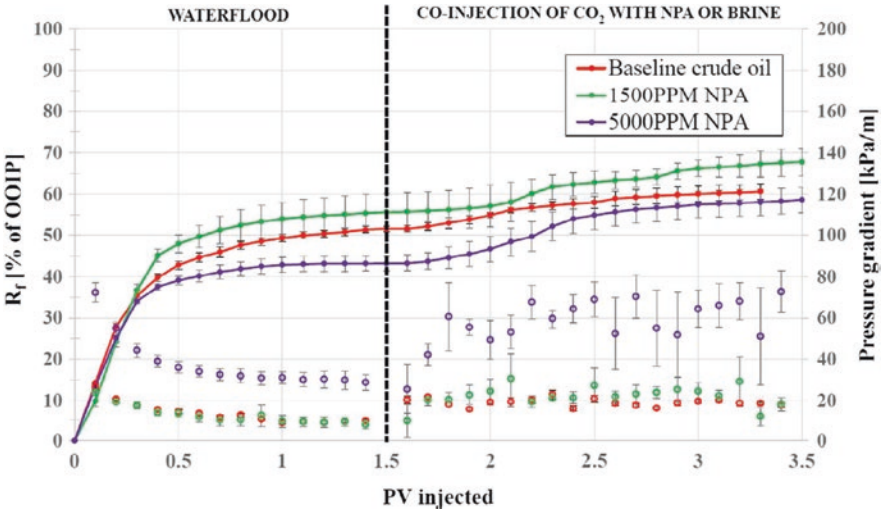

Fig. 8.38 Oil recovery (solid points and lines) and pressure drop comparison between CO_2 injection, 1500–5000 ppm by mass nanoparticle dispersion, and supercritical CO_2 at temperature, pressure, and salinity of 60 °C, 90 bar, and 1 wt.% NaCl [133]. Permissions related to the material excerpted were obtained from Elsevier, and further permission should be directed to Elsevier; Rognmo, A. U., Heldal, S., & Fernø, M. A. (2018). Silica nanoparticles to stabilize CO_2-foam for improved CO_2 utilization: Enhanced CO_2 storage and oil recovery from mature oil reservoirs. Fuel, 216, 621–626. doi: https://doi.org/10.1016/j.fuel.2017.11.144

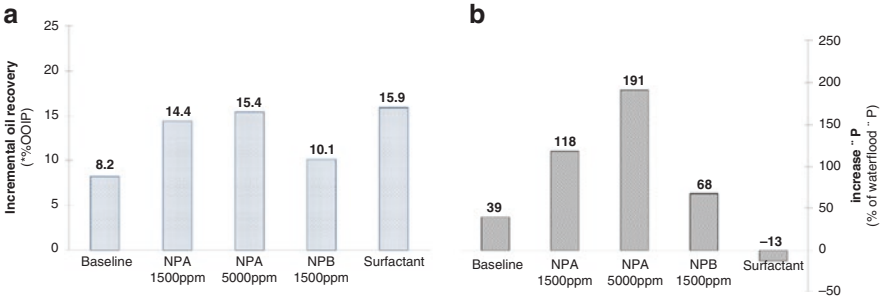

Fig. 8.39 (**a**) Additional oil recovery and (**b**) increase in pressure drop of supercritical CO_2 foam stabilized by nanoparticles (types NPA and NPB of different hydrophobicity) at temperature, pressure, salinity, surfactant concentration, and foam quality of 60 °C, 90 bar, 1 wt.% NaCl, 10,000 ppm, and 70%, respectively [133]. Permissions related to the material excerpted were obtained from Elsevier, and further permission should be directed to Elsevier; Rognmo, A. U., Heldal, S., & Fernø, M. A. (2018). Silica nanoparticles to stabilize CO_2-foam for improved CO_2 utilization: Enhanced CO_2 storage and oil recovery from mature oil reservoirs. Fuel, 216, 621–626. doi: https://doi.org/10.1016/j.fuel.2017.11.144

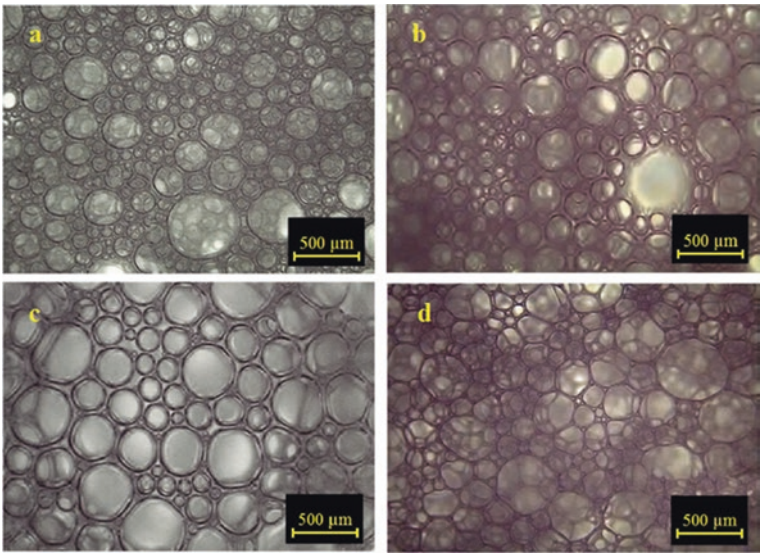

Fig. 8.40 Comparison between bubble sizes of CO_2 foam stabilized by (**a**) SiO_2, (**b**) Al_2O_3, (**c**) TiO_2, and (**d**) CuO nanoparticles [16]. Permissions related to the material excerpted were obtained from Elsevier, and further permission should be directed to Elsevier; Bayat, A. E., Rajaei, K., & Junin, R. (2016). Assessing the effects of nanoparticle type and concentration on the stability of CO_2 foams and the performance in enhanced oil recovery. Colloids and Surfaces A: Physicochemical and Engineering Aspects, 511, 222–231. doi: https://doi.org/10.1016/j.colsurfa.2016.09.083

8.6.2.2 Effect of Nanoparticle Surface Modification on CO_2 Foam Stability

The synergistic effect between nanoparticles and surfactants has received high attention as a significant mechanism for foam stability in EOR applications. Nevertheless, nanoparticles with certain hydrophobicity can be irreversibly adsorbed to the gas/liquid interface at lower energy compared to surfactant. Moreover, nanoparticles increase the density of surfactant molecules capable of stabilizing the foam interface. This effect can improve the interfacial tension between gas and liquid and increase the mechanical elasticity of foam lamellas, hence hindering the foam coalescence, rupturing, and liquid drainage compared to using surfactants only as a foam stabilizing agent. Main studies of CO_2 foam stabilization by modified nanoparticles and surfactants have been reported.

S. Li et al. [98] investigated the synergistic effect between hydrophilic silica nanoparticles (contact angle 38.63° with water) and CTAB on the stabilization of CO_2 foam. In their study, the concentration of silica nanoparticles was fixed at 1.5 wt.%, while CTAB concentration was changed from 0 to 0.3 wt.%. Initially, when surfactant concentration was low, the zeta potential of the silica nanoparticles and CTAB showed negative measurements indicating low adsorption between CTAB positive ions on the surface of the nanoparticles. Hence, the nanoparticles

Table 8.5 Selected studies of CO_2 foam stabilization by nanoparticles for enhancing oil recovery and maintaining high apparent foam viscosity

Nanoparticle type	Nanoparticle size (nm)	Nanoparticle surface modification	Experimental conditions											Effect on apparent viscosity/pressure drop/oil recovery	Reference
			Temperature (°C)	Pressure (psi)	Salinity	NPs concentration	Shear rate (s^{-1})	Porous media	Phi (%)	k (mD)	Oil	Gas	Gas quality (%)		
Silica	5	Hydrophilic coated with PEG	95	1352–1400	0	0.05 wt.%	1300	Glass bead pack column				Super critical CO_2	5.0–29.0	Flow resistance was 2–18 times gas viscosity	[55]
		Salt-tolerant coated with PEG			4 wt.% NaCl	0.5 wt.%									
Silica	20–100	Coated with PEG	25	1500 psig	Brine	2500–10,000 ppm	1419	Glass beadpack column				Super critical CO_2	2.0–11.0	(1) Apparent viscosity was between 1.5 and 2.5 times higher; (2) mobility was 9 times higher; (3) viscosity of foam was decreased when CO2/brine ratio was varied from 2 to 11	[176]
Silica	10.–40.	Coated silica	25	1500 psig	2 wt.% NaCl	5000 ppm		Berea sandstone	17.36	33.01		Super critical CO_2	20	(1) Pressure drop was 50 psi after brine flooding; (2) pressure drop increased up to 870 psi after CO2/brine-nano-dispersion flooding	[114]
Silica	17–20	Coated silica	20	1200 psig	2 wt.% NaCl	5000 ppm		Berea sandstone	17.4	31		Super critical CO_2	50%	(1) Pressure drop decreased from 834 to 786 psig during brine flooding; (2) as 5 PV of CO2/nanoparticles injected, pressure drop increased to 1750 psig; (3) additional oil recovery CO2/nanoparticles was 48.7%	[178]
									20.5	270				Additional oil recovery CO2/nanoparticles was 35.8%	

Silica	12	50% methyl-coated silica nanoparticles	22	600	1 wt.%	1 wt.%		Glass micromodel			Light oil (API 37)	CO_2		Additional oil recovery was 11%	[118]
											Medium to heavy oil (API 24)			Additional oil recovery was 15%	
											Heavy oil (API 14)			Additional oil recovery was 8%	
Silica	40	Hydrophilic	27		2.5 wt.% brine saturate, water flooding 0.3 wt% NaCl	0.008 wt.%		Sand packs	~43.4	~2300	Malaysian crude oil (density of 0.863 g/cm^3 and viscosity of 21.7 ± 0.02 cp at 26 °C)	CO_2		Additional oil recovery was 17.4%	[16]
AlO_3														Additional oil recovery was 12.3%	
TiO_2														Additional oil recovery was 6.5%	
CuO														Additional oil recovery was 5.1%	
Silica	Less than 50	Low coverage (LC), medium coverage (MC), high coverage (HC) ligands grafted to the nanoparticles	25–80	3000 psig	15 wt.% TDS	1 wt.%	2270	Glass bead pack	34	22,000		CO_2	70–90	(1) Apparent viscosity increased with increase in ligand grafting; (2) maximum apparent viscosity was 36 CP; (3) average bubble size was 40 micrometer	[8]
		MC, HC	25–70	2800 psig										Maximum apparent viscosity was 26 cP	
Silica		Hydrophilic	60–80	90 bar	2–20 wt%	1500–5000 ppm		Bentheimer sandstone	20–25	1100–2600	Crude oil (density of 0.849 g/cm^3 at 20 °C)	Super critical CO_2		Oil recovery increased to 14.1%, and the effects of high temperature and salinity were minimal	[132, 133]

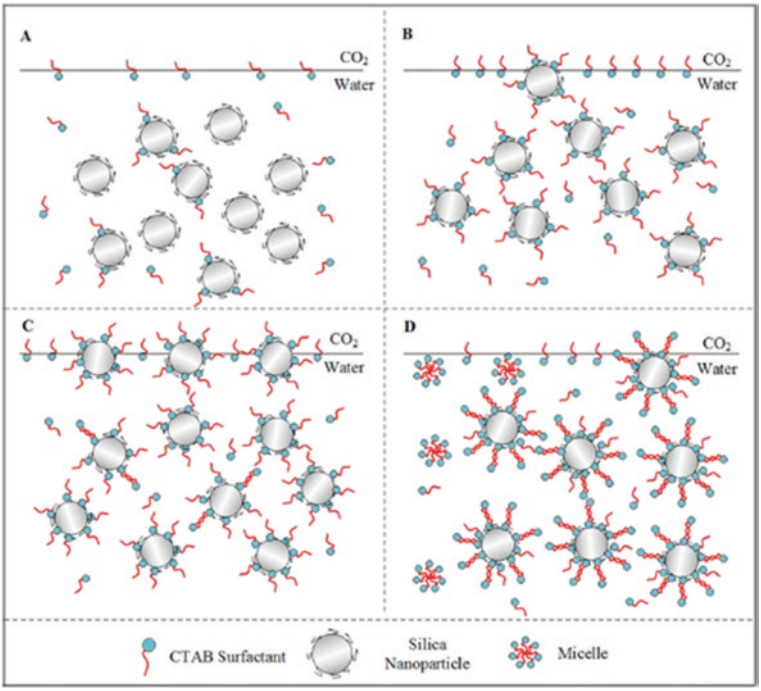

Fig. 8.41 Adsorption of the silica nanoparticles to the interface with an increase in surfactant concentration [98]. Permissions related to the material excerpted were obtained from ACS, and further permission should be directed to ACS; Li, S., Qiao, C., Li, Z., & Wanambwa, S. (2017). Properties of Carbon Dioxide Foam Stabilized by Hydrophilic Nanoparticles and Hexadecyltrimethylammonium Bromide. Energy & Fuels, 31(2), 1478–1488. doi: https://doi.org/10.1021/acs.energyfuels.6b03130

were still hydrophilic. As surfactant concentration was increased, more surfactant molecules were able to adsorb on the surface of the nanoparticles resulting in the formation of a monolayer of adsorption stage (CTAB/SiO_2 ratio between 0.02 and 0.033). This behavior was indicated by the positive zeta potential measurements. Due to the adsorption of surfactant molecules on the silica nanoparticles, the silica nanoparticles became hydrophobic hence escaping from the bulk phase and starts adsorbing on the gas/liquid interface. On the other hand, the double adsorption stage of surfactant molecules on the surface of the nanoparticles occurred due to further increase in surfactant concentration (CTAB/SiO_2 ratio between 0.033 and0.07) resulting in movement of nanoparticles from the gas/liquid interface back to the bulk phase as demonstrated in Fig. 8.41.

CO_2 foam half-life time and viscoelasticity were significantly increased due to the alternation of nanoparticle hydrophobicity by CTAB compared to using CTAB only. The rate of foam coalescence was delayed, and liquid hold up was significantly enhanced at CTAB/SiO_2 ratio of 0.033 (0.05 wt.% CTAB, 1.5 wt.% SiO_2) due to adsorption of nanoparticles at the gas/liquid interface. On the other hand, CO_2

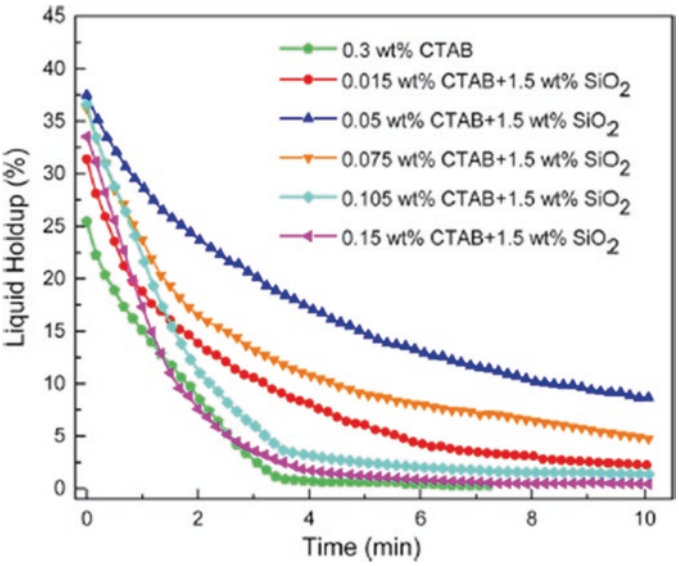

Fig. 8.42 CO_2 foam liquid holdup at different CTAB concentrations [98]. Permissions related to the material excerpted were obtained from ACS, and further permission should be directed to ACS; Li, S., Qiao, C., Li, Z., & Wanambwa, S. (2017). Properties of Carbon Dioxide Foam Stabilized by Hydrophilic Nanoparticles and Hexadecyltrimethylammonium Bromide. Energy & Fuels, 31(2), 1478–1488. doi: https://doi.org/10.1021/acs.energyfuels.6b03130

foam stabilized by CTAB at 0.3 wt.% without nanoparticles showed lower foam liquid holdup and half-life time and thus lower foam stability. Figure 8.42 shows the liquid holdup of CO_2 foam at different CTAB/SiO_2 concentrations. Finally, micromodel displacement experiments showed that CO_2 foam was able to increase the total oil recovery from 45% OOIP (at the end of water flooding) to 74.3% OOIP.

P. Wang et al. [163] compared the effect of several types of surfactants and hydrophilic silica nanoparticles on CO_2 foam stability. Surfactants used in this study include CTAB (cationic), SDBS (anionic), TX-100 (nonionic), and OA-12 (zwitterionic). The stability of CO_2 foam was decreased for all surfactant/nano-dispersion as salinity and temperature were increased from 0 to 30,000 mg/L and 30 to 70 °C, respectively. The best foam stability effect was achieved by a zwitterionic surfactant (OA-12) at nanoparticle and surfactant concentrations of 0.5 wt.% and 0.02 wt.%, respectively. The synergy between hydrophilic silica nanoparticles and OA-12 enhanced the CO_2 foam stability by lowering the surface tension and increasing the viscoelasticity modulus. Moreover, the intensity of CO_2 foam lamellas was reinforced by the formation of the three-dimensional network structure. Figure 8.43 illustrates the effect of hydrophilic silica nanoparticles in CO_2 foam stabilization. S. Li et al. [99] investigated the effect of silica nanoparticles hydrophilicity on CO_2 foam stability in the presence of nonionic surfactant ($C_{12}E_{23}$).

The best synergistic effect between four types of hydrophilic silica nanoparticles and $C_{12}E_{23}$ was reported when contact angle with water was minimum (20.12°). Due

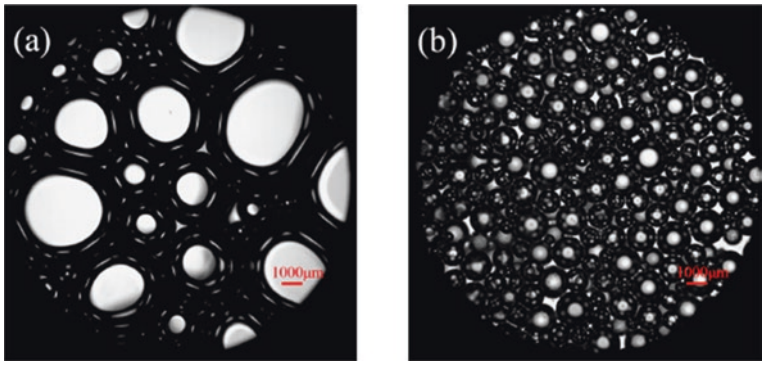

Fig. 8.43 Comparison between CO_2 foam morphology: (**a**) foam stabilized by surfactant (0.02 wt.% OA-12), (**b**) foam stabilized by surfactant-NPs (0.02 wt.% OA-12, 0.5 wt.% SiO_2) [163]. Permissions related to the material excerpted were obtained from ACS, and further permission should be directed to ACS; Wang, P., You, Q., Han, L., Deng, W., Liu, Y., Fang, J., … Dai, C. (2018). Experimental Study on the Stabilization Mechanisms of CO_2 Foams by Hydrophilic Silica Nanoparticles. Energy & Fuels, 32(3), 3709–3715. doi: https://doi.org/10.1021/acs.energyfuels.7b04125

to surfactant adsorption on the surface of the nanoparticles, the contact angle became 78° achieving the best foam stability at a surfactant concentration of 2.49 mM and nanoparticle concentration of 1.5 wt.%. As a result of the synergistic effect between hydrophilic silica and $C_{12}E_{23}$, CO_2 foam half-life was 30 times greater than surfactant foam, and interfacial viscoelastic modulus increased from 5.1 to 25.2 mN/m. Figure 8.44 shows the delay in CO_2 bubble coalescence of $C_{12}E_{23}$/SiO_2 dispersion compared to $C_{12}E_{23}$ foam in the microscopic model.

The role of hydrophobic nanoparticles in foam stability have also been reported. S. Li et al. [97] studied the synergistic effect between anionic surfactant (SDS) and hydrophobic silica nanoparticles (122.22° contact angle with water) at SDS/SiO_2 concentration ratio of 0.1–0.4 for CO_2 foam stabilization. Zeta potential measurements of SDS/SiO_2 dispersion revealed that the silica particle had a positive charge. Hence, most of the nanoparticles would be in the gas phase when SDS concentration is low. As the SDS/SiO_2 ratio increased, zeta potential started decreasing and reached zero when the SDS/SiO_2 ratio was 0.17. This indicates a reduction in nanoparticle hydrophobicity resulting in modulating the position of silica nanoparticles from the gas phase to the gas/liquid interface. Further increase in the SDS/SiO_2 ratio results in negative zeta potential measurements. When SDS/SiO_2 ratio reaches 0.4, nanoparticles become mostly hydrophilic. Hence, the stabilization effect of SDS/SiO_2 will be minimal since most of the nanoparticles will be already dispersed in the liquid phase. Figure 8.45 illustrates the position of the silica nanoparticles concerning the gas/liquid interface when SDS/SiO_2 concentration ratio was increased from 0.05 to 0.67.

S. Li et al. [97] reported that the synergistic effect between SDS/SiO_2 enhanced the CO_2 foam stability by the alternation of the interfacial properties. Viscoelastic

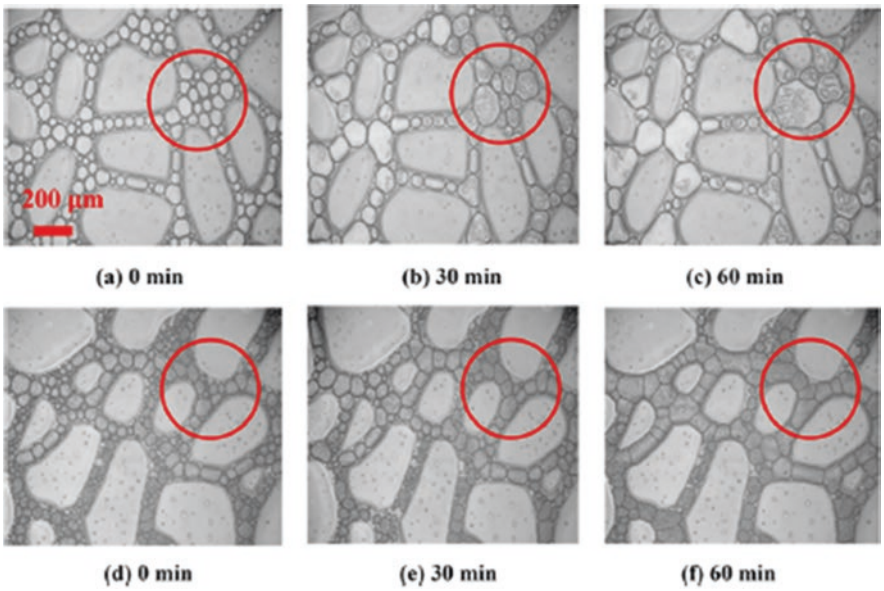

Fig. 8.44 (**a**–**c**) Stability of 2.49 mM $C_{12}E_{23}$ foam with time, (**d**–**f**) stability of 2.49 mM $C_{12}E_{23}$ and 1.5 wt.% silica foam with time [99]. Permissions related to the material excerpted were obtained from ACS, and further permission should be directed to ACS; Li, S., Yang, K., Li, Z., Zhang, K., & Jia, N. (2019). Properties of CO2 Foam Stabilized by Hydrophilic Nanoparticles and Nonionic Surfactants. Energy & Fuels, 33(6), 5043–5054. doi: https://doi.org/10.1021/acs.energyfuels.9b00773

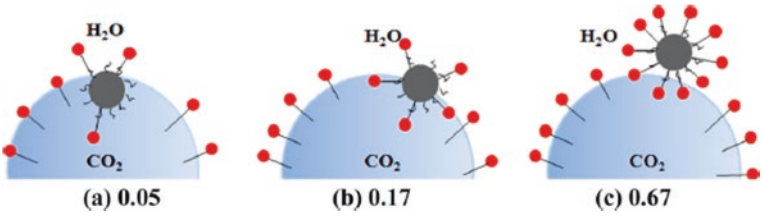

Fig. 8.45 Modulating the silica nanoparticle position from: (**a**) gas phase, (**b**) gas/liquid interface, (**c**) liquid phase. This figure indicates a middle section of a foam column [97]. Permissions related to the material excerpted were obtained from ACS, and further permission should be directed to ACS; Li, S., Yang, K., Li, Z., Zhang, K., & Jia, N. (2019). Properties of CO2 Foam Stabilized by Hydrophilic Nanoparticles and Nonionic Surfactants. Energy & Fuels, 33(6), 5043–5054. doi: https://doi.org/10.1021/acs.energyfuels.9b00773

modulus increased gradually as SDS/SiO_2 was increased to 0.17; then it decreased due to a further increase in SDS/SiO_2 ratio. At elevated temperatures, CO_2 foam stability was enhanced by addition of SiO_2 compared to using SDS alone. Increasing temperature lowers the viscoelastic modulus and increases the interfacial tension of SDS/SiO_2 dispersion. On the other hand, increasing pressure is beneficial for foam

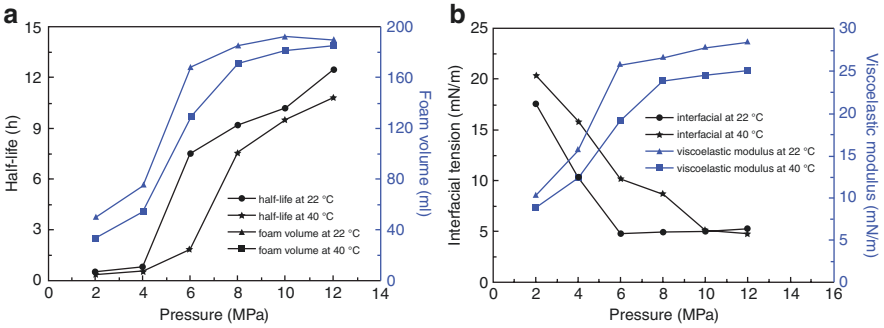

Fig. 8.46 (**a**) Foam half-life and volume of SDS/SiO_2 CO_2 foam at different temperatures and pressures, (**b**) interfacial properties of SDS/SiO_2 CO_2 foam at different temperatures and pressures [97]. Permissions related to the material excerpted were obtained from ACS, and further permission should be directed to ACS; Li, S., Li, Z., & Wang, P. (2016). Experimental Study of the Stabilization of CO2 Foam by Sodium Dodecyl Sulfate and Hydrophobic Nanoparticles. Industrial & Engineering Chemistry Research, 55(5), 1243–1253. doi: https://doi.org/10.1021/acs.iecr.5b04443

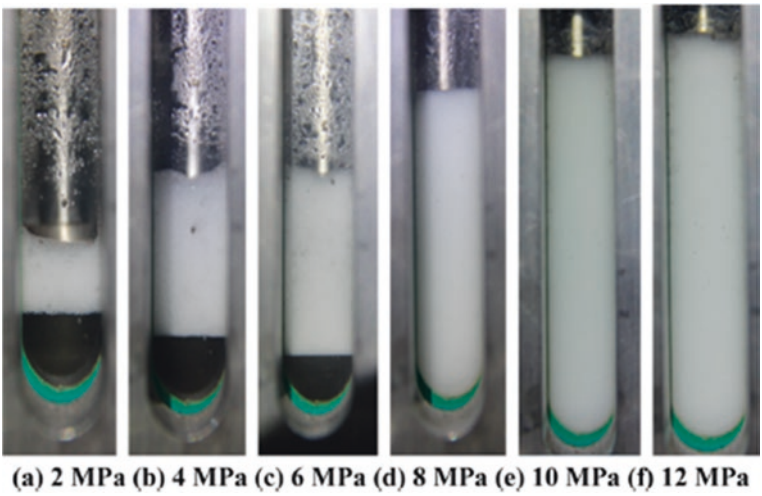

Fig. 8.47 Increase in SDS/SiO_2 CO_2 foam volume with an increase in pressure at 40 °C [97]. Permissions related to the material excerpted were obtained from ACS, and further permission should be directed to ACS; Li, S., Li, Z., & Wang, P. (2016). Experimental Study of the Stabilization of CO2 Foam by Sodium Dodecyl Sulfate and Hydrophobic Nanoparticles. Industrial & Engineering Chemistry Research, 55(5), 1243–1253. doi: https://doi.org/10.1021/acs.iecr.5b04443

stability by increasing foam half-life (foam half-life is 10 times higher) and interfacial properties as shown in Fig. 8.46. This effect was reported due to achieving the supercritical state of CO_2. Hence, CO_2 becomes liquid above 31.2 °C and 7.28 MPa. Figure 8.47 shows the increase in CO_2 foam volume due to pressure increase.

S. Li et al. [97] tested the efficiency of CO_2 foam in oil recovery stabilized by several SDS/SiO_2 concentration ratios at 50 °C and 8 MPa backpressure. Pressure difference and oil recovery results were optimum when SDS/SiO_2 concentration was 0.17. These results indicate that the best surfactant-nanoparticle concentration ratio to achieve CO_2 foam stability in the static foamability test is also the same as in the oil displacement tests. The maximum pressure difference and additional oil recovery results by water flooding followed by CO_2 foam stabilized by SDS/SiO_2 were 1.4 MPa and 75%, respectively.

Q. Liu et al. [102] studied the effect of surface modification of Fe_3O_4 nanoparticles on enhancing CO_2 foam stability. In the nanoparticle surface modification, 1,2-epoxy dodecane was grafted to the surface of the nanoparticles to alter its hydrophobicity. The alternation process of the hydrophobicity of the nanoparticles included the dispersion of Fe_3O_4 nanoparticles into a 4-methyl-2-pentanone solution while using NaOH aqueous solution as a catalyst. Then, the 1,2-epoxy dodecane was added to the aqueous dispersions. The surface modification reaction of the nanoparticles was conducted at 110 °C, while mechanical stirring speed was 300 rpm for 4 h under N_2 protection. More details of the Fe_3O_4 nanoparticles surface modification procedure are explained by Q. Liu et al. [102].

The identification of the surface functional groups by FTIR and TGA of the modified Fe_3O_4 nanoparticles indicated an effective grafting of the 1,2-epoxy dodecane (the hydrophobic functional group) to the surface of the nanoparticles. The contact angle between deionized water and the unmodified Fe_3O_4 nanoparticles was 12.7°, while the prepared Fe_3O_4 nanoparticles had the following contact angles: 20.6°, 57.5°, and 94.3°.

Evaluation of CO_2 foam stability of 0.1 wt.% Fe_3O_4, 0.2 wt.% SDS, and 0.1 wt.% HPAM dispersions by static foam stability tests, surface shear viscosity measurements, and core flooding experiments demonstrated the capability of surface-modified Fe_3O_4 to enhance foam stability. The best foam stability performance was achieved by the 94.3° wetting angle nanoparticles. They were able to increase the shear viscosity from 2650 to 5200 mPa.s, while enhancement in oil recovery was only 0.86% in a low permeability core oil displacement experiment by nano-dispersion foam.

8.7 Challenges of Field Implementation of Nanoparticle-Stabilized Foams

Although nanoparticle-stabilized foam is one of the most promising technologies for enhanced oil recovery and mitigation of the drawbacks of gas EOR, no pilot/field implementation of nanoparticle-stabilized foams have been reported in the literature [175]. However, the current status of nanoparticle-stabilized foams is still an important research focus. Yekeen et al. [175] summarized the main obstacles of field implementation of nanoparticle-stabilized foams including the uncertainty of the

economic aspects of nanoparticle-stabilized foams within the current low oil prices, nanoparticle agglomeration, and the environmental consequences of nanoparticles. Nanoparticles investigated in the literature for foam stabilization are developed from low-cost and commercially available raw materials including silica, fly ashes, and metal oxides; then surface modification is applied to the surface of the nanoparticles such as polyethene glycol (PEG) [82]. However, there is still no cost analysis demonstrating the economic advantages of nanoparticle utilization as a foam stabilizing agent in contrast with other foaming stabilization agents including surfactants or polymers [175]. Stability of a nanoparticle dispersion is crucially impacted by media conditions including salinity, temperature, pH, and nanoparticle concentration. In lab-scale foam studies, homogenous nanoparticle-surfactant dispersion can be prepared by ultrasonic vibration and surface modification of nanoparticles to avoid nanoparticle agglomeration [157]. However, the stability of nanoparticle dispersion in field-scale foam EOR is still unknown due to the lack of foam implementation in field or pilot applications [175]. In high salinity and high temperature environments, the screening effect of an electrostatic double layer (EDL) by reservoir electrolytes and the increased effect of particle collisions at high-temperature increments increase the risk of particle agglomeration [72, 73, 175] Hence, the aggregation of nanoparticles increases the hydrodynamic diameter of particles which could be in microns resulting in serious reservoir damage due to pore throats blockage. Finally, log-jamming and mechanical entrapment are the main identified mechanisms of nanoparticle pore channel blockage [49, 151, 157].

8.8 Conclusion, Recommendations, and Future Remarks

In this chapter, an extensive review of nanoparticle application for foam stability has been performed. Based on the existing literature, and from the phenomenological point of view, it can be argued that nanoparticle-stabilized foam offers a better alternative compared to surfactant-stabilized foam during gas EOR. Furthermore, nanoparticles of a given type and moderately hydrophobic surface at given optimum concentrations offer better stabilization options at the interfaces between immiscible fluids. Nevertheless, understanding the fundamental foam mechanisms, involved at the pore scale in the porous media coupled with nanoparticle agglomeration, is some of the current challenges of foam stabilized nanoparticles. Experimental studies and reported findings on the essential parameters of nanoparticle-stabilized foam performance are limited, and those that are reported are contradicting. It is important to note that the presence of nanoparticles at the air-water interface of the foam results in the draining of the oil from the foam films and their migration and accumulation at the edges enhance the foam stability and delay coalescence of the bubbles. Furthermore, the synergistic effect between nanoparticles and surfactants enhances the foam stabilization process. However, optimum nanoparticle concentration will depend largely on the surfactant type used and the concentration and operating conditions. It is also important to note that the aggregation of

nanoparticles at high salinity and high temperature and pressure could significantly increase or decrease foam stability depending on the aggregation magnitude. The potential benefit of producing nanoparticle-stabilized foam from fly ash and other low-cost nanoparticles, coupled with nanoparticle-stabilized foam visualization at the pore scale, and the fluid diversion mechanisms of nanoparticle-stabilized foam are exhilarating areas for further studies. Despite the extensive studies available in the literature, there are still some gaps in the nanoparticle-stabilized foam studies. Most of nanoparticle foam stabilization studies focus on sandstone formation, glass bead, or sand pack porous media, while less research has been conducted on carbonate formations. Also, the uncertainty of economic viability, nanoparticle agglomeration coupled with the uncertainty of health, and environmental hazards of nanoparticles are some of the existing challenges of nanoparticle-stabilized foam applications. In field applications, the purity of injected gases will differ over time due to gas recycling during the production process [170]. The effect of variation in gas composition or gas dilution on nanoparticle-stabilized foams is still unclear. Additionally, grafting surfactants on the surface of nanoparticles instead of physical mixing is another direction of research that has not been addressed recently that requires further investigations. Finally, there is still a need for pilot applications of nanoparticle-stabilized foams for field-scale performance evaluation of nanoparticle-stabilized foams.

Acknowledgments The authors gratefully acknowledge the Natural Sciences and Engineering Research Council of Canada (NSERC). The second author thanks the Islamic Development Bank (IDB) for its support during his internship at Dr. Nassar Research Group at the University of Calgary.

Nomenclature

A	Surface area, also used as the cross-sectional area of a core
B	Bridging coefficient
C_s	Surfactant concentration in solution
D_i	Diameter of a foam bubble
D_{med}	Median of the volume-averaged bubble diameter in the foam
D_{sm}	Sauter mean diameter
E	Entering coefficient
ΔE	Energy required to remove particle from the gas/liquid interface
E_G	Gibbs surface elasticity
E_M	Marangoni surface elasticity
f_g	Foam quality
k	Core permeability
L	Lamella number, core length
MRF	Mobility reduction ratio
$P_c^{\max}$	Maximum capillary pressure

P_c^*	Limiting capillary pressure
P_G, P_L	Pressure on each side of an interface (gas, liquid)
ΔP	Pressure difference across an interface or pressure change
p	Nanoparticle packing parameter
Q	Injection rate
R	Radius of a curved surface or interface, also used as the gas constant, radius of nanoparticles
S	Spreading coefficient
R_1, R_2	Principal radii of curvature of a surface or interface
T	Absolute temperature
U_g	The superficial velocity of the gas
U_{poly}	Polydispersity
U_w	The superficial velocity of water
u_t	The total foam superficial velocity
σ	Surface or interfacial tension
σ_{og}	The interfacial tension between oil and gas
σ_{wo}	The interfacial tension between water and oil
σ_{wg}	The interfacial tension between water and gas
ε	Viscoelastic modulus
θ	Contact angle
Γ_s	Surface excess concentration of surfactant

References

1. M.G. Aarra, P.A. Ormehaug, A. Skauge, S.K. Masalmeh, Experimental study of CO2- and methane- foam using carbonate core material at reservoir conditions. Paper presented at the SPE Middle East oil and gas show and conference, Manama, Bahrain, 2011. https://doi.org/10.2118/141614-MS
2. M.G. Aarra, A. Skauge, J. Solbakken, P.A. Ormehaug, Properties of N2- and CO2-foams as a function of pressure. J. Pet. Sci. Eng. **116**, 72–80 (2014). https://doi.org/10.1016/j.petrol.2014.02.017
3. V.O. Abramov, A.V. Abramova, V.M. Bayazitov, L.K. Altunina, A.S. Gerasin, D.M. Pashin, T.J. Mason, Sonochemical approaches to enhanced oil recovery. Ultrason. Sonochem. **25**, 76–81 (2015). https://doi.org/10.1016/j.ultsonch.2014.08.014
4. S. Akbari, A. Nour, R. Yunus, A. Farhan, Biosurfactants as promising multifunctional agent: A mini review. Int. J. Innov. Res. Sci. Stud. **1**, 1–6 (2018)
5. A. Al Sumaiti, A.R. Shaik, E.S. Mathew, W. Al Ameri, Tuning foam parameters for mobility control using CO2 foam: Field application to maximize oil recovery from a high temperature high salinity layered carbonate reservoir. Energy Fuel **31**(5), 4637–4654 (2017). https://doi.org/10.1021/acs.energyfuels.6b02595
6. Z. AlYousef, D. Schechter, The synergy of surfactant and nanoparticles: Towards enhancing foam stability. Paper presented at the SPE Kuwait oil & gas show and conference, Mishref, Kuwait, 2019. https://doi.org/10.2118/198190-MS

7. Z. AlYousef, M. Almobarky, D. Schechter, Enhancing the stability of foam by the use of nanoparticles. Energy Fuel **31**(10), 10620–10627 (2017). https://doi.org/10.1021/acs.energyfuels.7b01697
8. S. Alzobaidi, M. Lotfollahi, I. Kim, K.P. Johnston, D.A. DiCarlo, Carbon dioxide-in-brine foams at high temperatures and extreme salinities stabilized with silica nanoparticles. Energy Fuel **31**(10), 10680–10690 (2017). https://doi.org/10.1021/acs.energyfuels.7b01814
9. A. Andrianov, R. Farajzadeh, M. Mahmoodi Nick, M. Talanana, P.L.J. Zitha, Immiscible foam for enhancing oil recovery: Bulk and porous media experiments. Ind. Eng. Chem. Res. **51**(5), 2214–2226 (2012). https://doi.org/10.1021/ie201872v
10. N. Anuar, M.H. Yunan, F. Sagala, A. Katende, The effect of WAG ratio and oil density on oil recovery by immiscible water alternating gas flooding. Am. J. Sci. Technol. **4**(5), 80–90 (2017)
11. A. Aronson, V. Bergeron, M.E. Fagan, C.J.C. Radke, S.A. Physicochemical, E. Aspects, The influence of disjoining pressure on foam stability and flow in porous media. Colloids Surf. A Physicochem. Eng. Asp. **83**(2), 109–120 (1994)
12. A. Aroonsri, A.J. Worthen, T. Hariz, K.P. Johnston, C. Huh, S.L. Bryant, Conditions for generating nanoparticle-stabilized CO2 foams in fracture and matrix flow. Paper presented at the SPE annual technical conference and exhibition, New Orleans, LA, USA, 2013. https://doi.org/10.2118/166319-MS
13. S. Banerjee, E. Hassenklöver, J.M. Kleijn, M.A. Cohen Stuart, F.A.M. Leermakers, Interfacial tension and wettability in water–carbon dioxide systems: Experiments and self-consistent field modeling. J. Phys. Chem. B **117**(28), 8524–8535 (2013). https://doi.org/10.1021/jp400940s
14. A. Barrabino, T. Holt, E. Lindeberg, An evaluation of graphene oxides as possible foam stabilizing agents for CO_2 based enhanced oil recovery. Nanomaterials (Basel, Switzerland) **8**(8), 603 (2018). https://doi.org/10.3390/nano8080603
15. G. Batôt, M. Fleury, E. Rosenberg, L. Nabzar, M. Chabert, Foam propagation in rock samples: Impact of oil and flow characterization. Paper presented at the SPE EOR conference at oil and gas West Asia, Muscat, Oman, 2016. https://doi.org/10.2118/179855-MS
16. A.E. Bayat, K. Rajaei, R. Junin, Assessing the effects of nanoparticle type and concentration on the stability of CO2 foams and the performance in enhanced oil recovery. Colloids Surf. A Physicochem. Eng. Asp. **511**, 222–231 (2016). https://doi.org/10.1016/j.colsurfa.2016.09.083
17. E.J. Behrens, *Investigation of Loss of Surfactants During Enhanced Oil Recovery Applications-Adsorption of Surfactants onto Clay Materials* (Institutt for kjemisk prosessteknologi, 2013)
18. D. Beneventi, B. Carre, A. Gandini, Role of surfactant structure on surface and foaming properties. Colloids Surf. A Physicochem. Eng. Asp. **189**(1), 65–73 (2001). https://doi.org/10.1016/S0927-7757(01)00602-1
19. B.P. Binks, Particles as surfactants – Similarities and differences. Curr. Opin. Colloid Interface Sci. **7**(1), 21–41 (2002). https://doi.org/10.1016/S1359-0294(02)00008-0
20. B.P. Binks, S.O. Lumsdon, Influence of particle wettability on the type and stability of surfactant-free emulsions. Langmuir **16**(23), 8622–8631 (2000). https://doi.org/10.1021/la000189s
21. B.P. Binks, M. Kirkland, J.A. Rodrigues, Origin of stabilisation of aqueous foams in nanoparticle–surfactant mixtures. Soft Matter **4**(12), 2373–2382 (2008). https://doi.org/10.1039/B811291F
22. C.S. Boeije, W. Rossen, Fitting foam-simulation-model parameters to data: I. Coinjection of gas and liquid. SPE Reserv. Eval. Eng. **18**(02), 264–272 (2015). https://doi.org/10.2118/174544-PA
23. J. Boos, W. Drenckhan, C. Stubenrauch, Protocol for studying aqueous foams stabilized by surfactant mixtures. J. Surfactant Deterg. **16**(1), 1–12 (2013). https://doi.org/10.1007/s11743-012-1416-2

24. C. Boyère, C. Jérôme, A. Debuigne, Input of supercritical carbon dioxide to polymer synthesis: An overview. Eur. Polym. J. **61**, 45–63 (2014). https://doi.org/10.1016/j.eurpolymj.2014.07.019
25. R. Butler, I. Hopkinson, A.I. Cooper, Synthesis of porous emulsion-templated polymers using high internal phase CO2-in-water emulsions. J. Am. Chem. Soc. **125**(47), 14473–14481 (2003). https://doi.org/10.1021/ja037570u
26. B.T. Campbell, F.M. Orr, Jr., *Flow Visualization for CO2/Crude Oil Displacements* (1985)
27. E. Carey, C. Stubenrauch, Foaming properties of mixtures of a non-ionic (C12DMPO) and an ionic surfactant (C12TAB). J. Colloid Interface Sci. **346**(2), 414–423 (2010). https://doi.org/10.1016/j.jcis.2010.03.013
28. F. Carn, A. Colin, O. Pitois, M. Vignes-Adler, R. Backov, Foam drainage in the presence of nanoparticle−surfactant mixtures. Langmuir **25**(14), 7847–7856 (2009). https://doi.org/10.1021/la900414q
29. D. Chakravarthy, V. Muralidharan, E. Putra, D.S. Schechter, Application of x-ray CT for investigation of CO2 and WAG injection in fractured reservoirs. Paper presented at the Canadian International Petroleum Conference, Calgary, AB, USA, 2004. https://doi.org/10.2118/2004-232
30. Q. Chen, M. Gerritsen, A.R. Kovscek, Modeling foam displacement with the local equilibrium approximation: Theory and experiment verification. Paper presented at the SPE Annual Technical Conference and Exhibition, Denver, CO, USA, 2008. https://doi.org/10.2118/116735-MS
31. Y. Chen, A.S. Elhag, B.M. Poon, L. Cui, K. Ma, S.Y. Liao, … K.P. Johnston, Ethoxylated cationic surfactants for CO2 EOR in high temperature, high salinity reservoirs. Paper presented at the SPE improved oil recovery symposium, Tulsa, OK, USA, 2012. https://doi.org/10.2118/154222-MS
32. Y. Chen, A.S. Elhag, B.M. Poon, L. Cui, K. Ma, S.Y. Liao, et al., Switchable nonionic to cationic ethoxylated amine surfactants for CO2 enhanced oil recovery in high-temperature, high-salinity carbonate reservoirs. SPE J. **19**(02), 249–259 (2014). https://doi.org/10.2118/154222-PA
33. Y. Chen, A.S. Elhag, P.P. Reddy, H. Chen, L. Cui, A.J. Worthen, et al., Phase behavior and interfacial properties of a switchable ethoxylated amine surfactant at high temperature and effects on CO2-in-water foams. J. Colloid Interface Sci. **470**, 80–91 (2016). https://doi.org/10.1016/j.jcis.2016.02.028
34. K.-O. Choi, N.P. Aditya, S. Ko, Effect of aqueous pH and electrolyte concentration on structure, stability and flow behavior of non-ionic surfactant based solid lipid nanoparticles. Food Chem. **147**, 239–244 (2014). https://doi.org/10.1016/j.foodchem.2013.09.095
35. B.C. Craft, M. Hawkins, *Applied Petroleum Reservoir Engineering* (Pearson, Upper Saddle River, 2015)
36. Z.G. Cui, Y.Z. Cui, C.F. Cui, Z. Chen, B.P. Binks, Aqueous foams stabilized by in situ surface activation of CaCO3 nanoparticles via adsorption of anionic surfactant. Langmuir **26**(15), 12567–12574 (2010). https://doi.org/10.1021/la1016559
37. L. Cui, K. Ma, M. Puerto, A.A. Abdala, I. Tanakov, L.J. Lu, et al., Mobility of Ethomeen C12 and carbon dioxide (CO2) foam at high temperature/high salinity and in carbonate cores. SPE J. **21**(04), 1151–1163 (2016). https://doi.org/10.2118/179726-PA
38. C. Da, G. Jian, S. Alzobaidi, J. Yang, S.L. Biswal, G.J. Hirasaki, K.P. Johnston, Design of CO2-in-water foam stabilized with switchable amine surfactants at high temperature in high-salinity brine and effect of oil. Energy Fuel **32**(12), 12259–12267 (2018). https://doi.org/10.1021/acs.energyfuels.8b02959
39. T.W. de Haas, H. Fadaei, U. Guerrero, D. Sinton, Steam-on-a-chip for oil recovery: The role of alkaline additives in steam assisted gravity drainage. Lab Chip **13**(19), 3832–3839 (2013). https://doi.org/10.1039/C3LC50612F
40. R. Deleurence, C. Parneix, C. Monteux, Mixtures of latex particles and the surfactant of opposite charge used as interface stabilizers – Influence of particle contact angle, zeta

potential, flocculation and shear energy. Soft Matter **10**(36), 7088–7095 (2014). https://doi.org/10.1039/C4SM00237G
41. N.D. Denkov, Mechanisms of foam destruction by oil-based antifoams. Langmuir **20**(22), 9463–9505 (2004). https://doi.org/10.1021/la049676o
42. N.D. Denkov, I.B. Ivanov, P.A. Kralchevsky, D.T. Wasan, A possible mechanism of stabilization of emulsions by solid particles. *J. Colloid Interface Sci.* **150**(2), 589–593 (1992). https://doi.org/10.1016/0021-9797(92)90228-E
43. N.D. Denkov, P. Cooper, J.-Y. Martin, Mechanisms of action of mixed solid−liquid antifoams. 1. Dynamics of foam film rupture. Langmuir **15**(24), 8514–8529 (1999). https://doi.org/10.1021/la9902136
44. J.L. Dickson, B.P. Binks, K.P. Johnston, Stabilization of carbon dioxide-in-water emulsions with silica nanoparticles. Langmuir **20**(19), 7976–7983 (2004). https://doi.org/10.1021/la0488102
45. W. Drenckhan, S. Hutzler, Structure and energy of liquid foams. Adv. Colloid Interf. Sci. **224**, 1–16 (2015). https://doi.org/10.1016/j.cis.2015.05.004
46. W. Drenckhan, D. Langevin, Monodisperse foams in one to three dimensions. Curr. Opin. Colloid Interface Sci. **15**(5), 341–358 (2010). https://doi.org/10.1016/j.cocis.2010.06.002
47. Z. Du, M.P. Bilbao-Montoya, B.P. Binks, E. Dickinson, R. Ettelaie, B.S. Murray, Outstanding stability of particle-stabilized bubbles. Langmuir **19**(8), 3106–3108 (2003). https://doi.org/10.1021/la034042n
48. A.A. Eftekhari, R. Krastev, R. Farajzadeh, Foam stabilized by fly ash nanoparticles for enhancing oil recovery. Ind. Eng. Chem. Res. **54**(50), 12482–12491 (2015). https://doi.org/10.1021/acs.iecr.5b03955
49. H. Ehtesabi, M.M. Ahadian, V.J.E. Taghikhani, Enhanced heavy oil recovery using TiO2 nanoparticles: Investigation of deposition during transport in core plug. Energy Fuel **29**(1), 1–8 (2015)
50. A.S. Elhag, C. Da, Y. Chen, N. Mukherjee, J.A. Noguera, S. Alzobaidi, et al., Viscoelastic diamine surfactant for stable carbon dioxide/water foams over a wide range in salinity and temperature. J. Colloid Interface Sci. **522**, 151–162 (2018). https://doi.org/10.1016/j.jcis.2018.03.037
51. A.S. Emrani, H.A. Nasr-El-Din, Stabilizing CO2-foam using nanoparticles. Paper presented at the SPE European formation damage conference and exhibition, Budapest, Hungary, 2015. https://doi.org/10.2118/174254-MS
52. A.S. Emrani, H.A. Nasr-El-Din, An experimental study of nanoparticle-polymer-stabilized CO2 foam. Colloids Surf. A Physicochem. Eng. Asp. **524**, 17–27 (2017a). https://doi.org/10.1016/j.colsurfa.2017.04.023
53. A.S. Emrani, H.A. Nasr-El-Din, Stabilizing CO2 foam by use of nanoparticles. SPE J. **22**(02), 494–504 (2017b). https://doi.org/10.2118/174254-PA
54. R.M. Enick, D.K. Olsen, J.R. Ammer, W. Schuller, Mobility and conformance control for CO2 eor via thickeners, foams, and gels – A literature review of 40 years of research and pilot tests. Paper presented at the SPE improved oil recovery symposium, Tulsa, OK, USA, 2012. https://doi.org/10.2118/154122-MS
55. D.A. Espinoza, F.M. Caldelas, K.P. Johnston, S.L. Bryant, C. Huh, Nanoparticle-stabilized supercritical CO2 foams for potential mobility control applications. Paper presented at the SPE improved oil recovery symposium, Tulsa, OK, USA, 2010. https://doi.org/10.2118/129925-MS
56. A.H. Falls, G.J. Hirasaki, T.W. Patzek, D.A. Gauglitz, D.D. Miller, T. Ratulowski, Development of a mechanistic foam simulator: The population balance and generation by snap-off. SPE Reserv. Eng. **3**(03), 884–892 (1988). https://doi.org/10.2118/14961-PA
57. A.H. Falls, J.J. Musters, J. Ratulowski, The apparent viscosity of foams in homogeneous bead packs. SPE Reserv. Eng. **4**(02), 155–164 (1989). https://doi.org/10.2118/16048-PA

58. S. Farad, H.K. Nsamba, A. Al Hassan, W. Joseph, I. Kabenge, Effect of pH and slug ratio of alkaline surfactant polymer alternating gas flooding on oil recovery. Am. Assoc. Sci. Technol. **3**(2), 47–52 (2016)
59. R. Farajzadeh, A. Andrianov, H. Bruining, P.L.J. Zitha, Comparative study of CO2 and N2 foams in porous media at low and high pressure−temperatures. Ind. Eng. Chem. Res. **48**(9), 4542–4552 (2009). https://doi.org/10.1021/ie801760u
60. R. Farajzadeh, A. Andrianov, P.L.J. Zitha, Investigation of immiscible and miscible foam for enhancing oil recovery. Ind. Eng. Chem. Res. **49**(4), 1910–1919 (2010). https://doi.org/10.1021/ie901109d
61. R. Farajzadeh, M. Lotfollahi, A.A. Eftekhari, W.R. Rossen, G.J.H. Hirasaki, Effect of permeability on implicit-texture foam model parameters and the limiting capillary pressure. Energy Fuel **29**(5), 3011–3018 (2015). https://doi.org/10.1021/acs.energyfuels.5b00248
62. R.N. Gajbhiye, S.I. Kam, Characterization of foam flow in horizontal pipes by using two-flow-regime concept. Chem. Eng. Sci. **66**(8), 1536–1549 (2011). https://doi.org/10.1016/j.ces.2010.12.012
63. D. Georgieva, V. Schmitt, F. Leal-Calderon, D. Langevin, On the possible role of surface elasticity in emulsion stability. Langmuir **25**(10), 5565–5573 (2009). https://doi.org/10.1021/la804240e
64. R.B. Ghahfarokhi, United States Patent No. (2019)
65. D.W. Green, G.P. Willhite, *Enhanced Oil Recovery*, vol 8 (Texas, United States of America: Society of Petroleum Engineers, 1998)
66. F. Guo, S. Aryana, An experimental investigation of nanoparticle-stabilized CO2 foam used in enhanced oil recovery. Fuel **186**, 430–442 (2016). https://doi.org/10.1016/j.fuel.2016.08.058
67. F. Guo, J. He, P.A. Johnson, S.A. Aryana, Stabilization of CO2 foam using by-product fly ash and recyclable iron oxide nanoparticles to improve carbon utilization in EOR processes. Sustain. Energy Fuels **1**(4), 814–822 (2017). https://doi.org/10.1039/c7se00098g
68. J.E. Hanssen, M. Dalland, Increased oil tolerance of polymer-enhanced foams: Deep chemistry or just "Simple" displacement effects? Paper presented at the SPE/DOE Improved Oil Recovery Symposium, Tulsa, OK, USA, 2000. https://doi.org/10.2118/59282-MS
69. T.R. Hariz, *Nanoparticle-Stabilized CO2 Foams for Potential Mobility Control Applications* (The University of Texas at Austin, Austin, 2012)
70. W.D. Harkins, A general thermodynamic theory of the spreading of liquids to form duplex films and of liquids or solids to form monolayers. J. Chem. Phys. **9**, 552 (1941)
71. P.C. Harris, Dynamic fluid-loss characteristics of CO2-foam fracturing fluids. SPE Prod. Eng. **2**(02), 89–94 (1987). https://doi.org/10.2118/13180-PA
72. R. Hashemi, N.N. Nassar, P. Pereira-Almao, Transport behavior of multimetallic ultradispersed nanoparticles in an oil-sands-packed bed column at a high temperature and pressure. Energy Fuel **26**(3), 1645–1655 (2012). https://doi.org/10.1021/ef201939f
73. R. Hashemi, N.N. Nassar, P. Pereira Almao, Nanoparticle technology for heavy oil in-situ upgrading and recovery enhancement: Opportunities and challenges. Appl. Energy **133**, 374–387 (2014). https://doi.org/10.1016/j.apenergy.2014.07.069
74. A. Heydarian, R. Kharrat, S. Heydarian, A. Hashemi, Impact of nano-particles on static performance of surfactant foams. J. Am. Sci. **9**(6) (2013)
75. G.J. Hirasaki, J.B. Lawson, Mechanisms of foam flow in porous media: Apparent viscosity in smooth capillaries. Soc. Pet. Eng. J. **25**(02), 176–190 (1985). https://doi.org/10.2118/12129-PA
76. G. Hirasaki, C.A. Miller, M. Puerto, Recent advances in surfactant EOR. SPE J. **16**(04), 889–907 (2011). https://doi.org/10.2118/115386-PA
77. T.S. Horozov, Foams and foam films stabilised by solid particles. Curr. Opin. Colloid Interface Sci. **13**(3), 134–140 (2008). https://doi.org/10.1016/j.cocis.2007.11.009
78. J. Hou, Z. Liu, S. Zhang, X.a. Yue, J. Yang, The role of viscoelasticity of alkali/surfactant/polymer solutions in enhanced oil recovery. J. Pet. Sci. Eng. **47**, 219–235 (2005). https://doi.org/10.1016/j.petrol.2005.04.001

79. A.M. Howe, A. Clarke, J. Mitchell, J. Staniland, L. Hawkes, C. Whalan, Visualising surfactant enhanced oil recovery. Colloids Surf. A Physicochem. Eng. Asp. **480**, 449–461 (2015). https://doi.org/10.1016/j.colsurfa.2014.08.032
80. T.N. Hunter, R.J. Pugh, G.V. Franks, G.J. Jameson, The role of particles in stabilising foams and emulsions. Adv. Colloid Interf. Sci. **137**(2), 57–81 (2008). https://doi.org/10.1016/j.cis.2007.07.007
81. A.F. Ibrahim, A. Emrani, H. Nasraldin, Stabilized CO2 foam for EOR applications. Paper presented at the Carbon Management Technology conference, Houston, TX, USA, 2017. https://doi.org/10.7122/486215-MS
82. S. Jikich, CO2 EOR: Nanotechnology for mobility control studied. J. Pet. Technol. **64**(07), 28–31 (2012). https://doi.org/10.2118/0712-0028-JPT
83. S.I. Kam, W.R. Rossen, Anomalous capillary pressure, stress, and stability of solids-coated bubbles. J. Colloid Interface Sci. **213**, 329 (1999)
84. M.S. Kamal, I.A. Hussein, A.S. Sultan, Review on surfactant flooding: Phase behavior, retention, IFT, and field applications. Energy Fuel **31**(8), 7701–7720 (2017). https://doi.org/10.1021/acs.energyfuels.7b00353
85. S.I. Karakashev, O. Ozdemir, M.A. Hampton, A.V. Nguyen, Formation and stability of foams stabilized by fine particles with similar size, contact angle and different shapes. Colloids Surf. A Physicochem. Eng. Asp. **382**(1), 132–138 (2011). https://doi.org/10.1016/j.colsurfa.2010.09.023
86. M. Khajehpour, S.R. Etminan, J. Goldman, F. Wassmuth, S. Bryant, Nanoparticles as foam stabilizer for steam-foam process. SPE J. **23**(06), 2232–2242 (2018). https://doi.org/10.2118/179826-PA
87. J. Kim, L. Cote, F. Kim, W. Yuan, K. Shull, J. Huang, Graphene oxide sheets at interfaces. J. Am. Chem. Soc. **132**(23), 8180–8186 (2010). https://doi.org/10.1021/ja102777p
88. I. Kim, A. Taghavy, D. DiCarlo, C. Huh, Aggregation of silica nanoparticles and its impact on particle mobility under high-salinity conditions. J. Pet. Sci. Eng. **133**, 376–383 (2015). https://doi.org/10.1016/j.petrol.2015.06.019
89. I. Kim, A.J. Worthen, K.P. Johnston, D.A. DiCarlo, C. Huh, Size-dependent properties of silica nanoparticles for Pickering stabilization of emulsions and foams. J. Nanopart. Res. **18**(4), 82 (2016). https://doi.org/10.1007/s11051-016-3395-0
90. K. Koczo, L.A. Lobo, D.T. Wasan, Effect of oil on foam stability: Aqueous foams stabilized by emulsions. J. Colloid Interface Sci. **150**(2), 492–506 (1992). https://doi.org/10.1016/0021-9797(92)90218-B
91. T. Kostakis, R. Ettelaie, B.S. Murray, Effect of high salt concentrations on the stabilization of bubbles by silica particles. Langmuir **22**(3), 1273–1280 (2006). https://doi.org/10.1021/la052193f
92. P.M. Kruglyakov, S.I. Elaneva, N.G. Vilkova, About mechanism of foam stabilization by solid particles. Adv. Colloid Interf. Sci. **165**(2), 108–116 (2011). https://doi.org/10.1016/j.cis.2011.02.003
93. S. Kumar, A. Mandal, Investigation on stabilization of CO2 foam by ionic and nonionic surfactants in presence of different additives for application in enhanced oil recovery. Appl. Surf. Sci. **420**, 9–20 (2017). https://doi.org/10.1016/j.apsusc.2017.05.126
94. L.W. Lake, *Enhanced Oil Recovery* (Prentice Hall, Englewood Cliffs, 1989)
95. D. Lee, H. Cho, J. Lee, C. Huh, K. Mohanty, Fly ash nanoparticles as a CO2 foam stabilizer. Powder Technol. **283**, 77–84 (2015). https://doi.org/10.1016/j.powtec.2015.05.010
96. Z. Li, Z. Liu, B. Li, S. Li, Q. Sun, S. Wang, Aqueous foams stabilized with particles and surfactants. Paper presented at the SPE Saudi Arabia section technical symposium and exhibition, Al-Khobar, Saudi Arabia, 2012. https://doi.org/10.2118/160840-MS
97. S. Li, Z. Li, P. Wang, Experimental study of the stabilization of CO2 foam by sodium dodecyl sulfate and hydrophobic nanoparticles. Ind. Eng. Chem. Res. **55**(5), 1243–1253 (2016). https://doi.org/10.1021/acs.iecr.5b04443

98. S. Li, C. Qiao, Z. Li, S. Wanambwa, Properties of carbon dioxide foam stabilized by hydrophilic nanoparticles and hexadecyltrimethylammonium bromide. Energy Fuel **31**(2), 1478–1488 (2017). https://doi.org/10.1021/acs.energyfuels.6b03130
99. S. Li, K. Yang, Z. Li, K. Zhang, N. Jia, Properties of CO2 foam stabilized by hydrophilic nanoparticles and nonionic surfactants. Energy Fuel **33**(6), 5043–5054 (2019). https://doi.org/10.1021/acs.energyfuels.9b00773
100. M. Liu, A. Andrianov, W.R. Rossen, Sweep efficiency in CO2 foam simulations with oil. Paper presented at the IOR 2011-16th European symposium on improved oil recovery, 2011
101. C. Liu, J. Zhang, I. Orcid, X. Sang, X. Kang, B. Zhang, et al., CO(2)/water emulsions stabilized by partially reduced graphene oxide. ACS Appl. Mater. Interfaces **9**(20), 17613–17619 (2017)
102. Q. Liu, H. Qu, S. Liu, Y. Zhang, S. Zhang, J. Liu, et al., Modified Fe3O4 nanoparticle used for stabilizing foam flooding for enhanced oil recovery. Colloids Surf. A Physicochem. Eng. Asp., 125383 (2020). https://doi.org/10.1016/j.colsurfa.2020.125383
103. L. Lobo, D.T. Wasan, Mechanisms of aqueous foam stability in the presence of emulsified non-aqueous-phase liquids: Structure and stability of the pseudoemulsion film. Langmuir **9**(7), 1668–1677 (1993). https://doi.org/10.1021/la00031a012
104. T. Lu, Z. Li, D. Hou, Z. Xu, X. Ban, B. Zhou, Experimental and numerical evaluation of surfactant-nanoparticles foam for enhanced oil recovery under high temperature. Energy Fuel **34**(1), 1005–1013 (2020). https://doi.org/10.1021/acs.energyfuels.9b03000
105. J. Luo, L. Cote, V. Tung, A. Tan, P. Goins, J. Wu, J. Huang, Graphene oxide nanocolloids. J. Am. Chem. Soc. **132**(50), 17667–17669 (2010). https://doi.org/10.1021/ja1078943
106. Q. Lv, T. Zhou, X. Zhang, B. Zuo, Z. Dong, J. Zhang, Enhanced oil recovery using aqueous CO2 foam stabilized by particulate matter from coal combustion. Energy Fuel **34**(3), 2880–2892 (2020). https://doi.org/10.1021/acs.energyfuels.9b04066
107. K. Ma, *Transport of Surfactant and Foam in Porous Media for Enhanced Oil Recovery Process* (Rice University, 2013)
108. M. Manan, S. Farad, A. Piroozian, M. Esmail, Effects of nanoparticle types on carbon dioxide foam flooding in enhanced oil recovery. Pet. Sci. Technol. **33**(12), 1286–1294 (2015)
109. D.J. Manlowe, C.J. Radke, A pore-level investigation of foam/oil interactions in porous media. SPE Reserv. Eng. **5**(04), 495–502 (1990). https://doi.org/10.2118/18069-PA
110. S.K. Masalmeh, H. Hillgartner, R.A.-M. Al-Mjeni, X. Jing, Simultaneous injection of miscible gas and polymer (SIMGAP) to improve oil recovery and sweep efficiency from layered carbonate reservoirs. Paper presented at the SPE EOR Conference at Oil & Gas West Asia, Muscat, Oman, 2010. https://doi.org/10.2118/129645-MS
111. E.S. Mathew, A.R. Shaik, A. Al Sumaiti, W. AlAmeri, Effect of oil presence on CO2 foam based mobility control in high temperature high salinity carbonate reservoirs. Energy Fuel **32**(3), 2983–2992 (2018). https://doi.org/10.1021/acs.energyfuels.7b03490
112. W.D. McCain, *The Properties of Petroleum Fluids* (Pennwell Books, Tulsa, 1990), p. 19900301
113. M.B.J. Meinders, T. van Vliet, The role of interfacial rheological properties on Ostwald ripening in emulsions. Adv. Colloid Interf. Sci. **108–109**, 119–126 (2004). https://doi.org/10.1016/j.cis.2003.10.005
114. D. Mo, J. Yu, N. Liu, R.L. Lee, Study of the effect of different factors on nanoparticle-stablized CO2 foam for mobility control. Paper presented at the SPE Annual Technical Conference and Exhibition, San Antonio, TX, USA, 2012. https://doi.org/10.2118/159282-MS
115. D. Mo, B. Jia, J. Yu, N. Liu, R. Lee, Study nanoparticle-stabilized CO2 foam for oil recovery at different pressure, temperature, and rock samples. Paper presented at the SPE Improved Oil Recovery Symposium, Tulsa, OK, USA, 2014. https://doi.org/10.2118/169110-MS
116. M. Morvan, P. Moreau, G. Degre, J. Leng, C. Masselon, J. Bouillot, A. Zaitoun, New viscoelastic fluid for chemical EOR. Paper presented at the SPE international symposium on oilfield chemistry, The Woodlands, TX, USA, 2009. https://doi.org/10.2118/121675-MS
117. C. Negin, A. Saeedi, Q. Xie, Most common surfactants employed in chemical enhanced oil recovery. Petroleum **3** (2016). https://doi.org/10.1016/j.petlm.2016.11.007

118. P. Nguyen, H. Fadaei, D. Sinton, Pore-scale assessment of nanoparticle-stabilized CO2 foam for enhanced oil recovery. Energy Fuel **28**(10), 6221–6227 (2014). https://doi.org/10.1021/ef5011995
119. A.D. Nikolov, D.T. Wasan, D.W. Huang, D.A. Edwards, The effect of oil on foam stability: Mechanisms and implications for oil displacement by foam in porous media. Paper presented at the SPE annual technical conference and exhibition, New Orleans, LA, USA, 1986. https://doi.org/10.2118/15443-MS
120. G. Palazzo, D. Berti, *Colloidal Foundations of Nanoscience* (Elsevier, 2014)
121. C. Palocci, A. Barbetta, A. La Grotta, M. Dentini, Porous biomaterials obtained using supercritical CO2−water emulsions. Langmuir **23**(15), 8243–8251 (2007). https://doi.org/10.1021/la700947g
122. R.J. Pugh, Foaming, foam films, antifoaming and defoaming. Adv. Colloid Interf. Sci. **64**, 67–142 (1996). https://doi.org/10.1016/0001-8686(95)00280-4
123. C. Qian, A. Telmadarreie, M. Dong, S. Bryant, Synergistic effect between surfactant and nanoparticles on the stability of foam in EOR processes. SPE J. **25**(02), 883–894 (2020). https://doi.org/10.2118/195310-PA
124. M.D. Rad, *Natural Gas Foam Stabilization by a Mixture of Oppositely Charged Nanoparticle and Surfactant and the Underlying Mechanisms.* Master of Science, University of Calgary. (2018)
125. R. Rafati, A.S. Haddad, H. Hamidi, Experimental study on stability and rheological properties of aqueous foam in the presence of reservoir natural solid particles. Colloids Surf. A Physicochem. Eng. Asp. **509**, 19–31 (2016). https://doi.org/10.1016/j.colsurfa.2016.08.087
126. K. Raghav Chaturvedi, R. Kumar, J. Trivedi, J.J. Sheng, T. Sharma, Stable silica nanofluids of an oilfield polymer for enhanced CO2 absorption for oilfield applications. Energy Fuel **32**(12), 12730–12741 (2018). https://doi.org/10.1021/acs.energyfuels.8b02969
127. K.T. Raterman, An investigation of oil destabilization of nitrogen foams in porous media. Paper presented at the SPE annual technical conference and exhibition, San Antonio, TX, USA, 1989. https://doi.org/10.2118/19692-MS
128. P. Rattanaudom, B.-J. Shiau, U. Suriyapraphadilok, A. Charoensaeng, Effect of pH on silica nanoparticle-stabilized foam for enhanced oil recovery using carboxylate-based extended surfactants. J. Pet. Sci. Eng. **196**, 107729 (2021). https://doi.org/10.1016/j.petrol.2020.107729
129. F. Ravera, E. Santini, G. Loglio, M. Ferrari, L. Liggieri, Effect of nanoparticles on the interfacial properties of liquid/liquid and liquid/air surface layers. J. Phys. Chem. B **110**(39), 19543–19551 (2006). https://doi.org/10.1021/jp0636468
130. V.G. Reidenbach, P.C. Harris, Y.N. Lee, D.L. Lord, Rheological study of foam fracturing fluids using nitrogen and carbon dioxide. SPE Prod. Eng. **1**(01), 31–41 (1986). https://doi.org/10.2118/12026-PA
131. J.V. Robinson, W.W. Woods, A method of selecting foam inhibitors. J. Soc. Chem. Ind. **67**(9), 361–365 (1948). https://doi.org/10.1002/jctb.5000670908
132. A.U. Rognmo, N. Al-Khayyat, S. Heldal, I. Vikingstad, O. Eide, S.B. Fredriksen, … M.A. Ferno, Performance of silica nanoparticles in CO2-foam for EOR and CCUS at tough reservoir conditions. Paper presented at the SPE Norway one day seminar, Bergen, Norway, 2018a. https://doi.org/10.2118/191318-MS
133. A.U. Rognmo, S. Heldal, M.A. Fernø, Silica nanoparticles to stabilize CO2-foam for improved CO2 utilization: Enhanced CO2 storage and oil recovery from mature oil reservoirs. Fuel **216**, 621–626 (2018b). https://doi.org/10.1016/j.fuel.2017.11.144
134. W.R. Rossen, W.J. Renkema, Success of foam SAG processes in heterogeneous reservoirs. Paper presented at the SPE annual technical conference and exhibition, Anaheim, CA, USA, 2007. https://doi.org/10.2118/110408-MS
135. W.R. Rossen, M.W. Wang, Modeling foams for acid diversion. SPE J. **4**(02), 92–100 (1999). https://doi.org/10.2118/56396-PA

136. S. Sakthivel, A. Adebayo, M.Y. Kanj, Experimental evaluation of carbon dots stabilized foam for enhanced oil recovery. Energy Fuel **33**(10), 9629–9643 (2019). https://doi.org/10.1021/acs.energyfuels.9b02235
137. O.O. Samuel, *Effect of Reservoir Heterogeneity on Immiscible Foam Enhanced Oil Recovery* (Delft University of Technology, 2009)
138. L.L. Schramm, J.J. Novosad, Micro-visualization of foam interactions with a crude oil. Colloids Surf. **46**(1), 21–43 (1990). https://doi.org/10.1016/0166-6622(90)80046-7
139. L.L. Schramm, J.J. Novosad, The destabilization of foams for improved oil recovery by crude oils: Effect of the nature of the oil. J. Pet. Sci. Eng. **7**(1), 77–90 (1992). https://doi.org/10.1016/0920-4105(92)90010-X
140. L.L. Schramm, F. Wassmuth, Foams: Basic principles, in *Foams: Fundamentals and Applications in the Petroleum Industry*, vol. 242, (American Chemical Society, 1994), pp. 3–45
141. D. Shan, W.R. Rossen, Optimal injection strategies for foam IOR. Paper presented at the SPE/DOE improved oil recovery symposium, Tulsa, OK, USA, 2002. https://doi.org/10.2118/75180-MS
142. S. Shayegi, P.A. Schenewerk, J.M. Wolcott, *Enhancement of Residual Oil Recovery Using a Mixture of Nitrogen or Methane Diluted with Carbon Dioxide in a Single-Well Injection Process* (Google Patents, 1998)
143. J. Sheng, *Enhanced Oil Recovery Field Case Studies* (Elsevier Science & Technology, Oxford, 2013)
144. L. Siggel, M. Santa, M. Hansch, M. Nowak, M. Ranft, H. Weiss, … J. Tinsley, A new class of viscoelastic surfactants for enhanced oil recovery. Paper presented at the SPE improved oil recovery symposium, Tulsa, OK, USA, 2012. https://doi.org/10.2118/153969-MS
145. R. Singh, K.K. Mohanty, Foams stabilized by in-situ surface activated nanoparticles in bulk and porous media. Paper presented at the SPE annual technical conference and exhibition, Amsterdam, The Netherlands, 2014. https://doi.org/10.2118/170942-MS
146. R. Singh, K.K. Mohanty, Synergy between nanoparticles and surfactants in stabilizing foams for oil recovery. Energy Fuel **29**(2), 467–479 (2015). https://doi.org/10.1021/ef5015007
147. R. Singh, K.K. Mohanty, Foams stabilized by in-situ surface-activated nanoparticles in bulk and porous media. SPE J. **21**(01), 121–130 (2016). https://doi.org/10.2118/170942-PA
148. R. Singh, K.K. Mohanty, Nanoparticle-stabilized foams for high-temperature, high-salinity oil reservoirs. Paper presented at the SPE annual technical conference and exhibition, San Antonio, TX, USA, 2017. https://doi.org/10.2118/187165-MS
149. R. Singh, A. Gupta, K.K. Mohanty, C. Huh, D. Lee, H. Cho, Fly ash nanoparticle-stabilized CO2-in-water foams for gas mobility control applications. Paper presented at the SPE annual technical conference and exhibition, Houston, TX, USA, 2015. https://doi.org/10.2118/175057-MS
150. R. Singh, K. Panthi, U. Weerasooriya, K.K. Mohanty, Multistimuli-responsive foams using an anionic surfactant. Langmuir **34**(37), 11010–11020 (2018). https://doi.org/10.1021/acs.langmuir.8b01796
151. T. Skauge, K. Spildo, A. Skauge, Nano-sized particles for EOR. Paper presented at the SPE improved oil recovery symposium, 2010
152. R.L. Slobod, H.A. Jr. Koch, High-pressure gas injection- mechanism of recovery increase. Paper presented at the drilling and production practice, New York, NY, USA, 1953
153. K. Spildo, A.M. Johannessen, A. Skauge, Low salinity waterflood at reduced capillarity. Paper presented at the SPE improved oil recovery symposium, Tulsa, OK, USA, 2012. https://doi.org/10.2118/154236-MS
154. A. Stocco, E. Rio, B.P. Binks, D. Langevin, Aqueous foams stabilized solely by particles. Soft Matter **7**(4), 1260–1267 (2011). https://doi.org/10.1039/C0SM01290D
155. Y.Q. Sun, T. Gao, The optimum wetting angle for the stabilization of liquid-metal foams by ceramic particles: Experimental simulations. Metall. Mater. Trans. A Phys. Metall. Mater. Sci. **33**, 3285–3292 (2002). https://doi.org/10.1007/s11661-002-0315-y

156. Q. Sun, Z. Li, S. Li, L. Jiang, J. Wang, P. Wang, Utilization of surfactant-stabilized foam for enhanced oil recovery by adding nanoparticles. Energy Fuel **28**(4), 2384–2394 (2014). https://doi.org/10.1021/ef402453b
157. X. Sun, Y. Zhang, G. Chen, Z.J.E. Gai, Application of nanoparticles in enhanced oil recovery: A critical review of recent progress. Energies **10**(3), 345 (2017)
158. F.-Q. Tang, Z. Xiao, J.-A. Tang, L. Jiang, The effect of SiO2 particles upon stabilization of foam. J. Colloid Interface Sci. **131**(2), 498–502 (1989). https://doi.org/10.1016/0021-9797(89)90192-6
159. S. Tcholakova, Z. Mitrinova, K. Golemanov, N.D. Denkov, M. Vethamuthu, K.P. Ananthapadmanabhan, Control of Ostwald ripening by using surfactants with high surface modulus. Langmuir **27**(24), 14807–14819 (2011). https://doi.org/10.1021/la203952p
160. A.K. Vikingstad, *Static and Dynamic Studies of Foam and Foam-Oil Interactions.* PhD, University of Bergen, (2006)
161. T.-F. Wang, J.-X. Wang, L. Han, J.-H. Wang, Y. Zhu, Study on the stabilizing effect of aluminum hydroxide nanoparticles on foams. J. Xian Shiyou Univ., 78–81 (2012)
162. S. Wang, Y. Shi, B.-M. Li, Neural representation of cost–benefit selections in rat anterior cingulate cortex in self-paced decision making. Neurobiol. Learn. Mem. **139**, 1–10 (2017). https://doi.org/10.1016/j.nlm.2016.12.003
163. P. Wang, Q. You, L. Han, W. Deng, Y. Liu, J. Fang, et al., Experimental study on the stabilization mechanisms of CO2 foams by hydrophilic silica nanoparticles. Energy Fuel **32**(3), 3709–3715 (2018). https://doi.org/10.1021/acs.energyfuels.7b04125
164. D.T. Wasan, K. Koczo, A.D. Nikolov, Mechanisms of aqueous foam stability and antifoaming action with and without oil, in *Foams: Fundamentals and Applications in the Petroleum Industry*, vol. 242, (American Chemical Society, 1994), pp. 47–114
165. D. Weaire, S. Hutzler, P.-G. Gennes, The physics of foams. Phys. Today **54** (2001). https://doi.org/10.1063/1.1366070
166. T. Witten, P. Pincus, *Structured Fluids: Polymers, Colloids* (Surfactants, 2010)
167. A. Worthen, H. Bagaria, Y. Chen, S.L. Bryant, C. Huh, K.P. Johnston, Nanoparticle stabilized carbon dioxide in water foams for enhanced oil recovery. Paper presented at the SPE improved oil recovery symposium, Tulsa, OK, USA, 2012. https://doi.org/10.2118/154285-MS
168. A. Worthen, H. Bagaria, Y. Chen, S. Bryant, C. Huh, K. Johnston, Nanoparticle-stabilized carbon dioxide-in-water foams with fine texture. J. Colloid Interface Sci. **391**, 142–151 (2013). https://doi.org/10.1016/j.jcis.2012.09.043
169. D. Xing, B. Wei, W. McLendon, R. Enick, S. McNulty, K. Trickett, et al., CO2-soluble/nonionic, water-soluble surfactants that stabilize CO2-in-brine foams. SPE J. **17**(4), 1172–1185 (2012). https://doi.org/10.2118/129907-PA
170. Z. Xue, K. Panthi, Y. Fei, K.P. Johnston, K.K. Mohanty, CO2-soluble ionic surfactants and CO2 foams for high-temperature and high-salinity sandstone reservoirs. Energy Fuel **29**(9), 5750–5760 (2015). https://doi.org/10.1021/acs.energyfuels.5b01568
171. Z. Xue, A. Worthen, A. Qajar, I. Robert, S.L. Bryant, C. Huh, et al., Viscosity and stability of ultra-high internal phase CO2-in-water foams stabilized with surfactants and nanoparticles with or without polyelectrolytes. J. Colloid Interface Sci. **461**, 383–395 (2016). https://doi.org/10.1016/j.jcis.2015.08.031
172. W. Yang, T. Wang, Z. Fan, Highly stable foam stabilized by alumina nanoparticles for EOR: Effects of sodium cumenesulfonate and electrolyte concentrations. Energy Fuel **31**(9), 9016–9025 (2017a). https://doi.org/10.1021/acs.energyfuels.7b01248
173. W. Yang, T. Wang, Z. Fan, Q. Miao, Z. Deng, Y. Zhu, Foams stabilized by in situ-modified nanoparticles and anionic surfactants for enhanced oil recovery. Energy Fuel **31**(5), 4721–4730 (2017b). https://doi.org/10.1021/acs.energyfuels.6b03217
174. N. Yekeen, A.K. Idris, M.A. Manan, A.M. Samin, A.R. Risal, T.X. Kun, Bulk and bubble-scale experimental studies of influence of nanoparticles on foam stability. Chin. J. Chem. Eng. **25**(3), 347–357 (2017). https://doi.org/10.1016/j.cjche.2016.08.012

175. N. Yekeen, M.A. Manan, A.K. Idris, E. Padmanabhan, R. Junin, A.M. Samin, et al., A comprehensive review of experimental studies of nanoparticles-stabilized foam for enhanced oil recovery. J. Pet. Sci. Eng. **164**, 43–74 (2018). https://doi.org/10.1016/j.petrol.2018.01.035
176. J. Yu, C. An, D. Mo, N. Liu, R.L. Lee, Foam mobility control for nanoparticle-stabilized supercritical CO2 foam. Paper presented at the SPE improved oil recovery symposium, Tulsa, OK, USA, 2012a. https://doi.org/10.2118/153336-MS
177. J. Yu, N. Liu, L. Li, R.L. Lee, Generation of nanoparticle-stabilized supercritical CO2 foams. Paper presented at the Carbon Management Technology conference, Orlando, FL, USA, 2012b. https://doi.org/10.7122/150849-MS
178. J. Yu, D. Mo, N. Liu, R. Lee, The application of nanoparticle-stabilized CO2 foam for oil recovery. Paper presented at the SPE international symposium on oilfield chemistry, The Woodlands, TX, USA, 2013. https://doi.org/10.2118/164074-MS
179. Y. Zeng, R. Farajzadeh, A.A. Eftekhari, S. Vincent-Bonnieu, A. Muthuswamy, W.R. Rossen, et al., Role of gas type on foam transport in porous media. Langmuir **32**(25), 6239–6245 (2016). https://doi.org/10.1021/acs.langmuir.6b00949
180. S.Y. Zhang, *Foams Stabilized by Laponite/Surfactants and HMHEC/Surfactants* (Shandong University, Shandong, 2008)
181. X. Zhang, G. Zhang, J. Ge, Y. Wang, CO foam stabilized with switchable surfactants and modified nanoparticles effected by PH and salinity. Paper presented at the SPE Europec featured at 82nd EAGE Conference and Exhibition, Amsterdam, The Netherlands, 2020. https://doi.org/10.2118/200584-MS